Response to reviewers for the paper "Real-time measurements of secondary organic aerosol formation and aging from ambient air in an oxidation flow reactor in the Los Angeles area." – A. Ortega et al. ACPD, 15, 21907–21958, 2015

We thank the reviewers for their comments on our paper. To guide the review process we have copied the reviewer comments in black text. Our responses are in regular blue font. We have responded to all the referee comments and made alterations to our paper (**in bold text**).

Anonymous Referee #1

R1.0. The authors report a study investigating the aging of ambient air masses using an oxidation flow reactor. By exposing the samples in real-time to high OH exposures, they replicate the equivalent oxidative aging of 0.8 days to 6 weeks. A clear day/night cycle is observed in the enhancement of organic aerosol formation, attributed to the depletion of short-lived VOC precursors during daytime photo-oxidation. High reactor exposures were associated with a decrease in the SOA formation enhancement as heterogeneous oxidation leading to fragmentation and evaporation becomes dominant. The study highlights the advantages and insights that may be made by application of traditionally laboratory-based instrumentation to a field campaign, which may provide crucial measurements to help constrain model predictions of SOA formation. The scope of the study is fully appropriate for publication in ACP.

Overall the manuscript is well-written and insightful. The following comments should be addressed to improve the clarity of the manuscript.

R1.1. The authors should make the outlet configuration in the text (p21915 lines 1-4) and in the experimental schematic clearer. How narrow is the residence time distribution using this method? Have the "plug-flow" conditions been verified, either experimentally or using fluid dynamics simulations?

The use of "plug flow" was not accurate, what we meant to say is that the residence time distribution should be narrower when the inlet plate is removed. We have rephrased this text to clarify these issues, and also added results of CFD simulations, as:

"The configuration with the large inlet strongly reduces recirculation in the reactor and narrows the residence time distribution (RTD) (Fig. S1). To further reduce the width of the RTD, output flow was sampled from both a central stainless steel 1/4 inch OD tube at 2.0 L min^{-1} for aerosol measurements and a 3/8 inch OD PTFE Teflon perforated ring with 14 cm diameter for gas-phase measurements at 2.4 L min^{-1}. In addition, Peng et al. (2015) has shown that variations in the residence time distribution in the OFR had limited impact on the estimated OH_{exp}."

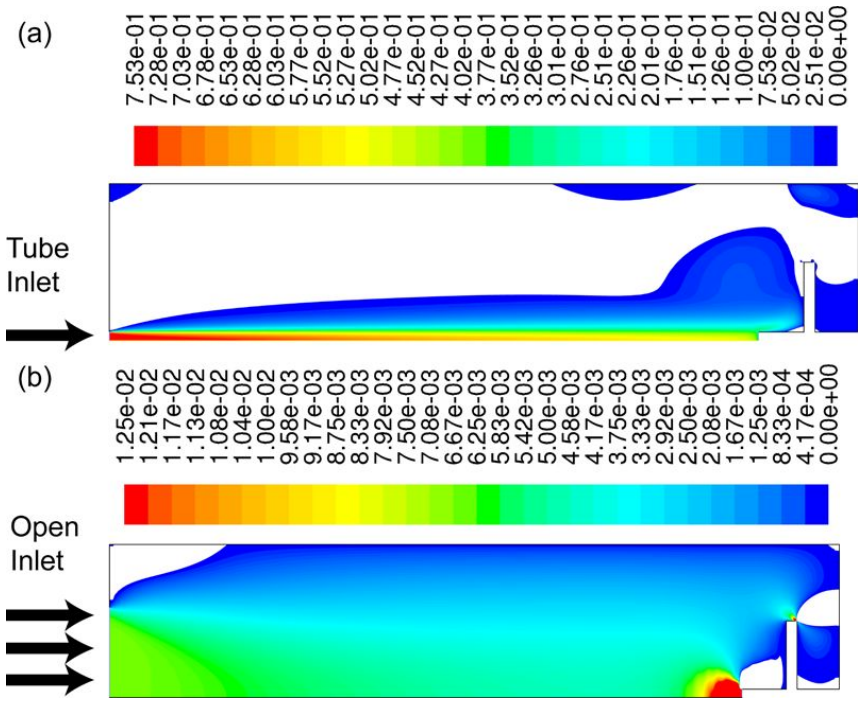

Figure S1. Results of computerized fluid dynamics (CFD) simulations comparing two OFR configurations. (a) Tube inlet, similar to Lambe et al. (2011); (b) Large open face inlet (11.9 cm diameter) as used in this field study. Colors are contours of positive horizontal velocity. White regions involve negative horizontal velocities, i.e. recirculation regions. The extensive recirculation regions of case (a) are almost completely removed in case (b), resulting in a narrower residence time distribution. Simulations were conducted using the FLUENT software, using cylindrical symmetry, with air at 1 atm and 293 K.

R1.2. Explain in more detail the particle loss correction. For instance, what does a “time varying way” mean in the context of applying the correction? A figure in the SI showing the uncorrected mass concentrations from the ambient and reactor sampling lines would help clarify. Further, might the temperature changes in the reactor with the lights on influence wall losses? Any temperature perturbation in the chamber should be reported.

The text describing the particle loss correction has been expanded to read:

“To correct for the effect of particle losses we compared concentrations measured in the reactor output when UV lights are turned off with those measured through the ambient inlet. The loss of particle mass in this aluminum reactor is small, of the order of a few percent of the ambient concentrations (see also Palm et al., 2016). Losses in an OFR with a quartz body were observed to be ~35% in a previous study (presumably due to nearly complete loss of charged particles), which led to our use of the all-aluminum reactor. A time-dependent correction factor was estimated by comparing each reactor output measurement (for each period when the lights were off) with the average of the two ambient measurements immediately before and after. This correction is interpolated in

time and applied to all reactor output measurements with lights on. The resulting average correction was +5.8 %. Although losses may have some size dependence, given the broad distributions covering the same size ranges for both ambient air and OFR output, and the small magnitude of the correction, this effect has not been considered in detail."

This correction seems too small and simple to warrant another supplementary figure.

We have added the following text to P21915/L18 to describe the second question:

"The lights are housed in Teflon sleeves which are purged with N_2 gas to remove heat and avoid exposing the lamp surfaces to O_3 or other oxidants. When operated at full power the lights result in an increase of ~2°C above ambient conditions. Given the low volatility of ambient OA (Huffman et al., 2009; see also Fig. S12 in this paper and associated discussion below), very little OA evaporation is expected in the reactor due to this heating."

R1.3. It seems the OH exposure is established in part by assuming the reactivity of the constituents. I'd be interested to see how an appropriate uncertainty placed on the assumed rate constant influences the inferred OH exposure.

OH exposure is calculated using a retrieval in which ambient OH reactivity is an input, as detailed in Li et al., (2015). During CalNex, an ambient direct measurement of total OH reactivity by the Stevens Group at the Indiana University was available, as stated on P21916/L9 of the ACPD manuscript. In this method, there is no assumption about the rate constants of different constituents. Other estimates of OH reactivity were available for the campaign, such as OH reactivity based on VOC measurements, but those values were not used due to the assumptions the reviewer highlights would be required. The following text has been modified to clarify this point:

"The equation uses ambient H_2O concentration, reactor output O_3 concentrations, residence time, and ambient OH reactivity from collocated measurements (total OH reactivity data measurement from the Stevens Group, Indiana University; in this method there is no assumption about the rate constants of different constituents)."

R1.4. In section 2.4, the possible reasons for underestimating SOA are discussed, all consequences of the short residence time and high oxidant concentration – (ambient) aerosol condensation, wall condensation, further reaction with OH, or reactor exit. The discussion that follows on the correction for these is unclear. Is all loss of SVOC by condensation onto aerosol, rather than formation of SOA, corrected? For example, at an exposure of 10^{12} (note units on x-axis of figure S6), approximately half of the SVOC is lost by condensation onto aerosol. Thus, dividing by this gives a correction of a factor 2×, much larger than the 1.2× reported. There is some confusion here that should be made clear.

We are confused by the reviewer's question "Is all loss of SVOC by condensation onto aerosol, rather than formation of SOA, corrected?", since condensation onto aerosol and SOA formation are the same thing.

The following text is added to P21918/L9 to clarify:

"The analyses leading to the correction terms were developed in Palm et al. (2016) and are applied here. As Palm et al. (2016) is now published in final form in ACP, we refer readers to that manuscript for the full details of the method."

The magnitude of the correction is different at different OH_{exp}. The factor of x1.2 applies at the point of maximum SOA production, while larger corrections apply at higher ages. We have modified this text to give typical values as:

"At OH_{exp} lower than 1×10^{12} molec cm^{-3} s (~ 10 days) the dominant LVOC fate (50-75%) is condensation to the aerosol (see Fig. S7). At higher OH_{exp}, the fate of organic gases is dominated (>45%) by loss to reaction with OH rather than condensing on aerosol. LVOC lost to the walls (~7%) or exiting the reactor (~2%) play only small roles under the conditions of this study, due to the relatively high ambient aerosol surface area."

R1.5. In Figure 3, the pie charts display average fractions – are these averages over the whole sampling period or just for the time shown in panel b? Why are the inorganic components enhanced in the reactor relative to ambient (nitrate in particular)? Does this suggest NOx chemistry in the reactor? Does this distribution change as a function of exposure in the reactor?

The pie charts are made from all data in panel (a), and this has been clarified in the figure caption. As stated in the figure caption the reactor data excludes dark reactor, "lights off" periods. I.e. periods are included only if OH_{exp} > ambient. We have added the following text for clarification on P21920/L1:

"The fact that the inorganic components are enhanced in the reactor is not surprising but expected. SO_2 and NO_x in ambient air are expected to be oxidized to H_2SO_4 and HNO_3 by the OH in the reactor, and can then condense onto the aerosols (together with ambient NH_3 for HNO_3). See e.g. Kang et al. (2007) and Li et al. (2015) for further details."

R1.6. The discussion of Ox species suggests the enhancement is brought about due to there being less Ox (as stated in reference to the "steep inverse relationship"). Ox results from photochemistry, and SOA result from photochemistry. It should be made clearer than Ox as discussed here is a proxy for ambient photochemistry, and that Ox itself is not playing a role in the reactor (unless I've misinterpreted the discussion, in which case I recommend clarifying it). Also, the plot in Figure 5 needs appropriate error bars.

The reviewer's interpretation is correct. We note that the ACPD text reads (P21922/L7) "oxidants are generated internally and are not dependent on ambient Ox." To clarify the discussion, the following text has been added to P21922/L14:

”**As ambient O_x is not itself playing a role in reactor aging, but rather is a proxy for ambient photochemistry, these results further confirm that as the degree of ambient photochemical processing of the sampled air increases (during daytime), […]**”.

We have also added the following text to the caption of Figure 5:

“**Note that ambient O_x is not itself playing a role in reactor aging, but rather is a proxy for ambient photochemistry.**”

Figure 5 has been updated with standard error bars for the quantiles and noted in the figure caption. The updated figure is shown below:

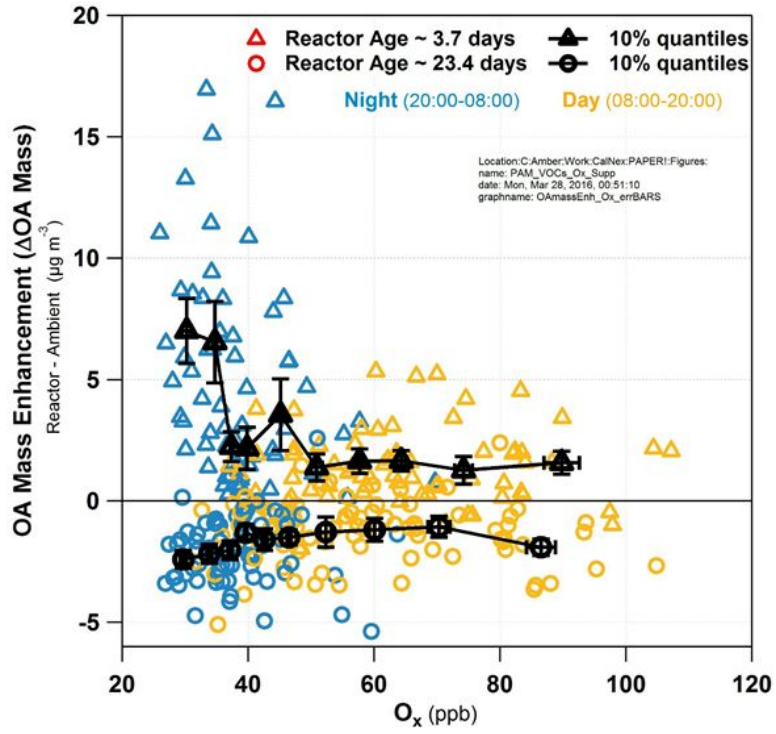

R1.7. Please clarify line 14, starting “At the same…” on page 21925.

We have modified the text to include an example for clarity (P21925/L14) as:

“At the same OH exposure, i.e. 8 days, higher OS_C is observed (~1) for conditions of high reactor SOA production (ER_{OA}~2) compared to no net SOA production (ER_{OA}~1, OS_C~0).”

R1.8. In Figure 9, the reactor data with wall loss correction and without are binned differently, and the uncorrected data spans a wider range on the x-axis. Why is this?

We note that, as stated in the legend and caption of the figure in the ACPD version,the figure is not “wall loss corrected”, but rather “vapor loss corrected” per the discussion in Section 2.4. We

have updated the figure legend and caption to say **"LVOC loss corrected"** to avoid confusion. The updated figure is reproduced below:

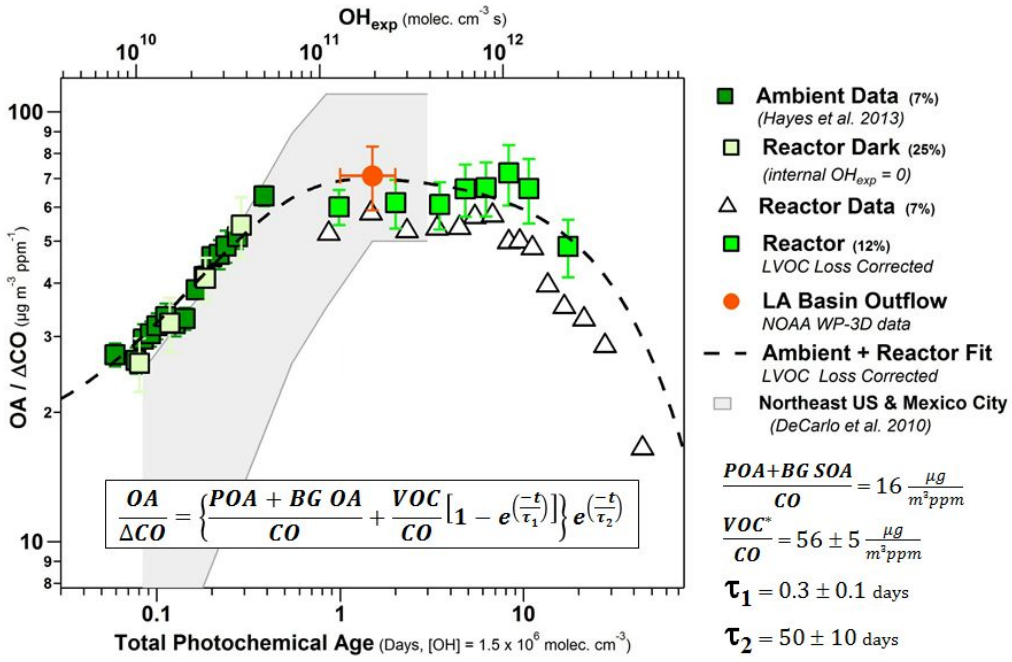

As discussed in Section 2.4 of the ACPD version, we state the LVOC loss correction cannot be applied when reactor OA is less than ambient OA. The range of LVOC loss-corrected data is thus smaller due to this fact. The number of bins was chosen to best illustrate trends of the data while not allowing too high an influence of noise, which is observed for high bin numbers. We have added the following text to the figure caption to avoid confusion:

"Note that the LVOC loss correction can only be applied when reactor output OA is larger than ambient OA, which reduces the number of datapoints."

R1.9. The errors bars used throughout do not appear to be representative of the variance in the data. Given that you are reporting on a single sample population, the standard deviation, rather than the standard error, is more appropriate.

The standard error is used when presenting quantile averages of data. For each quantile we calculate the average of the X and Y data in that bin. The quantity of most interest is how well those averages are known, i.e. the standard error. The full variability of the data can be seen from the full 2.5 min dataset in several figures (e.g. Fig. 4, 5, 12). Showing the standard deviation as another measure of the full variability of the data would be redundant, would clutter the figures, and would prevent showing the more relevant quantity. We have double-checked that the error bars are clearly explained as standard errors in all the relevant plots.

R1.10. On page 21930 line 20, a diameter of 285 nm is reported as the volume averaged value. From Figure S7, the average looks like it should be closer to 500nm. Please check this and

clarify any difference. Furthermore, for estimating the OH surface flux, the surface-weighted diameter should be used. How different are these values?

Perhaps the reviewer is confusing the two different diameters (d_{va} and d_{ve}), which are clearly discussed in the main text and in the caption and X-axis label of Figure S8. To avoid confusion, the manuscript text has been updated with a reference to the key paper describing their relationship, as:

"Heterogeneous oxidation calculations use surface-weighted diameter calculated from the peak of the mass distribution and estimated particle density from AMS components (DeCarlo et al., 2004) [...]."

With a typical material density of 1.45 g cm^{-3} estimated from the composition of this study, d_{va} ~ density * d_{ve} ~ 415 nm.

The value used in the calculation is an average of all size distribution observations, while only a subset of those is shown in (now) Figure S8 for clarity.

We have modified the calculation using the surface-weighted average diameter, with the results discussed in response to comment R3.9 below.

Anonymous Referee #2

R2.0. The authors present results from an experimental study in which the aging of ambient air is oxidized using a PAM reactor. This paper demonstrates of the PAM reactor as a tool evaluation of SOA formation during field studies. The study and the manuscript are well organized and documented and I recommend for publication. However, I have several comments (most minor and for my own curiosity) before this manuscript can be accepted for publication in Atmospheric Chemistry and Physics.

Questions:

Experimental Methods

R2.1. Page 21914: Line 10: The PAM reactor operates similar to a batch reactor giving you the spatial average of oxidized particles rather than with a traditional flow-tube you have particles with the same oxidative lifetime. Do you expect this to affect your results?

We are confused by this comment. The OFR (PAM reactor), at least as used in this study as described in the methods section, was used as a flow reactor with a short residence time. Thus its output corresponds to the processing of the air present at a given time at the field site, and not to a "spatial average." The relevant text of the methods section in the ACPD version is:

- (P21914/L15): "Ambient air was continuously sampled in an open flow-through configuration via a 14 cm diameter opening with coarse-grid mesh screen coated with an inert silicon coating (Sulfinert by SilcoTek, Bellefonte, PA)."
- (P21915/L6) "The total flow rate through the reactor was 4.4 L min^{-1} corresponding to a residence time of 3 min."
- (P21915/L19): "Oxidant concentrations in the reactor were stepped in 20 min intervals, through six levels (including lights off, i.e. no added oxidants) comprising a two-hour cycle (Fig. 2). Only data from the last five minutes of each 20 min period are used, to avoid including reactor transient periods."
- (P21916/L4): "OH_{exp} was estimated using a calibration equation developed by multivariate fitting of the output from a kinetic model of reactor (OFR185) operation, and verified against data from several field and laboratory experiments including CalNex (Li et al., 2015)"

Thus it is clear from the text already in the manuscript that the PAM is used here as a flow reactor and not a batch reactor. The use of a large inlet opening was also designed to narrow the residence time distribution, and this is a difference with how the reactor is run in laboratory studies.

See also the response to comment R1.1.

R2.2. Page 21914; Line 10: How long does it take the PAM reactor to reach equilibrium, in other words how long does the reactor need in order for complete replacement of particles? (I think this is 20 minutes if so please make it clearer in the text)

As stated in P21915/L6 of the ACPD version: "The total flow rate through the reactor was 4.4 L min^{-1} corresponding to a residence time of 3 min." and (P21915/L19): "Oxidant concentrations in the reactor were stepped in 20 min intervals [...]. Only data from the last five minutes of each 20 min period are used, to avoid including reactor transient periods."

We have added the following text at that point to further clarify this issue:

"Thus, five full residence times have elapsed after changes to the UV lights and before starting to sample reactor outputs, to allow full replacement of the contents of the reactor."

See also response to R2.1, as well as Figure 2 in the ACPD manuscript.

R2.3. Page 21914; Line 10: Since the output of your photolysis lamps are 254 nm do you expect any significant photo-degradgation from any of your organic species of interest? Do you expect any of these reactions to lead to SOA formation?

The possibility of photolysis of gases or aerosols under the light conditions of the flow reactor during our specific study has been reported by Peng et al. (2016), which was submitted to ACPD shortly after this paper and is now published in final form in ACP. We have added the following text to summarize their findings at P21915/L13:

"Peng et al. (2015) have investigated the possibility of photolysis of gases and aerosol species under the OFR conditions. OH reaction dominated the fate of all gases studied. Under most conditions in this study, photolysis was estimated to be responsible for only several percent of the fractional destruction of the gas-phase primary species most susceptible to it (aromatic species) even if photolysis quantum yield was assumed to be 1. The upper limit of the fractional destruction of possible oxidation intermediates was ~x2 that of primary species. Photolysis of SOA already present in the atmosphere may have played some role at the medium and high UV settings studied here when assuming upper limit quantum yields. However, photolysis e-fold decays in the reactor are estimated to be orders-of-magnitude lower than for the atmosphere for equivalent OH exposures."

R2.4. Page 21915; Line 11: Do you expect loss of your compounds to be from ozonolysis rather than OH given that O_3 is being used as the precursor for OH? Were any experiments performed using HOOH? Were blank experiments performed to make sure there was not loss from photochemistry?

The reviewer may be confusing our experimental method (in which O_3 is NOT added to the reactor) with the method used in other applications of the PAM reactor, in which O_3 is added to

the reactor as the OH precursor. This was discussed in the experimental section, although perhaps not clearly enough. We have clarified the text on P21915/L7 to read:

"The reactor was used to expose ambient air to high levels of OH and O_3, produced when UV light from two low-pressure mercury lamps (model no. 82-9304-03, BHK Inc., with discrete emission peaks at 254 and 185 nm) initiated O_2, H_2O and O_3 photochemistry. This mode of operation is referred to as OFR185, and OH is formed from both H_2O and O_3 photolysis (Li et al., 2015). In this mode, O_3 is formed in the reactor but is not added to the reactor, contrary to the OFR254 mode that has been used mainly in laboratory studies (Peng et al., 2015). Given that most known urban SOA precursors do not react with O_3 (e.g. Hayes et al., 2015), we expect OH to dominate the observed SOA formation. Consistent with this, no SOA was formed in test experiments during CalNex when ambient air was exposed to O_3 only without OH."

To avoid the possibility of contamination and the possibility of incomplete mixing, we prefer to not add anything other than ambient air and UV light to the reactor, whenever possible. We have not explored using HOOH as an OH precursor, but that is not necessary given that high OH concentrations can be produced from ambient H_2O photolysis and from the photolysis of O_3 formed in the reactor.

R2.5. Page 21916; Line 1: Is there a reason a gas-phase tracer (for example hexane) was not used to monitor your OH concentrations? This seems like it would be a more accurate method of quantification.

Using a gas-phase tracer is easy in a laboratory setting, but more difficult when adding to ambient air with a large inlet as used here. We have done so successfully on later field deployments, e.g. adding CO during the SOAS 2013 field study (Li et al., 2015), but during this initial field deployment of the reactor such a tracer delivery and detection system was not available.

It is actually preferable to use the decay of species already present in ambient air, which removes the need to mix a flow of the tracer species, thus diluting the ambient air and creating the possibility of contamination and additional leaks, as well as additional cost and complexity. During CalNex we used ambient SO_2 measured before and after the reactor to quantify OH_{exp}. This was only possible during periods of higher SO_2 concentrations (> 1 ppbv). The model-based OH_{exp} estimation equation was fit to the SO_2 decay data from CalNex as well as to data from other studies, and used to estimate OH_{exp} in our study. To clarify this detail we have revised the text on P21916/L4 to read:

"OH_{exp} was estimated using an equation developed by multivariate fitting of the output from a kinetic model of reactor (OFR185) operation, and verified against data from several field and laboratory experiments (Li et al., 2015). Data from the decay of ambient SO_2 in the OFR during CalNex, which was only reliable during periods with higher

ambient SO_2 concentrations (> 1 ppbv), was used to verify the OH_{exp} estimation equation."

R2.6. Page 21917; Line 15: Is there a reason why SVOC is not discussed in this manuscript? If there is could you please explain some of the issues of quantification of these species? (I assumed this will be a topic of an additional paper but this question is more out of curiosity)

Primary SVOC as precursors of the SOA observed to form in the OFR are discussed in the paper, see section 4.3 and Figure 10 (Fig. 11 in the revised version).

The formation of secondary SVOC in the reactor and their condensation to form SOA are not explicitly considered for several reasons. We have revised the text in P21917/L15 to clarify this point:

"Semivolatile organic compounds (SVOC) will also be formed, but we focus this discussion on LVOC for several reasons. As shown in Figure S12 (discussed in Section 4.4), the volatility distribution of the SOA present during CalNex shows very limited importance of SVOCs as SOA constituents. Second, discussion and modeling of LVOC fate in the reactor is conceptually simpler. Third, the amount of SOA formed in the reactor is significantly higher than can be explained by the speciated precursors, consistent with other studies (Palm et al., 2016). The assumption of LVOCs results in higher SOA formation than if SVOC were assumed, and is thus a the most conservative assumption in terms of closure of measured vs. predicted SOA. Thus adding complexity to the loss model for species that are likely of limited importance was not a priority for our study."

R2.7. Page 21918; Line 13: How much loss of LVOC did you measure on the walls or exiting the reactor? What is the percentage of wall loss?

In this study, LVOCs were not measured directly, as instruments such as CIMS were not available to us at the time. To clarify this detail, we have modified the manuscript (P21917/L26) to read:

"To account for vapor losses, we follow the modeling method detailed in Palm et al. (2016)..."

See also response to R1.5.

R2.8. Page 21918; Line 15: What are the rough percentages of LVOC fate of each pathway (condensation, wall loss, fragmentation) in each OH concentration regime (low, medium, high)?

See responses to R1.5 and R2.7.

Observations

R2.9. Page 21919; Line 5: It is explained later in the paper but it would help orient the reader if a brief discussion of the type of ambient precursors you might expect at your location?

We have added the following text to P21919/L9 to clarify this point:

"The precursors that are expected to be important contributors to SOA at this location include aromatic VOCs and semivolatile and intermediate volatility species (mostly alkanes and aromatics), with low importance for biogenic species (Hayes et al., 2015)."

R2.10. Page 21919; Line 25: What type of precursors for SOA do you expect to be depleted in the ambient air?

See response to R2.9, as well as sections 3.3.2 and 4.3 in the manuscript. We feel that repeating some additional details here would be confusing.

R2.11. Page 21920; Line 28: Could the loss of OA be due to the high OH concentrations that are forcing chemistry through channels that don't typically exist (ie, RO2 + RO2 chemistry)? How much of this OA loss do you expect to be through this pathway? (Reason I asked for rough percentages above).

We have investigated in detail some of the pathways that could lead to deviations between OFR chemistry and that relevant to the ambient atmosphere. The pathway that comes closest to playing a role in the OFR chemistry in this study, while still being of minor importance, is photolysis, as discussed in the response to R2.3 above.

Modeling results (unpublished) indicate that RO_2+RO_2 chemistry is typically unimportant in the reactor under the conditions of this study. HO_2 concentrations are also greatly enhanced in the reactor (Li et al., 2015) and the rate constants of its reactions with RO_2 are orders-of-magnitude higher than those of RO_2+RO_2. As a result, RO_2+HO_2 is faster than RO_2+RO_2 under most OFR conditions, and the main reaction channel of RO_2 is RO_2 + HO_2.

General Questions:

R2.12. Was NOx measured and if so was there any effect you would expect in SOA formation?

Ambient NO_x was measured, but it was not measured after the reactor. Previously published results (Li et al., 2015) indicate that NO_x is converted to HNO_3 very rapidly in the reactor. Thus it is not expected to play an important role in our results.

Figures:

R2.13. Page 21948: Please add part c to the figure which is a picture of the sampling site.

We have added the following picture of the sampling site as requested:

And added the following text to the caption of Figure 1:

"(c) Photograph of the sampling site showing the different trailers and inlets. The OFR can be seen on top of the leftmost trailer, next to the AMS and SMPS ambient inlets."

R2.14. Page 21949: What is the error in the concentration of O3 and OH in the reactor?

We have added the following text to P21914/L24:

"The uncertainty in the O_3 measurement is +/- 1.5 ppb or 2% of the measurement, whichever is greater."

We have added the following text to P21916/L12:

"The uncertainty in the calculated OH_{exp} is estimated to be a factor of 3 (Li et al., 2015; Peng et al., 2015)."

R2.15. Page 21950: The differences in the reactor and ambient colors are really difficult to see. Is there a way that you could make this clearer?

We agree that this is a difficult figure, which is why the zoomed version in Figure 3b is essential. We have tried this figure with dashed lines for the reactor output as well as other alternatives, but they only complicated the visual appearance of this figure. As the five AMS species observed are the same for ambient and the reactor, and those colors are standardized within

the AMS community (and much of the larger community), showing the reactor in a lighter shade was the most intuitive option.

R2.16. Page 21951: Please explain where the error bars come from and whether they are 1s or 2s? Please put in the caption.

The figure caption already states “... with vertical error bars indicating standard errors.” Standard errors are a standard statistical metric, and are understood to be 1σ. Thus we feel that this is already clear enough. See also response to R1.9.

Anonymous Referee #3

R3.0. Ortega et al. report measurements of secondary organic aerosol generated by OH oxidation of ambient urban emissions in a PAM oxidation flow reactor during the CalNEX campaign. An aerosol mass spectrometer was used along with a scanning mobility particle sizer to obtain mass spectra, elemental ratios, and aerosol size distributions of the SOA. Selected VOCs were detected with a proton-transfer reaction mass spectrometer. The authors characterize organic aerosol enhancement factors as a function of OH exposure in the PAM reactor. The following results are obtained:

1. SOA formation peaks at an intermediate photochemical age in the reactor (~1-6 days' equivalent atmospheric OH exposure) prior to decreasing. This result is interpreted as a transition from functionalization- to fragmentation-dominated reactions.

2. SOA formation is largest during the nighttime. The authors interpret this result to suggest that the most SOA precursors have an atmospheric oxidation lifetime that is shorter than the source->receptor transit time (0.3 day) during the day, but not at night.

3. Campaign-average SOA oxidation state and Δ(SOA)/Δ(CO) emission factors are generally consistent with previous studies, although the magnitude and trend of observed Δ(SOA)/Δ(CO) emission factors is difficult to reproduce with conventional chemistry and transport models.

Overall, this manuscript addresses an important research topic regarding the characterization of ambient SOA formation and chemical evolution with oxidative aging. It demonstrates the unique capability of oxidation flow reactors to simulate in situ photochemical aging of air masses and complements previous studies through its application in an urban receptor location. I would support publication in Atmospheric Chemistry and Physics after incorporation of my comments below.

Main Comments

R3.1. P21914, L19-21: Please add data to the Supplement to support the claim that removal of the inlet plate reduces losses.

This text reads: "This configuration, with no inlet, was chosen because of the observation of reduced SOA formation when any inlet and/or an inlet plate was used in a previous experiment (Ortega et al., 2013)." The comparison of plate-on / plate-off SOA production was much easier to perform during the FLAME-3 study described in Ortega et al. (2013), as much higher concentrations of SOA precursors were maintained for several hours within a 3000 m^3 chamber. Thus the variations in SOA production were obvious and could be reproduced multiple times in a short period of time. In an ambient air study such as CalNex, SOA production is smaller, especially during the day when operators are typically present at the site, and the result of such short experiments is very noisy. Thus we have no direct evidence that this was true to CalNex,

but we did not state otherwise in the manuscript. We only stated that a decision was made to run without the plate because of the observations during FLAME-3.

R3.2. P21915, L1-4: Please add data (such as residence time distributions of tracer species) to the Supplement to support the claim that this flow configuration maintains plug flow characteristics.

See response to R1.1.

R3.3. P21915, L29: More information/clarification about the particle loss correction is needed. Specifically, it's not clear to me how the UV dependence to particle losses was determined if particle losses are measured with the lamps off. Also, shouldn't there be a size dependence to the magnitude of the particle losses?

The text "and accounting for variations in UV intensity" was erroneous and has been removed. We are not aware of any results or evidence that suggest that particle losses depend on UV light intensity.

See response to R1.2 for further details on the particle loss correction, including the size dependence.

R3.4. P21918, L3-4: "It is assumed that products after five oxidation steps with OH at kOH…." I found this sentence confusing. Couldn't you equivalently just state the OH exposure at which you assume that OH oxidation products no longer condense? For example, doesn't 5 oxidation lifetimes at kOH = $1*10^{-11}$ cm-3 molec sec correspond to an OH exposure of $5*10^{11}$ molec cm-3 sec? If so, the first sentence in the next paragraph states: "At OHexp lower than $1*10^{12}$ molec cm-3 sec … the dominant LVOC fate is condensation to the aerosol". While self-consistent, these two statements suggest a different OH exposure at which the transition to fragmentation-dominated reactions occurs (unless I am misinterpreting the method that is being applied). Please clarify.

5 oxidation lifetimes does approximately correspond to an OH_{exp} ~ 5 x 10^{11} molec. cm^{-3} s. However, because of the concatenation of exponential processes, at that OH_{exp} only ~56% of the initial molecules have undergone the 5 generations of oxidation. After OH_{exp} = 10^{12} molec. cm^{-3} s, 97% of the initial molecules have undergone all 5 generations of oxidation. This explains the factor of 2 difference that the reviewer brings up. To clarify this point we have modified the text on P21918/L3 to read:

"It is assumed that products after five consecutive oxidation steps with OH at k_{OH} = 1×10^{-11} molec cm^{-3} s^{-1} are lost (fragmented and too volatile to condense). We note that 56% (97%) of the initial molecules will have undergone five oxidation steps after an OH_{exp}= $5x10^{11}$ ($1x10^{12}$) molec. cm^{-3} s."

R3.5. P21918, L10-24: After reading this section, I found it difficult to come away with definitive conclusions about the relative importance of LVOC loss pathways as a function of OH

exposure. Figure S6 demonstrates the corrections that are used, but the information in this figure does not come across clearly in the text. I suggest moving this figure out of the supplement and into the main paper because it seems to be important for interpretation of results. Some suggested text to incorporate is provided below (paraphrase and update highlighted quantities as appropriate), which I think would make it clearer:

"The modeled fractional loss of LVOCs to condensation on pre-existing aerosols decreases from a maximum of 0.75 at OHexp = $1*10^{11}$ molec cm-3 sec to a minimum of 0.15 at OHexp = $1*10^{13}$ molec cm-3 sec. Over the OHexp range, the modeled fractional loss of LVOCs to gas-phase fragmentation reactions with OH increases from a minimum of 0.15 to a maximum of 0.83, and the fractional loss of LVOCs to the reactor walls and sampling line walls decreases from 0.10 to 0.02."

See the updated text in response to R2.7, which quotes the fraction of LVOCs undergoing the different fates, as also requested by reviewer #2.

We have considered moving Figure S6 from the supplementary information to the main paper as suggested. However, the primary paper describing those corrections was published recently in ACP (Palm et al., 2016), and thus we think it is more appropriate to refer readers to that publication for more detail, while documenting the application of the method to our study is suitable for the Supp. Info.

R3.6. P21919, L22-L24: I would be careful to avoid over-interpretation of a single event in claiming that the OFR can be used as a predictive tool. Figure 3b indicates that maximum nighttime OA concentrations ranging from 15 – 30 μg m-3 are observed at 6 separate intervals over 12 hours. Figure 2 shows a ~1.5 hr measurement cycle, suggesting that six OFR sampling cycles are conducted over this period. However, the corresponding OHexp at which these [OA] = 15 – 30 μg m-3 periods are attained is not discussed. If OHexp in the reactor is the same as the ambient OHexp during the following day (5-Jun-2010, peak OA ~ 25 μg m-3), over multiple days of the campaign (instead of just one day), then it might be appropriate to highlight "the reactor's potential for estimating the next day's OA concentrations." Otherwise, it is an interesting observation but (in my opinion) inconclusive. For example, Figure 2 suggests that maximum reactor OA concentration during a nighttime cycle on 2-Jun-2010 are observed at OHexp ~ $2*10^{12}$ molec cm-3 sec (15 days of equivalent atmospheric oxidation), which is presumably much higher than the ambient OHexp later that day.

Individual data points can be affected by noise and experimental uncertainties in both the X (OH_{exp}) and Y (SOA produced) variables. However, the results shown later in the paper in Figure 9 show that this statement is approximately true on the average. Note in Figure 9 that the amount of SOA produced after ~15 days OH_{exp} and under the highest ambient OH_{exp} is still similar. The wording at this point in the paper is more tentative ("suggesting"), since the latter evidence has not been shown. We have revised that text to read:

"The nighttime reactor-aged OA mass peaks at approximately the same concentration as the following day's ambient OA concentration, suggesting the reactor's potential for

estimating the next day's OA concentrations. A more quantitative evaluation of this potential is discussed below (Sect. 4.1. and Figure 9)."

R3.7. P21920, Section 3.2: The mean inorganic aerosol concentration is greater than the mean organic aerosol concentration (11 µg m-3 INORG versus 8.4 µg m-3 ORG in reactor, 8.2 µg m-3 INORG versus 6.8 µg m-3 ORG in ambient). However, aside from a brief mention in the Supplement relating to discussion AMS collection efficiency, the magnitude and OH exposure-dependent inorganic aerosol enhancements in the reactor are never discussed despite being comparable to the organic aerosol enhancements. This is especially evident from the nitrate time series in Figures 3a and 3b. There is likely valuable information here that complements the discussion of OA enhancements: Nitrate, sulfate, ammonium and chloride enhancements as a function of photochemical age. Are the trends the same or different as OA trends, and what does this reveal about their sources? Are nitrate and sulfate neutralized by ammonium in the reactor and in ambient? At the moment this information is buried in L21-L29 of the Supplement.

It is true that there are additional promising observations from this field deployment that are not reported in this manuscript. SOA formation was the topic of highest interest and resulted in a large paper already (12 figures in the main paper and another 12 in the Supp. Info, for a total of 35 figure panels). The formation of inorganic species in the OFR, together with other observations that we did not include in this manuscript either such as the variation of new particle formation with time, should be the focus of future publications. We have added the following text to the Supp. Info. (P1/L13) to briefly document these details:

"Although the focus of this paper is OA formation and aging, a brief summary of the observed evolution of the inorganic species: (a) Sulfate formation proceeds as expected from the OH + SO_2 reaction. A quantitative analysis of sulfate formation is shown in Palm et al. (2016), which reports results from a similar experiment from our group, but in a forest environment. That analysis provides evidence that the corrections for losses of low volatility species developed in that work are appropriate. (b) Nitrate formation is more complex since OH + NO_2 is a fast reaction, but HNO_3 is semivolatile and the formation of NH_4NO_3 also depends on the availability of NH_3(g). (c) The aerosols in the output of the flow reactor during CalNex are neutralized, similarly to the ambient aerosols (Hayes et al., 2013).

As an aside, as noted in Comment #13 below, the mean "total mass" listed in Figure 3c (22.4 µg m-3 in reactor, 14.9 µg m-3 in ambient) is not equal to the sum of the organic, nitrate, sulfate, ammonium and chloride components (19.4 µg m-3 in reactor, 15.0 µg m-3 in ambient). If this is a typo it should be fixed, if it is a real difference it should be explained.

This was a typo on the total mass, which has been corrected in the revised version.

R3.8. P21930, L12-L15. It is not clear how you distinguish gas-phase fragmentation of condensable species from heterogenous oxidation of SOA here because to first order, the timescales for gas-phase fragmentation of condensable species and heterogeneous oxidation of

SOA appear to be similar. Because this comparison is speculative and doesn't seem to add much to the discussion anyway, I would consider removing it.

We have revised this text to clarify the point that we were trying to make:

"Note that the George and Abbatt (2010) vs. Lambe et al. (2012) studies are qualitatively different, and thus the explanations of the decrease in OA at high ages may be different. George and Abbatt (2010) started their oxidation experiment with particles only, after removing gases with a denuder. Any decreases in OA in their study must result from heterogeneous oxidation. The Lambe et al. (2012) study started with gas-phase precursors only and no particles. Thus the reduction in SOA at high OH_{exp} may be due to either gas-phase fragmentation of condensable species, so that SOA is never formed, or to formation of SOA followed by its heterogeneous oxidation and revolatilization. Results in Fig. S7 suggest that gas-phase oxidation would prevent the formation of SOA, and thus the second explanation is more likely."

R3.9. P21930, L16-L29: To complement this discussion, I suggest adding a scatter plot of "measured oxygen added" versus "predicted oxygen added" to the main paper, and rephrasing the discussion accordingly. I am unable to draw this conclusion from Figure S10; I think this alternative figure would make the point a little clearer. Figure S10 could then be removed.

We have made a new figure illustrating this point that should be clearer. We have also updated this calculation to use the surface-averaged diameter, as detailed in response to comment R1.10. The new figure S10 is reproduced below, and the ACPD Figure S10 has been removed as suggested (now Fig. S11 in revised manuscript). The text in P21930/L16-29 has been revised to read:

"To evaluate directly whether heterogeneous oxidation could explain the gain of oxygen observed in the aerosol, we follow the method outlined in appendix A of DeCarlo et al. (2008). Figure S11 shows the ratio of the gain of oxygen of OA observed in the reactor (ΔOxygen in OA = $O_{atoms,\ reactor} - O_{atoms,\ ambient}$) to the total number of OH collisions with OA in the reactor, plotted vs. total photochemical age. Heterogeneous oxidation calculations use surface-weighted diameter calculated from the peak of the mass distribution and estimated particle density from AMS components (DeCarlo et al., 2004), assume every collision results in reaction ($\gamma = 1$). If it is assumed that each OH collision with OA results in one O atom addition, the number of O atoms added is underpredicted by a factor of 5 at ages ~ 1 day, decreasing to a factor of 2 at ~ 10 days, and lower values at high ages (> 10 days). This analysis supports that heterogeneous oxidation is not dominant in contributing to SOA mass at low-to-intermediate ages, but it likely plays a role in OA evolution at the highest photochemical ages in the reactor."

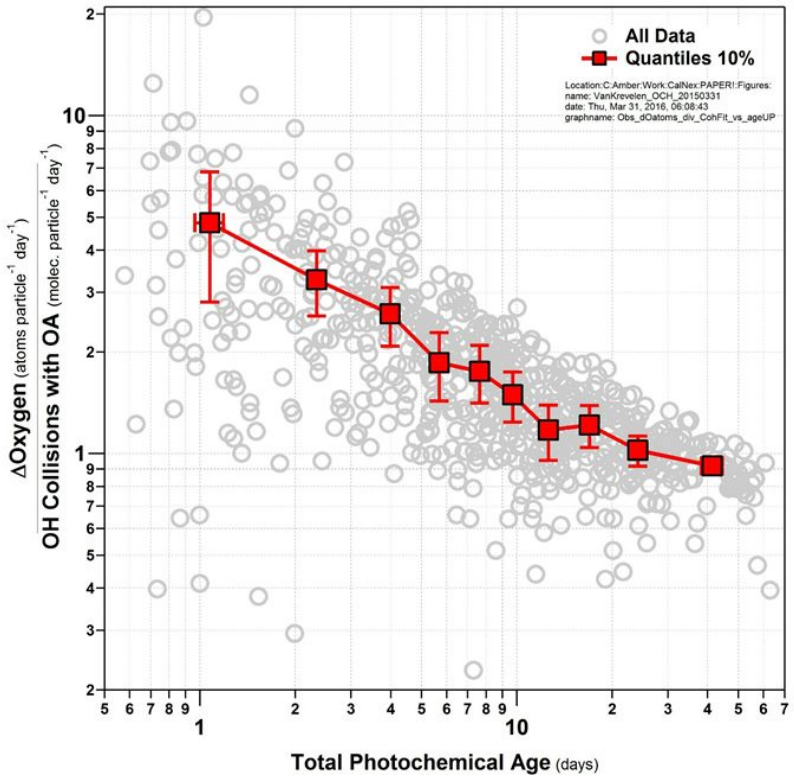

R3.10. P21932, L8-L29 and P21934-P21935, L28-2: In making the comparison with Tkacik et al. (2014), I would consider the following points in the discussion. High NO levels (>400 ppb) in Tkacik et al. might minimize the relative rate of RO2 + HO2 reactions in their reactor that would otherwise lead to multifunctional, condensable species (and possibly higher ΔOA/ΔCO). High NO and NH3 levels in Tkacik et al. result in nitrate and ammonium enhancements ~3x higher than the organic aerosol enhancements. Thus, while vehicle emissions presumably dominate SOA formation in both studies, the ensuing RO2 oxidation chemistry could be very different. Given that inlet losses of semivolatiles is pretty much discounted in this discussion, I would remove (or significantly shorten) that discussion and instead focus on the different photochemical conditions and how they might result in different secondary aerosol composition despite similar precursor makeup.The sum Δ(OA + Nitrate + Sulfate + Ammonium)/Δ(CO) would also be worth calculating and comparing between the two studies.

We have added the following text to the manuscript (P21932/L26) to clarify these issues:

"(3) It may appear at first that the tunnel SOA may have been dominated by RO_2+NO, compared to RO_2+HO_2 for our ambient air results, thus making the results less comparable. However, while the initial NO levels in the tunnel may be high, the lifetime of NO under the conditions of the OFR is typically very low (Li et al., 2015). O_3 levels in OFR185 are typically 1-25 ppm, which result in NO lifetimes of 0.1-2 s. Since HO_2 levels are greatly enhanced by the reactor chemistry, the majority of the RO_2 radicals are still

expected to react via RO_2 + HO_2 under the tunnel conditions, similar to our study. The model of Peng et al. (2015) was used to estimate the fraction of RO_2 reacting with NO vs. HO_2 for the tunnel study. At the point of peak SOA production we estimate that 81% of the RO_2 radicals are reacting with HO_2 and 19% with NO. Therefore the chemistry of the OFR in the tunnel study is proceeding mostly through the HO_2 channel, similar to our ambient study."

We have also added the following text to address a related point:

"(4) A difference between the studies that may explain somewhat higher SOA formation in the tunnel study is the larger partitioning of semivolatile species, given the higher OA concentrations (~50 μg m^{-3} in the tunnel vs ~15 μg m^{-3} for our study). However, this effect is estimated to be a factor of ~1.5 for the aromatic and alkane precursors that are thought to dominate SOA formation from vehicle emissions (Barsanti et al., 2013), and it reduces the difference observed here, thus further supporting our conclusions."

While the enhancements of the inorganic species are of some interest, those of sulfate are straightforward to explain (see response to R3.7), and those of nitrate depend on complex ways on NH_3(g) present which may be quite different in the two studies. Thus a comparison would be a complex subject that exceeds the scope of this paper.

In addition, during the revision process of Peng et al. (2015) we realized that there was an error on the inputs used for the simulation of OH_{exp} for the tunnel study of Tkacik et al. (2014), as discussed in Peng et al (AMTD, 8, C3671 ; see response to comment SC.2 in http://www.atmos-meas-tech-discuss.net/8/C3671/2015/amtd-8-C3671-2015-supplement.pdf). Figure 12 has been updated to add the results using the correct inputs, which result in improved agreement between the ambient and tunnel observations. We have corrected the text on P21932/L28 to read:

"Thus it is most likely that the observed difference between the tunnel and our study is due to overestimation of OH_{exp} at lower ages in the tunnel study. We have used the model of Peng et al. (2015) to estimate the corrected OH_{exp} under the tunnel conditions. The corrected curve is also shown in Fig. 12b, and shows much improved agreement with our urban air observations."

The updated Figure 12b is shown below:

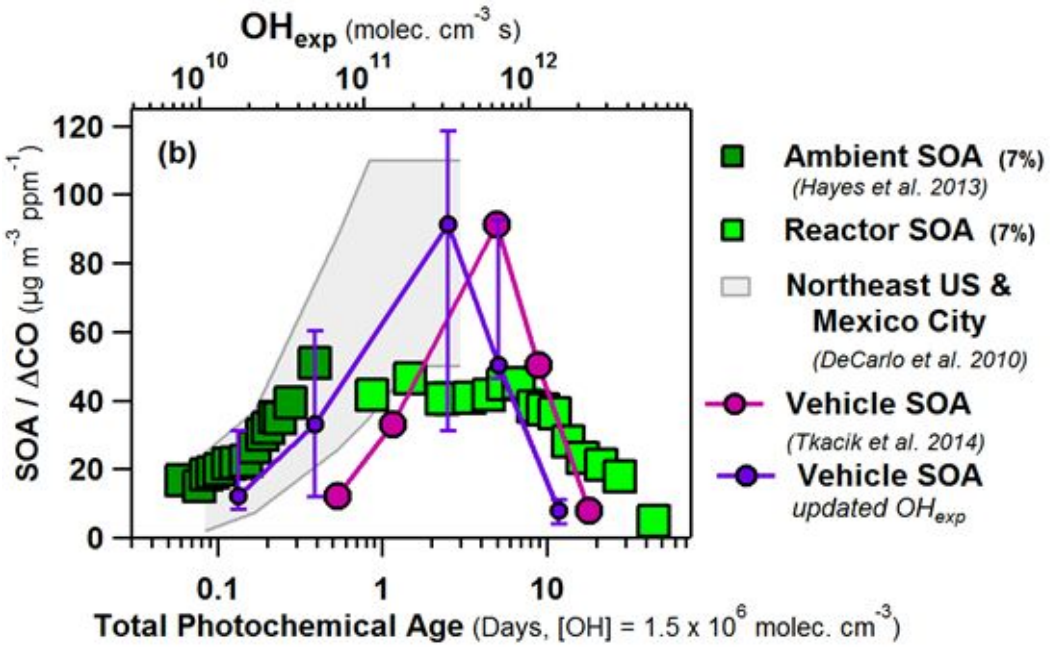

Figure Comments

R3.11. Figure 1: This figure could be moved to the supplement.

We prefer to keep the figure in the main paper, since this was the first time that anyone demonstrated this type of reactor operation or our knowledge, and thus a visual reference for the experiment may help reduce confusion about our setup and results.

R3.12. Figure 2:

- Given the range of [O3] (up to ~16 ppm), I suggest plotting in parts per million instead of parts per billion.

We have made this change as suggested. The updated figure is shown below:

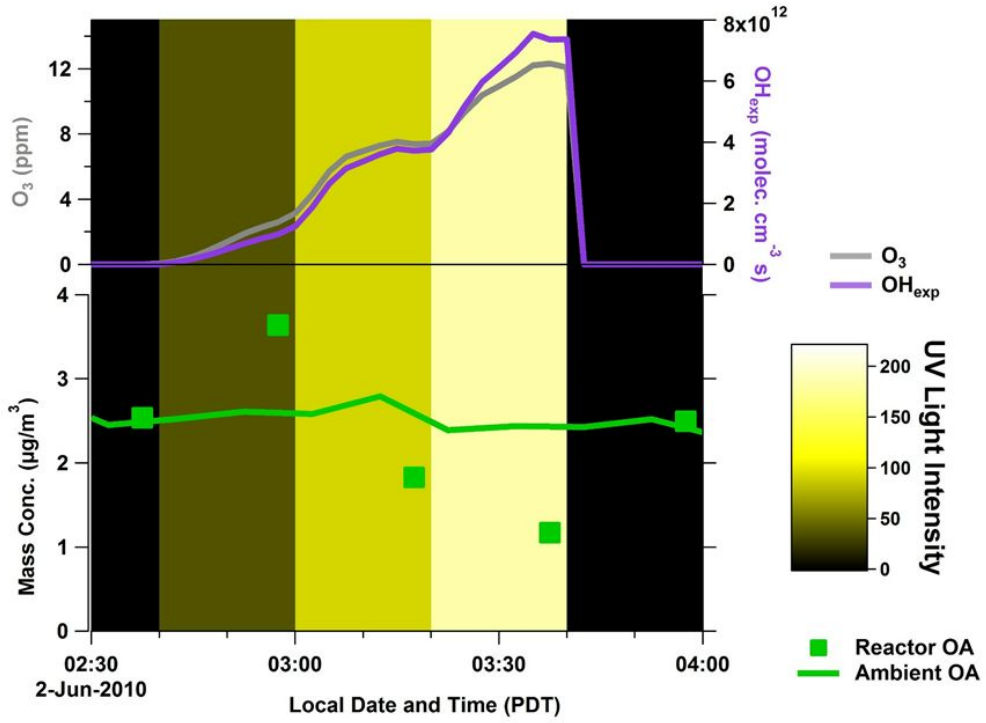

- I think it would be useful to have the colorbar scaled by the lamp voltages so that readers better the specific conditions that were used, especially if they want to reproduce the sampling protocols that were used here in their own work.

The UV light intensity colorscale was actually already the sum of the voltages applied to both lamps. We have added the following text to the figure caption to clarify this point:

"The UV light intensity color scale corresponds to the sum of the AC voltages applied to the two lamps in the reactor. Only at the highest lamp setting are both lamps on, while at lower settings only one of the lamps is used."

- In the caption, "oxidant cycle" is vague - something like "A typical OFR sampling cycle" would better describe the figure.

Figure caption text was changed to:

"A typical OFR sampling cycle, including four steps in lamp intensity in the reactor."

R3.13. Figure 3c: The "total mass" is not equal to the sum of the non-refractory components listed here (OA + Nitrate + Sulfate + Ammonium + Chloride): 22.4 µg m-3 stated versus 19.4 µg m-3 calculated (PAM reactor) 14.9 µg m-3 stated versus 15.0 µg m-3 calculated (ambient). This discrepancy should be explained or sorted out as appropriate. Also, is there a reason why the reactor" and ambient pie charts are different sizes?

The comment for the total mass is the same as R3.7, and it has been addressed in that response.

The following text has been added to the figure caption to explain the second point:

"The pie chart areas are proportional to the total mass concentrations."

R3.14. Figure 4: Analogous figures should be made for nitrate, sulfate and ammonium.

See response to R3.7.

R3.15. Figure 5: This figure could be removed or moved to the Supplement (see Comment #40)

See response to R1.6.

R3.16. Figure 6: It would make sense to show toluene here as well (rather than in Figure S8).

The VOCs highlighted in this figure were selected to serve as proxies for relative classes of reactivity. Thus, toluene has been left in supplemental as adding it would further complicate visually an already complex figure.

R3.17. Figure 7: I assume that symbols representing the PMF factors are the same in Figures 7a and 7b, but this should be made clear. The "ambient" and "reactor" symbols are also the same, but whereas they appear in two legends, the PMF factor symbols do not.

PMF factor symbols have been made larger and the legend now appears in both Fig. 7a and 7b.

R3.18. Figure 9:

- I suggest adding vertical lines at photochemical ages corresponding to one e-fold decay of 1,3,5-trimethylbenzene, toluene, and benzene, to illustrate the relevant range of kOH for important SOA precursors. This would convey the added information in Figure S9a in the main paper (and perhaps make that figure unnecessary in supplemental) more directly than the decay curves that are shown in Figure S9a.

This is an important figure for our conclusions and it is already pretty complex, and adding more lines would make its explanation more difficult. The issue of the VOC ages is already addressed also in Fig. 6, plus Fig. S9. Thus we prefer to keep Fig. 9 as is.

- Define "BG" as "background" and "POA" as "primary organic aerosol" in the figure caption.

The figure caption text has been adjusted as requested.

R3.19. Figure 10:

- The Hayes et al. 2014 ACPD citation shown in legend and caption is not in the listed references. Should this instead be Hayes et al. 2015?

Correct. The figure legend has been updated.

- In the figure caption, the text “This difference is due…photochemical ages less than 1.2 h” would probably be better in the main text.

We believe that this is a small detail, as it concerns a difference of 5 units in a graph with a scale up to 220. Thus we prefer to keep this text in the caption to facilitate the readability of the main text.

- Is there a reason why Figures 10a and 10b are different sizes?

Figure 10b was only meant as an inset. However we realize that the size difference may be distracting, and thus we have made both figures of the same size in the revised version (now Fig. 11).

R3.20. Figure S6: Move to main paper

See response to R3.5.

R3.21. In addition to (or instead of) Figure S10, Add a scatter plot of “measured oxygen added” versus “predicted oxygen added” to the main paper.

See response to R3.9.

Minor/technical comments

R3.22. P21909, L6: Define the “CalNEX” acronym (it is not definied until the last paragraph in the Introduction).

The Abstract text has been adjusted to, “An Oxidation Flow Reactor (OFR) was deployed to study SOA formation in real-time during the **California Research at the Nexus of Air Quality and Climate Change (CalNex)** campaign in Pasadena, CA, in 2010.”

R3.23. P21909, L7: Might it be useful to spell out “California” and indicate it’s in the United States?

Now, spelled out in the CalNex acronym definition.

We believe the fact that California is in the United States is already known for anyone who could be interested in our paper.

R3.24. P21909, L11-13: “OH radical concentration was continuously stepped […] 0.8 days – 6.4 weeks”. This sentence seems superfluous with the preceding sentence.

We have consolidated the text in L9-13 to read:

"The reactor produced OH concentrations up to 4 orders of magnitude higher than in ambient air. OH radical concentration was continuously stepped, achieving equivalent atmospheric aging of 0.8 days–6.4 weeks in 3 min of processing every 2 hrs."

R3.25. P21909, L19: Define LA-Basin

We have replaced "LA-Basin" with **"greater Los Angeles area."**

R3.26. P21909, L25-28: "The mass added […] fragmentation/evaporation." I'm not certain if the abstract is the best place for this text.

We believe that this is an important scientific contribution of our work, and thus that it should remain in the abstract.

R3.27. P21911, L12: Quantify "long" aging timescales.

Text has been modified to read, "SOA at long aging times **(>1 day).**"

R3.28. P21911, L19-21: "In order […] changing air masses." This sentence is unclear.

The sentence has been modified to read:

"In order to characterize the SOA formation potential of urban emissions, a rapid field deployable experimental method is needed, so that rapid changes of ambient SOA formation potential can be captured."

R3.29. P21913, L12-14: "By combining results from the ambient aerosol and aged ambient aerosol measurements, we provide a stronger test of current SOA models." Instead of 'stronger', I suggest "more rigorous." Also, explain why the combination of ambient and PAM-oxidized ambient measurements is a better test of SOA models.

The text "stronger**"** has been changed to **"more rigorous"** as suggested.

The last sentence of the paragraph has been updated to read:

"By combining results from the ambient aerosol and aged ambient aerosol measurements, we provide a more rigorous test of current SOA models, since they can now be compared with data from a much wider range of photochemical ages."

R3.30. P21915, L23: Add "and" between "reactor" and "resultant"

The text has been modified as requested.

R3.31. P21916, L8: Isn't residence time the governing parameter here (rather than flow rate)?

Correct. The text has been modified accordingly.

R3.32. P21916, L18-19: “OH concentrations averaged up to $4*10^6$ cm-3 during the daytime.” This sentence is confusing - was the mean daytime OH concentration $4*10^6$ cm-3 ? If so, delete “up to”.

This text has been modified, replacing “up to” with “**as high as.**”

R3.33. P21916, L19-22: “Since a significant part of SOA formation … peak OH observed during CalNex.” This sentence is unclear; please clarify or rephrase. Also, “peak OH” should be “peak [OH]” or “peak OH concentration”.

The text has been modified to read:

“Since a significant part of SOA formation happens during the first few hours after emission, the 0.8 day minimum photochemical age probed with the reactor would correspond to ~0.3 days of transport age at the peak OH concentration observed during CalNex.”

R3.34. P21918, L24: This is the first instance of “EROA” in the manuscript, so it needs to be defined here.

This text has been modified to read:

“Thus, correction is applied when reactor-measured OA is greater than ambient OA (relative OA enhancement ratio, ER_{OA} = reactor OA / ambient OA, $ER_{OA}>1$; and the absolute OA enhancement factor, ΔOA Mass = reactor OA – ambient OA, ΔOA Mass>0, Sect. 3.2).”

Text in Section 3.2 has been adjusted to remove the definition.

R3.35. P21919, L17: Typo (“attributes”->”attribute”)

Text has been modified as requested.

R3.36. P21919, L25: Replace “indicating” with “suggesting”

Text has been modified as requested.

R3.37. P21919-21920, L26-1: “At the peak of…removal by photochemical oxidation and condensation”. Delete, this is repetitive with the previous sentence.

Text has been modified as requested.

R3.38. P21921, L4-6: The last sentence of this paragraph is confusing.

Text has been modified to read:

"A smaller enhancement is observed during the day ~2 μg m^{-3}, or a factor of 1.2x of ambient, while at > 2 weeks of aging, day and night observations closely overlap, with a decrease up to ~2.5 μg m^{-3}, or a factor of 0.5x of ambient."

R3.39. P21921, L14: Please provide a reference for the stated 0.5 day transit time from downtown Los Angeles to Pasadena.

Reference has been added to Washenfelder et al. (2011).

R3.40. P21922, Section 3.3.1 and Figure 5: In my opinion this section is somewhat self evident because the oxidant exposures attainable in the reactor are much higher than the ambient photochemical age. I don't think it adds much to the paper and would delete or move to the Supplement.

See response to R1.6.

R3.41. P21922, L19-20: I suggest a slight modification to the title of Section 3.3.2: "Further constraints on urban SOA formation timescales from OH reactivity of measured VOCs."

Text has been modified as requested.

R3.42. P21923, L6: Typo ("moelcule"->"molecule")

Text has been modified as requested.

R3.43. P21923, L14: Typo ("theses"->"these")

Text has been modified as requested.

R3.44. P21923, L24-25: Somewhere in the paper S/IVOCs should be briefly defined. This sentence could be explained slightly to point out why these species are not often measured.

The definition of S/IVOCs is given here, and the following text has been added to the end of the sentence:

"due to the difficulty in measuring these compounds."

R3.45. P21924, L6: f43, f44, H:C and O:C are never defined.

The text on p. 21917, line 3 was modified to define O:C and H:C:

"The elemental analysis of OA (resulting in oxygen-to-carbon ratio, O:C, and hydrogen-to-carbon ratio, H:C)."

The text was also modified to define f_{43} and f_{44} as:

"f_{44} is a tracer for aged OA (fractional organic contribution at *m/z* 44, mostly CO_2^+), while f_{43} (fractional organic contribution at *m/z* 43, mostly $C_2H_3O^+$), due to non-acid oxygenates,

with some contribution from $C_3H_7^+$) is a tracer of POA and freshly formed SOA (Ng et al., 2011a).”

R3.46. P21924, L10: Rather than “move up and to the left”, I suggest “f44 increases and f43 decreases.”

Text has been modified as requested.

R3.47. P21924, L13: Typo (“lay”->”lie”)

Text has been modified as requested.

R3.48. P21924, L17-L18: “The Van Krevelen diagram … demonstrates results that are very consistent to those of the previous plot”. The connection between f44 – O/C and f43 – H/C has been documented in previous papers (e.g. the Ng et al. 2011b ref, among others), but is never made in this paper. Readers might not make this connection themselves. I suggest doing so here if you want to relate Figures 7a and 7b.

We respectfully disagree. Both diagrams have been used in many publications, and we believe that our discussion and referencing (e.g. the Ng et al. citation) are sufficient to explain these figures.

R3.49. P21925, L12-13: “While ambient OSc is within the range of …urban/anthropogenic OA”. Please provide reference(s).

Reference is provided at the end of the sentence to Kroll et al. (2011).

R3.50. P21925, L21: I suggest a modification to the title of Section 4.1: “Evolution of OA/ΔCO with photochemical age”

We have changed the title to read:

“Evolution of urban OA with photochemical age”

R3.51. P21926, L8-L19 and PL22-23: “Ambient photochemical age … Fig. S9a for reference” and “Reactor data are shown… vapor loss-correction applied (see Sect. 2.3)”. Can this text be deleted or shortened significantly? Most of it is already in the Figure 9 caption or self-evident from viewing the figure, and it breaks up the flow of discussion of data in Figure 9.

We have moved the following text to the figure caption, deleting duplicated text when necessary:

- L8-11 , “Ambient photochemical age [...] and reactor age.”
- L16-19: “Figure 9 [...] for reference.”
- L22-23: “Reactor data [...] applied.”

R3.52. P21926, L27: “To further illustrate the lifetimes of important urban SOA precursors”. This sentence confuses the point. Benzene, toluene, and 1,3,5-trimethylbenzene are not important urban SOA precursors. Rather, their OH oxidation lifetimes – in conjunction with timescale over which OA/ΔCO increases -- constrain the range of OH reactivity (kOH) of important urban SOA precursors: 5*10-12 < kOH < 5*10-11 cm-3 molec sec. This should be clarified here and elsewhere in the discussion.

While those specific species are not unimportant (e.g. see Hayes et al., 2015), this text was trying to make the same point that the reviewer is indicating. We gather that was not clear, and we have reworded this text as:

“To constrain the lifetimes of the important urban SOA precursors, the OH decays of three example gas-phase species (benzene, toluene, and 1,3,5-trimenthylbenzene (TMB)) are shown are overlaid in Fig. S10, together with data from Fig. 9 that illustrates the timescale over which OA/ΔCO increases. The correlation of different VOCs with maximum SOA formation in the reactor is shown vs. their reaction rate constants with OH (k_{OH}) in Figure 10. This analysis constrains the rate constants of the most important urban SOA precursors to the approximate k^{OH} ~ 3-5x10^{-11} cm^3 $molec.^{-1}$ s^{-1}. This constraint suggests that polyalkyl monoaromatics (such as TMB), substituted polyaromatics such as alkyl naphthalenes (Phousongphouang and Arey, 2002), or large alkanes with ~23 or more carbons (Calvert et al., 2008), or branched / cyclic species of similar size are (as a group) important contributors. The latter species are semivolatile and intermediate volatility species (S/IVOCs), and thus our results suggests a very important role for such species in urban SOA formation. ”

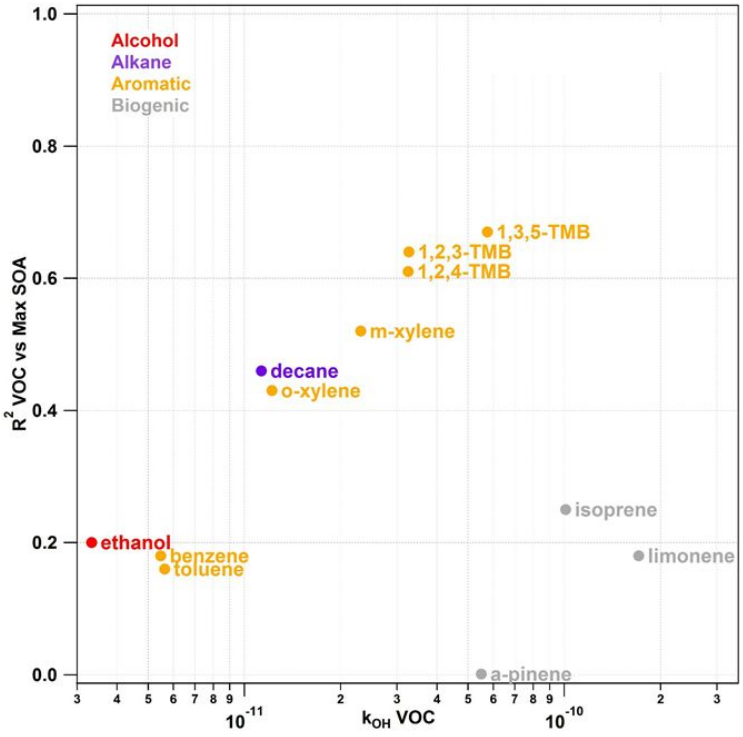

Figure 10: R^2 between the concentrations of different VOCs and the maximum amount of SOA formation in the OFR, plotted vs. the reaction rate constant of each VOC with OH (k_{OH}).

We have also modified the abstract to reflect this updated result as:

"**Reactor SOA formation was inversely correlated with ambient SOA and Ox, which along with the short-lived VOC correlation, indicates the importance of relatively reactive (OH ~0.3 day) SOA precursors (most likely semivolatile and intermediate volatility species, S/IVOC) in the greater Los Angeles Area.**"

R3.53. P21927, L15: I suggest a modification to the title of Section 4.2: "Fit to the observed ambient and reactor OA/ΔCO evolution" or perhaps "Parameterization of timescales for SOA functionalization and fragmentation processes."

We have modified the section title to:

"Parameterization of the Amount and Timescale for Urban SOA Formation"

R3.54. P21927, L22: "However, the evolution…": Evolution of OA/ΔCO?

Text has been modified as requested.

R3.55. P21928, L22: Isn't it implicit in the discussion that IVOCs and SVOCs are primary emissions? I suggest: "The second model variant represents SOA formation from IVOCs and SVOCs in addition to VOCs".

Text has been modified as requested.

R3.56. P21930, L6: Define "TPOT".

Definition added as requested.

R3.57. P21933, L14-L15: Didn't the George and Abbatt (2010) and Tkacik et al. (2014) studies that are already cited here also use an oxidation flow reactor to perturb ambient urban air?

Tkacik et al. (2014) was not a study of ambient urban air but a study of oxidation of vehicle emissions in a tunnel study. The George and Abbatt (2010) study used a denuder to remove VOCs and thus only studied heterogeneous oxidation. The latter point was not clear in the sentence that the reviewer is referring to, so we have updated that text to read:

"This work represents the first application of an oxidation flow reactor to investigate SOA formation from ambient urban air, to our knowledge."

References

Barsanti, K. C., Carlton, A. G., and Chung, S. H.: Analyzing experimental data and model parameters: implications for predictions of SOA using chemical transport models, Atmos. Chem. Phys., 13, 12073-12088, 10.5194/acp-13-12073-2013, 2013.

DeCarlo, P. F., Slowik, J. G., Worsnop, D. R., Davidovits, P., and Jimenez, J. L.: Particle morphology and density characterization by combined mobility and aerodynamic diameter measurements. Part 1: Theory, Aerosol Sci Tech, 38, 1185-1205, 2004.

George, I. J., and Abbatt, J. P. D.: Heterogeneous oxidation of atmospheric aerosol particles by gas-phase radicals, Nat Chem, 2, 713-722, 2010.

Hayes, P. L., Carlton, A. G., Baker, K. R., Ahmadov, R., Washenfelder, R. A., Alvarez, S., Rappenglück, B., Gilman, J. B., Kuster, W. C., de Gouw, J. A., Zotter, P., Prévôt, A. S. H., Szidat, S., Kleindienst, T. E., Offenberg, J. H., Ma, P. K., and Jimenez, J. L.: Modeling the formation and aging of secondary organic aerosols in Los Angeles during CalNex 2010, Atmos. Chem. Phys., 15, 5773-5801, 10.5194/acp-15-5773-2015, 2015.

Kang, E., Root, M. J., Toohey, D. W., and Brune, W. H.: Introducing the concept of Potential Aerosol Mass (PAM), Atmos. Chem. Phys., 7, 5727-5744, 10.5194/acp-7-5727-2007, 2007.

Kroll, J. H., Donahue, N. M., Jimenez, J. L., Kessler, S. H., Canagaratna, M. R., Wilson, K. R., Altieri, K. E., Mazzoleni, L. R., Wozniak, A. S., Bluhm, H., Mysak, E. R., Smith, J. D., Kolb, C. E.,

and Worsnop, D. R.: Carbon oxidation state as a metric for describing the chemistry of atmospheric organic aerosol, Nat Chem, 3, 133-139, 2011.

Lambe, A. T., Onasch, T. B., Croasdale, D. R., Wright, J. P., Martin, A. T., Franklin, J. P., Massoli, P., Kroll, J. H., Canagaratna, M. R., Brune, W. H., Worsnop, D. R., and Davidovits, P.: Transitions from Functionalization to Fragmentation Reactions of Laboratory Secondary Organic Aerosol (SOA) Generated from the OH Oxidation of Alkane Precursors, Environmental Science & Technology, 46, 5430–5437, 10.1021/es300274t, 2012.

Li, R., Palm, B. B., Ortega, A. M., Hlywiak, J. A., Hu, W., Peng, Z., Day, D. A., Knote, C., Brune, W. H., de Gouw, J. A., and Jimenez, J. L.: Modeling the Radical Chemistry in an Oxidation Flow Reactor: Radical Formation and Recycling, Sensitivities, and OH Exposure Estimation Equation, The Journal of Physical Chemistry A, 10.1021/jp509534k, 2015.

Ortega, A. M., Day, D. A., Cubison, M. J., Brune, W. H., Bon, D., de Gouw, J. A., and Jimenez, J. L.: Secondary organic aerosol formation and primary organic aerosol oxidation from biomass-burning smoke in a flow reactor during FLAME-3, Atmos. Chem. Phys., 13, 11551-11571, 10.5194/acp-13-11551-2013, 2013.

Palm, B. B., Campuzano-Jost, P., Ortega, A. M., Day, D. A., Kaser, L., Jud, W., Karl, T., Hansel, A., Hunter, J. F., Cross, E. S., Kroll, J. H., Peng, Z., Brune, W. H., and Jimenez, J. L.: In situ secondary organic aerosol formation from ambient pine forest air using an oxidation flow reactor, Atmos. Chem. Phys., 16, 2943-2970, 10.5194/acp-16-2943-2016, 2016.

Peng, Z., Day, D. A., Ortega, A. M., Palm, B. B., Hu, W. W., Stark, H., Li, R., Tsigaridis, K., Brune, W. H., and Jimenez, J. L.: Non-OH chemistry in oxidation flow reactors for the study of atmospheric chemistry systematically examined by modeling, Atmos. Chem. Phys. Discuss., 2015, 23543-23586, 10.5194/acpd-15-23543-2015, 2015a.

Peng, Z., Day, D. A., Stark, H., Li, R., Lee-Taylor, J., Palm, B. B., Brune, W. H., and Jimenez, J. L.: HOx radical chemistry in oxidation flow reactors with low-pressure mercury lamps systematically examined by modeling, Atmos. Meas. Tech., 8, 4863-4890, 10.5194/amt-8-4863-2015, 2015b.

Ryerson, T. B., Andrews, A. E., Angevine, W. M., Bates, T. S., Brock, C. A., Cairns, B., Cohen, R. C., Cooper, O. R., de Gouw, J. A., Fehsenfeld, F. C., Ferrare, R. A., Fischer, M. L., Flagan, R. C., Goldstein, A. H., Hair, J. W., Hardesty, R. M., Hostetler, C. A., Jimenez, J. L., Langford, A. O., McCauley, E., McKeen, S. A., Molina, L. T., Nenes, A., Oltmans, S. J., Parrish, D. D., Pederson, J. R., Pierce, R. B., Prather, K., Quinn, P. K., Seinfeld, J. H., Senff, C. J., Sorooshian, A., Stutz, J., Surratt, J. D., Trainer, M., Volkamer, R., Williams, E. J., and Wofsy, S. C.: The 2010 California Research at the Nexus of Air Quality and Climate Change (CalNex) field study, Journal of Geophysical Research: Atmospheres, 118, 5830-5866, 10.1002/jgrd.50331, 2013.

Tkacik, D. S., Lambe, A. T., Jathar, S., Li, X., Presto, A. A., Zhao, Y., Blake, D., Meinardi, S., Jayne, J. T., Croteau, P. L., and Robinson, A. L.: Secondary Organic Aerosol Formation from in-Use Motor Vehicle Emissions Using a Potential Aerosol Mass Reactor, Environmental Science & Technology, 48, 11235-11242, 10.1021/es502239v, 2014.

Washenfelder, R. A., Young, C. J., Brown, S. S., Angevine, W. M., Atlas, E. L., Blake, D. R., Bon, D. M., Cubison, M. J., de Gouw, J. A., Dusanter, S., Flynn, J., Gilman, J. B., Graus, M., Griffith, S., Grossberg, N., Hayes, P. L., Jimenez, J. L., Kuster, W. C., Lefer, B. L., Pollack, I. B., Ryerson, T. B., Stark, H., Stevens, P. S., and Trainer, M. K.: The glyoxal budget and its contribution to organic aerosol for Los Angeles, California, during CalNex 2010, Journal of Geophysical Research: Atmospheres, 116, D00V02, 10.1029/2011jd016314, 2011.

Real-time Measurements of Secondary Organic Aerosol Formation and Aging from Ambient Air in an Oxidation Flow Reactor in the Los Angeles Area

Amber M. Ortega[1,2], Patrick L. Hayes[3], Zhe Peng,[1,4], Brett B. Palm[1,4], Weiwei Hu,[1,4], Douglas A. Day[1,4], Rui Li,[1,2,5,*] Michael J. Cubison[1,4,+], William H. Brune[6], Martin Graus[1,5,++], Carsten Warneke[1,5], Jessica B. Gilman[1,5], William C. Kuster[1,5,^],Joost de Gouw[1,5], Cándido Gutiérrez-Montes[7], and Jose L. Jimenez[1,4]

[1]Cooperative Institute for Research in the Environmental Sciences, University of Colorado, Boulder, CO, USA
[2]Department of Atmospheric and Oceanic Sciences, University of Colorado, Boulder, CO, USA
[3]Department of Chemistry, Université de Montréal, Montreal, Quebec, Canada
[4]Department of Chemistry and Biochemistry, University of Colorado, Boulder, CO USA
[5]Chemical Sciences Division, NOAA Earth System Research Laboratory, Boulder, CO, USA
[6]Department of Meteorology, Pennsylvania State University, University Park, PA, USA
[7]Departamento de Ingeniería, Mecánica y Minera, Universidad de Jaen, Jaen, Spain
[*]now at Markes International Inc., Cincinnati, OH 45242
[+]now at: Tofwerk AG, Thun, Switzerland
[++]now at: Institute of Meteorology and Geophysics, University of Innsbruck, Innsbruck, Austria
[^]now retired

Abstract

Field studies in polluted areas over the last decade have observed large formation of secondary organic aerosol (SOA) that is often poorly captured by models. The study of SOA formation using ambient data is often confounded by the effects of advection, vertical mixing, emissions, and variable degrees of photochemical aging. An Oxidation Flow Reactor (OFR) was deployed to study SOA formation in real-time during the California Research at the Nexus of Air Quality and Climate Change (CalNex) ~~CalNex~~ campaign in Pasadena, CA, in 2010. A high-resolution aerosol mass spectrometer (AMS) and a scanning mobility particle sizer (SMPS) alternated sampling ambient and reactor-aged air. The reactor produced OH concentrations up to 4 orders of magnitude higher than in ambient air~~, achieving equivalent atmospheric aging from hours up to several weeks in 3 minutes of processing. OH radical concentration was continuously stepped, obtaining measurements of real-time SOA formation and oxidation at multiple equivalent ages from 0.8 days–6.4 weeks of age.~~. OH radical concentration was continuously stepped, achieving equivalent atmospheric aging of 0.8 days–6.4 weeks in 3 min of processing every 2 hrs. Enhancement of OA from aging showed a maximum net SOA production between 0.8–6 days of aging with net OA mass loss beyond 2 weeks. Reactor SOA mass peaked at night, in the absence of ambient photochemistry and correlated with trimethylbenzene concentrations. Reactor SOA formation was inversely correlated with ambient SOA and O_x, which along with the short-lived VOC correlation, indicates the importance of relatively reactive (τ_{OH} ~0.3 day) SOA precursors (most likely semivolatile and intermediate volatility species, S/IVOC) in the greater Los Angeles Area.~~Reactor SOA formation was inversely correlated with ambient SOA and O_x, which along with the short-lived VOC correlation, indicates the importance of relatively reactive (τ_{OH} ~0.3 day) SOA precursors in the LA Basin~~. Evolution of the elemental composition in the reactor was similar to trends observed in the atmosphere (O:C vs. H:C slope ~ -0.65). Oxidation state of carbon (OSc) in reactor SOA increased steeply with age and remained elevated (OS_C ~2) at the highest photochemical ages probed. The ratio of OA in the reactor output to excess CO (ΔCO, ambient CO above regional background) vs. photochemical age is similar to previous studies at low to moderate ages and also extends to higher ages where OA loss dominates. The mass added at low-

Formatted: Superscript
Formatted: Superscript
Formatted: Subscript
Formatted: Font: Symbol
Formatted: Subscript

to-intermediate ages is due primarily to condensation of oxidized species, not heterogeneous oxidation. The OA decrease at high photochemical ages is dominated by heterogeneous oxidation followed by fragmentation/evaporation. A comparison of urban SOA formation in this study with a similar study of vehicle SOA in a tunnel supports the dominance of vehicle emissions in urban SOA. Pre-2007 SOA models underpredict SOA formation by an order of magnitude, while a more recent model performs better but overpredicts at higher ages. These results demonstrate the value of the reactor as a tool for *in situ* evaluation of the SOA formation potential and OA evolution from ambient air.

1 Introduction

Atmospheric aerosols are the most uncertain aspect of the climate radiative forcing (Myhre et al., 2013), and have negative impacts on human health (Pope et al., 2002) and visibility (Watson, 2002). Organic aerosol (OA) represents a large fraction of fine particle mass (Murphy et al., 2006; Zhang et al., 2007) and is the least-characterized component of submicron aerosol due to its complexity and wide variety of emission sources and atmospheric processes (Jimenez et al., 2009). OA can be emitted directly into the atmosphere from primary OA sources (POA), such as traffic or biomass burning, or formed through atmospheric processing as secondary OA (SOA). SOA can be formed when volatile organic compounds (VOCs) react with atmospheric oxidants such as ozone and hydroxyl radicals (O_3 and OH), to form less-volatile products that can partition into the aerosol phase (Pankow, 1994; Donahue et al., 2006), as well as through heterogeneous and multiphase processes (Ervens et al., 2011). An improved understanding of the sources, atmospheric processes, and chemical properties of SOA is necessary to constrain and predict current impacts on human health and climate as well as shifting impacts with changing climate and emissions (Hallquist et al., 2009).

SOA concentrations are typically underestimated by over an order of magnitude when pre-2007 models are applied in urban regions (Volkamer et al., 2006; de Gouw and Jimenez, 2009; Hodzic et al., 2010; Morino et al., 2014; Hayes et al., 2015). These "traditional" models treated SOA formation as partitioning of semivolatile products from gas-phase oxidation of VOCs, using aerosol yields and saturation concentrations from older environmental chamber studies. More recently updated models have incorporated (higher) SOA yields from VOCs from more recent chamber studies. Some studies have used artificially higher yields based on "aging" of the VOC products, although these are unconstrained by chamber studies (e.g. Tsimpidi et al., 2010), or

increased yields to account for losses of semivolatile gases to chamber walls (Zhang et al., 2014; Hayes et al., 2015). Donahue et al. (2006) developed the volatility basis set (VBS) formalism for modeling OA partitioning, in which organic species are distributed into volatility bins, which has been adopted by many SOA modeling schemes. Semi-volatile and intermediate volatility compounds (S/IVOCs) have been identified as additional precursors that were not considered in traditional models (Robinson et al., 2007). These updated approaches have been applied to several urban datasets leading to better closure between measured and modeled bulk OA, but have resulted in other problems such as several-fold overpredictions of SOA at long aging times (>1 day; Dzepina et al., 2011; Hayes et al., 2015; Zhang et al., 2015) or SOA that is much too volatile compared to observations (Dzepina et al., 2011). These models remain under-constrained, and it is unclear whether the updated models increase predicted SOA formation for the right reasons. Targeted field studies in urban areas, with sufficient constraints and with novel approaches for focused investigation of SOA formation, are essential for continued model testing and improvement.

In order to characterize the SOA formation potential of urban emissions, ~~an~~ a rapid field deployable experimental ~~technique~~ method is needed, so that potentially rapid changes of ambient SOA formation potential can be captured. ~~that is capable of rapid operation to allow examination of the variable potential of changing air masses~~. The "Potential Aerosol Mass" (PAM) oxidation flow reactor (OFR), was developed by Kang et al., (2007; 2011), and used in many laboratory experiments and recent field studies. It is a small flow reactor that exposes air samples to high oxidant levels (100-10,000 times atmospheric concentrations) with short residence time (<5 min). Recent work with the reactor has examined SOA yield, oxidation, and physicochemical changes using single precursors or simple mixtures in laboratory experiments, producing results similar to

environmental chamber experiments (Massoli et al., 2010; Kang et al., 2011; Lambe et al., 2011a; Lambe et al., 2011b; Bruns et al., 2015). SOA yields in the reactor are comparable or somewhat lower than for similar OH exposures in large environmental chambers, which has been suggested to be due to the short residence time of the reactor not being sufficient to allow complete condensation of semivolatiles (Lambe et al., 2015) or increased wall losses of gas-phase species due to the higher surface area to volume ratios of the reactor (Bruns et al., 2015). OH oxidation of alkane SOA precursors in the reactor show the effect of functionalization (oxygen addition) and fragmentation (carbon loss) reactions (Lambe et al., 2012). Recent reactor application to aging of biomass burning smoke showed that total OA after reactor oxidation was on average 1.42±0.36 times the initial primary OA (POA) with similar aging of biomass burning tracers to that observed in aircraft measurements (Cubison et al., 2011; Ortega et al., 2013). Aging measurements of vehicular exhaust using the reactor in a highway tunnel in Pittsburgh, PA indicated peak SOA production after 2.5 days of atmospheric equivalent photochemical aging (at OH = 3×10^6 molec cm^{-3}) and concluded the chemical evolution of the OA inside the reactor appears to be similar to that observed in the atmosphere (Tkacik et al., 2014). Other studies also show that the reactor produces SOA with characteristics similar to that formed in the atmosphere for crude oil evaporation (Bahreini et al., 2012a; Li et al., 2013). The radical chemistry in the reactor has been recently characterized (Li et al., 2015; Peng et al., 2015).Thus, the reactor is a useful tool for elucidating SOA formation processes under field conditions where utilizing large-scale environmental chambers is not practical and/or if a higher degree of aging is targeted.

Due to meteorological conditions (e.g. diurnal fluctuations in land-sea breeze patterns with weak synoptic forcing) and topography (e.g. the surrounding coastal mountain ranges) ventilation of air in the greater Los Angeles area (LA-Basin) can be limited, historically resulting in high pollution

levels. Several field campaigns have investigated SOA in the LA-Basin, including the 2005 Study of Organic Aerosol at Riverside (SOAR; Docherty et al., 2011) and the 2009 Pasadena Aerosol Characterization Observatory (PACO; Hersey et al., 2011). These studies identified SOA as a major fraction of total OA in the LA Basin in the summer, consistent with findings in previous urban field campaigns (Volkamer et al., 2006; de Gouw and Jimenez, 2009). This situation is in contrast to previous studies in this region which reported that primary OA was higher than SOA, other than during severe photochemical smog episodes; however, these estimates were likely affected by apportionment biases or the greatly underestimated SOA production of traditional models (Docherty et al., 2008).

The 2010 California Research at the Nexus of Air Quality and Climate Change (CalNex) was a multiplatform large-scale field study, which utilized ground sites at Bakersfield and Pasadena, California, NOAA WP-3D and Twin Otter aircraft, and the research ship *R/V Atlantis* (Ryerson et al., 2013). In this study, we measured submicron aerosol size and composition alternately for ambient air and for ambient air that had been aged in an oxidation flow reactor by systematically changing the OH exposure. This work is compared to the previous literature but extends beyond it with the new information provided by the *in situ* aging studies. By combining results from the ambient aerosol and aged ambient aerosol measurements, we provide a stronger test of current SOA models, since they can now be compared with data from a much wider range of photochemical ages. ~~By combining results from the ambient aerosol and aged ambient aerosol measurements, we provide a stronger test of current SOA models.~~ In order to characterize the SOA formation potential of urban emissions, a field deployable experimental method is needed that is capable of rapid operation to allow examination of the variable potential of changing air masses.

2 Experimental Methods

2.1 CalNex Field Campaign

The work in this study will focus on measurements from the Pasadena ground site during CalNex. The Pasadena site was located on the California Institute of Technology (Caltech) campus in Pasadena, CA (34.1406 N, 118.1225 W, 236 m above mean sea level); the location, airmass transport, and key measurements have been described in detail previously (Washenfelder et al., 2011; Hayes et al., 2013). The measurement period for our reactor study is 29 May–10 June 2010, hereafter referred to as the "sampling period." Meteorological conditions, including prevailing winds, boundary layer height, temperature, and relative humidity information are summarized by Washenfelder et al. (2011) and Hayes et al. (2013). An overview of the 2010 CalNex field campaign (Ryerson et al., 2013) and aerosol observations at the Pasadena Supersite (Hayes et al., 2013) can be found in previous publications. A gas-chromatography mass spectrometer (GC-MS) from NOAA was located at the same field site (Hayes et al., 2013; Warneke et al., 2013) and used for VOC measurements reported in this study. The NOAA WP-3D research aircraft sampled *in situ* meteorological, trace gas, and aerosol conditions aloft during CalNex (Bahreini et al., 2012b; Ryerson et al., 2013). Non-refractory submicron aerosol composition measurements aboard the NOAA WP-3D were made using an Aerodyne compact time-of-flight aerosol mass spectrometer (C-ToF-AMS, Drewnick et al., 2005). Details of operation, analysis, and quantification can be found in Bahreini et al. (2012b).

2.2 Oxidation Flow Reactor

To study SOA formation and OA aging *in-situ*, we deployed a Potential Aerosol Mass (PAM) oxidation flow reactor (Kang et al., 2007; Kang et al., 2011) at the Pasadena ground site. Fig. 1a

shows a diagram of the operational setup. The reactor and ambient sample lines were located adjacent to one another, on the roof of the instrument trailer at 7.2 meters above ground (Fig. 1b). Ambient air was continuously sampled in an open flow-through configuration via a 14-cm diameter opening with coarse-grid mesh screen coated with an inert silicon coating (Sulfinert by SilcoTek, Bellefonte, PA). The mesh was designed to block debris and insects, as well as break up large eddies while allowing VOCs and oxidized gases to be sampled efficiently. This configuration, with no inlet, was chosen because of the observation of reduced SOA formation when any inlet and/or an inlet plate was used in a previous experiment (Ortega et al., 2013). The reactor output was measured by an AMS (described below), a scanning-mobility particle sizer (SMPS, TSI Inc., Model 3936 with TSI 3010 CPC), and an O_3 monitor (2B Technologies, Model 205). The uncertainty in the O_3 measurement is +/- 1.5 ppb or 2% of the measurement, whichever is greater. Fast switching valves were used to automatically alternate AMS and SMPS sampling between the reactor and unperturbed ambient sample line every 5 minutes. Bypass lines were used to maintain constant flow in both the reactor and ambient sample lines while instrumentation was sampling the other channel, to avoid artifacts due to particle or gas losses or re-equilibration that could occur if flow had been stagnant in the lines or modulated in the reactor. ~~To maintain plug-like flow characteristics in the reactor, output flow was sampled from both a central stainless steel 1/4-inch OD tube at 2.0 lpm for aerosol measurements and a 3/8-inch OD PTFE Teflon perforated ring with 14-cm diameter for gas-phase measurements at 2.4 lpm. This setup allowed continuous measurements of both photochemically-aged and ambient aerosol.~~ The configuration with the large inlet strongly reduces recirculation in the reactor and narrows the residence time distribution (RTD) (Fig. S1). To further reduce the width of the RTD, output flow was sampled from both a central stainless steel 1/4 inch OD tube at 2.0 L min^{-1} for aerosol measurements and a 3/8 inch OD

Formatted: Subscript

Formatted: Superscript

PTFE Teflon perforated ring with 14 cm diameter for gas-phase measurements at 2.4 L min^{-1}. In addition, Peng et al. (2015) has shown that variations in the residence time distribution in the OFR had limited impact on the estimated OH_{exp}.

The total flow rate through the reactor was 4.4 lpm corresponding to a residence time of 3 min. The reactor was used to expose ambient air to high levels of OH and O_3, produced when UV light from two low-pressure mercury lamps (model no. 82-9304-03, BHK Inc., with discrete emission peaks at 254 and 185 nm) initiated O_2, H_2O and O_3 photochemistry. This mode of operation is referred to as OFR185, and OH is formed from both H_2O and O_3 photolysis (Li et al., 2015). In this mode O_3 is formed in the reactor but is not added to the reactor, contrary to the OFR254 mode that has been used mainly in laboratory studies (Peng et al., 2015). Given that most known urban SOA precursors do not react with O_3 (e.g. Hayes et al., 2015), d using we expect OH to dominate the observed SOA formation. Consistent with this, no SOA was formed in test experiments during CalNex when ambient air was exposed to O_3 only without OH. ~~The reactor was used to expose ambient air to high levels of OH and O_3, produced when UV light from two low-pressure mercury lamps (model no. 82-9304-03, BHK Inc., with discrete emission peaks at 254 nm and 185 nm) initiated O_2, H_2O and O_3 photochemistry. This mode of operation is referred to as OFR185 (Li et al., 2015).~~ We use the term "aging" to refer to the combined effect of OH, O_3, and light exposure in the flow reactor, although reactions in the reactor are understood to be dominated by OH under typical operating conditions (Peng et al., 2016). Peng et al. (2016) have investigated the possibility of photolysis of gases and aerosol species under the OFR conditions. OH reaction dominated the fate of all gases studied. Under most conditions in this study, photolysis was estimated to be responsible for only several percent of the fractional destruction of the gas-phase primary species most susceptible to it (aromatic species) even if photolysis quantum yield was assumed to be 1.

Formatted: Superscript
Formatted: Subscript
Formatted: Subscript
Formatted: Subscript
Formatted: Subscript
Formatted: Subscript
Formatted: Subscript
Formatted: Subscript
Formatted: Subscript
Formatted: Subscript

The upper limit of the fractional destruction of possible oxidation intermediates was ~x2 that of primary species. Photolysis of SOA already present in the atmosphere may have played some role at the medium and high UV settings studied here when assuming upper limit quantum yields. However photolysis e-fold decays in the reactor are estimated to be orders-of-magnitude lower than for the atmosphere for equivalent OH exposures.

The intensity of aging was continuously stepped by computer-controlled lamp power supplies (custom made transformers from BHK Inc., controlled via Labview using a National Instruments analog output board NI USB-6501), resulting in systematic stepping of lamp input voltage from 50–110 VAC. This voltage stepping modulates the photon flux and consequently the OH concentrations in the reactor (Li et al., 2015). The lights are housed in Teflon sleeves which are purged with N_2 gas to remove heat and avoid exposing the lamp surfaces to O_3 or other oxidants. When operated at full power the lights result in an increase of ~2^{o}C above ambient conditions. Given the low volatility of ambient OA (Huffman et al., 2009; see Fig. S12 and associated discussion below), little OA evaporation is expected in the reactor due to this heating.

Formatted: Subscript

Formatted: Subscript

Formatted: Superscript

Oxidant concentrations in the reactor were stepped in 20-minute intervals, through six levels (including lights off, i.e. no added oxidants) comprising a two-hour cycle (Fig. 2). Only data from the last five minutes of each 20-minute period are used, to avoid including reactor transient periods. Thus, five full residence times have elapsed after changes to the UV lights and before starting to sample reactor outputs, to allow full replacement of the contents of the reactor. As lamp intensity increased, O_3 and OH concentrations increased in the reactor, and resultant OA concentrations were measured from the reactor after oxidant perturbation as seen in Fig. 2. To correct for the effect of particle losses we compared concentrations measured in the reactor output when UV lights are turned off with those measured through the ambient inlet. The loss of particle mass in

this aluminum reactor is small, of the order of a few percent of the ambient concentrations (see also Palm et al., 2016). Losses in an OFR with a quartz body were observed to be ~35% in a previous study (presumably due to nearly complete loss of charged particles), which led to our use of the all-aluminum reactor. A time-dependent correction factor was estimated by comparing each reactor output measurement (for each period when the lights were off) with the average of the two ambient measurements immediately before and after. This correction is interpolated in time and applied to all reactor output measurements with lights on. The resulting average correction was +5.8 %. Although losses may have some size dependence, given the broad distributions covering the same size ranges for both ambient air and OFR output, and the small magnitude of the correction, this effect has not been considered in detail.

~~To account for particle losses in the reactor, reactor AMS concentrations have been corrected by comparing particles measured through the ambient inlet (averaging two concurrent ambient measurements just before and after lights-off measurement) to the levels during the last 5 minutes of each period with lights off. This correction is applied over the sample period, in a time varying way and accounting for variations in UV intensity, resulting in an average correction of +5.8%.~~

The OH exposure (OH_{exp}, OH concentration integrated over the reactor residence time) achieved in this study is primarily a function of lamp photon flux (at 185 and 254 nm), residence time, and ambient H_2O concentration and OH reactivity (Li et al., 2015; Peng et al., 2015). OH_{exp} was estimated using an ~~calibration~~ equation developed by multivariate fitting of the output from a kinetic model of reactor (OFR185) operation, and verified against data from several field and laboratory experiments including CalNex (Li et al., 2015). Data from the decay of ambient SO_2 in the OFR during CalNex, which was only reliable during periods with higher ambient SO_2 concentrations (> 1 ppbv), was used to verify the OH_{exp} estimation equation. The equation uses

Formatted: Subscript

Formatted: Subscript

Formatted: Subscript

ambient H_2O concentration, reactor output O_3 concentrations, ~~flow rate~~residence time, and ambient OH reactivity from collocated measurements (total OH reactivity ~~data~~ measurement from the Stevens Group, Indiana University; in this method there is no assumption about the reactivity constituents). According to this equation, internal OH_{exp} in the reactor typically ranged from 1.1×10^{11}–5.8×10^{12} molec. cm^{-3} s, 0.8 days–6.4 weeks of photochemical age assuming 24-hr average ambient OH concentrations of 1.5×10^{6} molec. cm^{-3} (Mao et al., 2009). The uncertainty in the calculated OH_{exp} is estimated to be a factor of 3 (Li et al., 2015; Peng et al., 2015). "Total photochemical age" refers to the sum of ambient photochemical age and reactor internally-generated photochemical age, used throughout this work unless otherwise specified. Ambient photochemical age is calculated by the ratio of 1,2,4-trimethylbenzene to benzene (Borbon et al., 2013), using collocated gas-phase measurements as described in Hayes et al. (2013). Subsequent figures use total photochemical age in day-units applying the average OH concentration of 1.5×10^{6} molec. cm^{-3}. During CalNex, OH concentrations averaged ~~up to~~as high as 4×10^{6} molec. cm^{-3} during the daytime, from concurrent OH reactivity estimates. Since a significant part of SOA formation happens during the first few hours after emission, the 0.8 ~~equivalent~~ day minimum photochemical age probed with the reactor would correspond to ~0.3 days at the peak OH concentration observed during CalNex.

Formatted: Subscript

2.3 Particle Measurements

Particle concentration and composition were analyzed with a high-resolution time-of-flight aerosol mass spectrometer (HR-ToF-AMS, abbreviated as AMS hereafter; Aerodyne Research, Billerica, MA; DeCarlo et al., 2006; Canagaratna et al., 2007). The ambient measurement setup, instrument intercomparisons, scientific results, and their interpretation are reported in Hayes et al. (2013). he high-resolution (HR) fragmentation table (Aiken et al., 2008) and peak fitting (DeCarlo et al.,

2006) were applied to the reactor measurements with no additional adjustments beyond those performed for the ambient CalNex data by Hayes et al. (2013). The elemental analysis of OA (resulting in oxygen-to-carbon ratio, O:C, and hydrogen-to-carbon ratio, H:C) was performed using the "improved-ambient" method published by Canagaratna et al. (2015) for both reactor and ambient measurements, which increases O:C on average by 27% and H:C on average by 11% over the previous "Aiken ambient" method (Aiken et al., 2008). Details of the quantification of AMS reactor measurements (i.e. collection efficiency, inlet and particle lens losses) and intercomparison with the SMPS are discussed in supplementary Section S1 (Figs. ~~S1~~S2-~~S5~~S6). Hayes et al. (2015) performed a modeling study comparing the ambient AMS OA measurements with several box and 3-D SOA models. Here, we only discuss the modifications in post-processing and data analysis necessitated by the alternating sampling of the reactor output. ~~T~~

2.4 Fate of Low-Volatility Organic Gases in the Reactor

As organic gases are oxidized, they can form lower vapor pressure products, low-volatility organic compounds (LVOC). Semivolatile organic compounds (SVOC) will also be formed, but we focus this discussion on LVOC for several reasons. As shown in Figure S12 (discussed in Section 4.4), the volatility distribution of the SOA present during CalNex shows very limited importance of SVOCs as SOA constituents. Second, discussion and modeling of LVOC fate in the reactor is conceptually simpler. Third, the amount of SOA formed in reactor is significantly higher than can be explained by the speciated precursors, consistent with other studies (Palm et al., 2016). The assumption of LVOCs results in higher SOA formation than if SVOC were assumed, and is thus a the most conservative assumption in terms of closure of measured vs. predicted SOA. Thus adding complexity to the loss model for species that are likely of limited importance was a lower priority for our study.~~simplicity~~. In the atmosphere, the dominant fate of these LVOC is

condensation on aerosols, as OH lifetimes and dry deposition time scales are slower (Donahue et al., 2013; Knote et al., 2015). However, given the limited residence time, high surface/volume ratio, and the high oxidant concentrations in the OFR, other LVOC fates can be competitive with condensation on aerosols. LVOC in the reactor can either condense on aerosols, be lost due to condensation on the reactor walls, react further with OH resulting in condensable or non-condensable products, or exit the reactor in the gas phase to condense on the sampling line walls. Aerosol sampling instruments only measure the LVOC that condense on aerosols in the reactor. Given the short residence time and high OH_{exp} of the reactor, SOA formation could be underestimated due to these competing fates. To account for vapor losses, we follow the method detailed in Palm et al. (2016), using McMurry and Grosjean (1985) for wall loss estimation. The method of Pirjola et al. (1999) is used for estimating organic gas condensation to aerosols based on the measured SMPS size distributions with the Fuchs-Sutugin correction for gas diffusion in the transition regime (Seinfeld and Pandis, 1998). It is assumed that products after five oxidation steps with OH at k_{OH} = 1 x 10^{-11} molec cm^{-3} s^{-1} are lost (fragmented and too volatile to condense). We note that 56% (97%) of the initial molecules will have undergone five oxidation steps after an OH_{exp}= 5×10^{11} (1×10^{12}) molec. cm^{-3} s. This is used to simulate a typical C_{10} VOC oxidation in the reactor. Parameters used include the measured surface-area-to-volume ratio (A/V) of the reactor (25 m^{-1}), a coefficient of eddy diffusion k_e approximated as 0.0036 s^{-1}, and a diffusion coefficient D = 47×10^{-6} m^2 s^{-1}, corresponding approximately to the diffusivity of a molecule with a mass of 200 g mol^{-1}. The analyses leading to the correction terms were developed in Palm et al. (2016) and are applied here. As Palm et al. (2016) is now published in final form in ACP, we refer readers to that manuscript for the full details of the method.

Formatted: Subscript
Formatted: Superscript
Formatted: Superscript
Formatted: Superscript

At OH_{exp} lower than 1×10^{12} molec cm^{-3} s (~ 10 days) the dominant LVOC fate (50–75%) is condensation to the aerosol (see Fig. S7). At higher OH_{exp}, the fate of organic gases is dominated (>45%) by loss to reaction with OH rather than condensing on aerosol. LVOC lost to the walls (~7%) or exiting the reactor (~2%) play only small roles under the conditions of this study, due to the relatively high ambient aerosol surface area. ~~At OH_{exp} lower than 1×10^{12} molec. cm^{-3} s (~10 days) the dominant LVOC fate is condensation to the aerosol (see Fig. S6). At higher OH_{exp}, the fate of organic gases is dominated by loss to reaction with OH rather than condensing on aerosol. LVOCs lost to the walls or exiting the reactor play only a small role under the conditions of this study, due to the relatively high ambient aerosol surface area.~~ The amount of SOA formed in the reactor is corrected for the fraction of SOA that condense on the aerosol by fitting a line to the calculated fraction of LVOCs that condense on aerosol and dividing the measured SOA formed in the reactor by the fitted fraction of LVOCs that were lost by condensation on the aerosol (Fig. ~~S6~~S7). This correction is a minimum at low to moderate ages, and highest at longest ages where net OA production is lowest (Sect. 3.2). Thus, the maximum net SOA production was typically corrected by a factor of 1.2. At increasing ages, where OA loss due to heterogeneous oxidation begins to dominate over gas-phase oxidation, it becomes unfeasible to apply the correction, as the net OA enhancement in the reactor is negative. Thus, correction is applied when reactor-measured OA is greater than ambient OA (relative OA enhancement ratio, ER_{OA} = reactor OA / ambient OA, $ER_{OA}>1$; and the absolute OA enhancement factor, ΔOA Mass = reactor OA – ambient OA~~$ER_{OA}>1$~~, ΔOA Mass>0, Sect. 3.2).

Formatted: Subscript

Formatted: Superscript

Formatted: Superscript

Formatted: Subscript

3 Results and Discussion

3.1 Observations

The time series of the reactor sample period is shown in Fig. 3a. The ambient aerosol during the first third (30 May–3 June 2010) of the measurement period is characterized by OA dominance, while the remaining two-thirds of the period (3–11 June 2010) is characterized by high concentrations of OA and nitrate, moderate sulfate and ammonium, and low chloride, with a marked diurnal cycle. This second period was strongly affected by in-basin pollution and is the most useful in terms of studying urban SOA formation (Hayes et al., 2013). The precursors that are expected to be important contributors to SOA at this location include aromatic VOCs and semivolatile and intermediate volatility species (mostly alkanes and aromatics), with low importance for biogenic species (Hayes et al., 2015).

A 24-h~~our~~ snapshot of the time series of ambient and reactor data is shown in Fig. 3b. This period is representative of the diurnal profiles observed from 3–9 June 2010. The oscillations (zig-zag pattern) in reactor output concentrations are due to OH_{exp} stepping as shown in Fig. 2. Day and night periods are highlighted to indicate the period of inactive (20:00–8:00) and active ambient photochemistry (8:00–20:00) in Fig. 3b. Ambient nitrate and ammonium concentrations peak in early morning hours before sunrise, while OA peaks in the late afternoon, during the most photochemically active part of the day. Hayes et al. (2013) attribute~~s~~ this organic aerosol temporal pattern to the formation of fresh urban SOA as the LA-plume undergoes ~0.3 days of photochemical aging during transport to our field location, which is considered a receptor site as it experienced a strong impact from aged urban emissions. However, OA enhancement in the reactor peaked during night, ~12 h before the ambient OA peak. The nighttime reactor-aged OA mass peaks at approximately the same concentration as the following day's ambient OA concentration, suggesting the reactor's potential for estimating the next day's OA concentrations.

A more quantitative evaluation of this potential is discussed below (Sect. 4.1. and Figure 9). While this peak likely occurs at OH_{exp} higher than observed the following day, the similar OA mass added highlights the potential for further develop of the reactor as a predictive tool. Daytime reactor-aged OA mass shows very limited enhancement above the ambient OA mass, ~~indicating~~ suggesting that the precursors for SOA formation have been mostly depleted in ambient air. ~~At the peak of the ambient photochemical age during daytime, only small amounts of precursors are available to contribute to further SOA formation from oxidation in the reactor, likely due to previous removal by photochemical oxidation and condensation.~~The nighttime reactor-aged OA mass peaks at approximately the same concentration as the following day's ambient OA concentration, suggesting the reactor's potential for estimating the next day's OA concentrations. A more quantitative evaluation of this potential is discussed below (Sect. 4.1. and Figure 9). The fact that the inorganic components are enhanced in the reactor is not surprising but expected. SO_2 and NO_x in ambient air are expected to be oxidized to H_2SO_4 and HNO_3 by the OH in the reactor, and can then condense onto the aerosols (together with ambient NH_3 for HNO_3). See e.g. Kang et al. (2007) and Li et al. (2015) for further details. Figure 3c shows the average speciated contribution to total aerosol for ambient and the reactor (excluding dark reactor periods, "lights off" periods, periods are included only if OH_{exp} > ambient~~where OH_{exp} = ambient~~), indicating overall enhancement of all species from reactor aging with very similar composition to ambient aerosol.

Formatted: Subscript
Formatted: Subscript
Formatted: Subscript
Formatted: Subscript
Formatted: Subscript
Formatted: Subscript
Formatted: Subscript
Formatted: Subscript
Formatted: Subscript

Observations of the OA size distributions indicate reactor aging does not significantly shift the size of the accumulation mode for the average of nighttime ambient and three different reactor age ranges (age ~ ambient, 3.7 days, and 23.5 days), from 2–9 June 2010 (Fig. ~~S7~~S8). The reactor size distribution changes in intensity and shape are most pronounced during low ages (~3.7 days and lower), with an enhanced smaller size mode (d_{va} ~80 nm). While many daytime/nighttime average

size distributions and age ranges were explored, only ages at or below a few days at nighttime showed significant enhancement of small particle sizes. Highest ages (>14 days) show overall decrease in concentration across all size bins with the size of the accumulation mode unchanged from ambient within the uncertainty of the measurement. Given the high concentrations of large particles in this urban environment, we expect aging to enhance organic aerosol by condensation of semi- and low-volatile compounds on existing particles to dominate over new particle formation and growth. Reactor results are indicative of this process, although they also indicate the effect of new particle formation and/or of nanoparticle growth at lower OH exposures.

3.2 Aerosol Enhancements

Investigating reactor perturbation of ambient OA allows quantification of both relative and absolute OA changes vs. OH_{exp}. The relative OA enhancement ratio, ER_{OA} ~~= reactor OA / ambient OA~~, and the absolute OA enhancement factor, ΔOA Mass ~~= reactor OA – ambient OA~~, are plotted vs. OH_{exp} in Fig. 4a and Fig. 4b respectively for the sample period. OA mass is enhanced up to four times from ambient OA, with the majority of maximum ER_{OA} peaking around a factor of two increase. OA enhancement peaks and plateaus between 0.8–6 days of OH aging, then decreases at higher aging, eventually showing net OA loss beyond two weeks of aging. When separated into daytime and nighttime ER_{OA} and ΔOA mass (Fig. 4), the qualitative trends are the same in both cases, but OA was more enhanced from reactor aging during nighttime by 5 μg m^{-3}, or a factor of 1.7x of ambient. A smaller enhancement is observed during the day ~2 μg m^{-3}, or a factor of 1.2x of ambient, ~~. The data for greater than~~while at > 2 weeks of aging, day and night observations closely overlap~~s for day and night~~, with a decrease up to ~2.5 μg m^{-3}, or a factor of 0.5x of ambient.

The substantial difference between day- and nighttime enhancements can be explained as during the night the boundary layer is shallow and reactive precursors accumulate due to the absence of ambient photochemistry, with lower ambient photochemical ages of ~0.1 day (Hayes et al., 2015) and minimal loss mechanisms as the dominant urban VOCs do not react with O_3 or NO_3 (other than a small concentration of monoterpenes). In contrast, during the day reactive precursors in ambient air are depleted due to reaction with OH. Transport times from downtown LA, the dominant precursor source region impacting Pasadena, is ~0.5 days (Washenfelder et al., 2011; Hayes et al., 2013), with ambient photochemical ages reaching ~0.3 days. Thus most of the SOA precursors that can become SOA already have by the time the air was sampled in Pasadena and only about 20% more SOA could be produced from the precursors that remained. The trends in Fig. 4 indicate increased oxidation transitioning from a dominance of functionalization reactions and condensation at low-to-moderate exposures, to fragmentation-dominated reactions and evaporation of reaction products at the highest photochemical ages. Fragmentation can occur in the gas phase by reactions of SVOCs with OH, leading to non-condensable products and decreasing SOA formation. Fragmentation can also be due to heterogeneous oxidation of existing OA, producing more volatile species that may evaporate leading to OA mass loss. Discussion of the relative importance of these processes for this study is presented in Section 4.4 below.

3.3 Gas-Phase Observations

3.3.1 Odd Oxygen (O_x) Relation to SOA Formation

The day-night difference observed in both ER_{OA} and ΔOA mass merits examination of the relationship with ambient odd-oxygen, O_x (O_3 + NO_2). Ambient O_x correlates with freshly produced SOA in urban areas (Herndon et al., 2008; Wood et al., 2010; Hayes et al., 2013; Morino

et al., 2014; Zhang et al., 2015), both resulting from recent photochemistry. For the reactor, oxidants are generated internally and are not dependent on ambient O_x. As seen in Fig. 5, there is a steep inverse relationship between ΔOA mass and ambient O_x, at low to moderate aging (<4 days). As daytime ambient photochemical production of oxidants increases (O_x >50 ppbv), the reactor's SOA formation for moderate aging decreases to a near constant OA mass enhancement (2 μg m^{-3}). At high ages (>14 days), OA mass loss is fairly constant with ambient O_x, which is not surprising since the mechanisms responsible for OA depletion at long ages have little dependence on previous photochemical processing in the atmosphere. As O_x is not itself playing a role in reactor aging, but can be used as a proxy ambient photochemistry, ~~These~~ these results further confirm that as the degree of ambient photochemical processing of the sampled air increases (during daytime), SOA production in the reactor becomes more limited, likely due to the depletion of reactive SOA precursors in ambient air, consistent with the conclusions from Fig. 4.

Formatted: Subscript

Commented [AO1]: Check response doc

3.3.2 Further Constraints on Urban SOA Formation Timescales from OH Reactivity of Measured VOC ~~Observation~~s

To further constrain the timescales and precursors of urban SOA formation, ambient and reactor OA data are plotted together with ambient VOCs in Fig. 6. The maximum reactor OA enhancement has a similar diurnal profile to 1,3,5–trimenthylbenzene (TMB). Both TMB and OA enhancement have diurnal profiles that are out of phase with ambient SOA. In contrast, the concentration of benzene shows little correlation with reactor SOA formation in the reactor. The lifetime of TMB by reaction with OH is nearly 2 orders of magnitude shorter, τ_{OH} ~3 hours, $k_{OH} = 5.67\times10^{-11}$, than benzene, τ_{OH} ~6 days, $k_{OH} = 1.22\times10^{-12}$ (Atkinson et al., 2006). The anti-correlation of TMB and reactor enhancement in OA and ambient SOA concentrations suggests that only in the absence of

Formatted: Font: Italic

Formatted: Font: Italic

ambient photochemistry, substantial amounts of short-lived SOA precursors are present to produce most of the SOA formed in the reactor. Toluene, a VOC with a lifetime of 1.4 days and k_{OH} = 5.63×10^{-12} cm^3 ~~moelcule~~molecule$^{-1}s^{-1}$ does not have the same diurnal structure as reactor OA and TMB (Fig. ~~S8~~S9). The shape of the diurnal-scale time series in Fig. 6 and ~~S8~~ S9 can be explained as the sunrises ambient photochemistry begins at sunrise, very short lived precursors, such as TMB, begin decay rapidly due to gas-phase oxidation as well as boundary layer growth. As these gas-phase oxidation products condense, SOA forms and ambient OA reaches its daytime peak. At the daytime ambient OA peak, most of these short-lived precursors have been consumed, thus the reactor only forms an additional 1–2 μg m^{-3} of SOA as opposed to the greater than 10 μg m^{-3} possible when these~~s~~ precursors are allowed to build in a shallow boundary layer and in the absence of photochemical sinks. Note that in the afternoon the boundary layer is significantly deeper than at night, and thus the total afternoon SOA formation potential may not be that different than at night, even though the potential per unit volume of air is much smaller.

The inset in Fig. 6 is a scatter plot of maximum reactor SOA formation (per OH_{exp} cycle) vs. TMB (slope ~52, R^2=0.7). TMB's SOA yield is on the order of 10% (Cao and Jang, 2007). Thus its concentration is insufficient to explain reactor SOA formation by a factor of ~500, though it is not expected to be the sole SOA precursor. This correlation suggests species with a similar source footprint and lifetime as TMB produce most of the urban SOA. Such species likely include semivolatile and intermediate volatility precursors (S/IVOC) that are rarely measured in ambient air (Dzepina et al., 2009; Zhao et al., 2014; Hayes et al., 2015), due to the difficulty in measuring these compounds. A comparison of observed reactor SOA formation with a model that uses all the measured VOCs is discussed in section 4.3 below.

Formatted: Font: Italic

3.4 OA Chemical Composition and Evolution with Aging

The evolution of OA chemical composition upon aging has been the subject of several studies, both for ambient (Heald et al., 2010; Kroll et al., 2011; Ng et al., 2011a; Ng et al., 2011b) and reactor conditions (Kang et al., 2011; Ortega et al., 2013; Tkacik et al., 2014; Lambe et al., 2015). This evolution results in characteristic trends in specific diagrams: AMS fragments f_{44} vs. f_{43}, and H:C vs. O:C. Both diagrams are shown for the CalNex ambient and reactor data in Fig. 7. f_{44} is a tracer for aged OA (fractional organic contribution at *m/z* 44, mostly CO_2^+), while f_{43} (fractional organic contribution at *m/z* 43, mostly $C_2H_3O^+$), due to non-acid oxygenates, with some contribution from $C_3H_7^+$) is a tracer of POA and freshly formed SOA (Ng et al., 2011a). In Figure 7a, ambient and reactor data evolve consistently ~~and~~ as f_{44} ~~move up and to the left~~ increases and f_{43} decreases with aging, consistent with previous ambient field observations from multiple field campaigns (Ng et al., 2010)~~(Ng et al 2010)~~. As expected, reactor data with the highest age has the highest f_{44}. Positive Matrix Factorization (PMF) factors from Hayes et al. (2013) ~~lay~~ lie within ambient observations and data for lower OH_{exp} in the reactor. Reactor data stays within the boundary of flow reactor results from Lambe et al. (2011a) and below the location of oxalic acid, as expected.

The Van Krevelen diagram (H:C vs. O:C) is shown in Fig. 7b and demonstrates results that are very consistent to those of the previous plot. The reactor data follows a similar trend to ambient data, with slopes of -0.64 and -0.68, respectively. A slope between -1 and -0.5 is consistent with the addition of acid and alcohol functional groups without fragmentation or the addition of acid groups with carbon–carbon bond breakage (Ng et al., 2011b). The consistency of ambient and reactor OA aging suggest that the reactor produces similar SOA composition upon aging to that in the atmosphere within the LA-Basin.

Formatted: Font: Italic

Formatted: Not Superscript/ Subscript

Formatted: Font: Italic

Formatted: Font: Italic, Subscript

Reactor O:C ratios increase with age and span a wider range than ambient observations (O:C up to 1.4). While O:C (and f_{44}) continually increased with additional OH_{exp}, peak reactor OA enhancement is observed at intermediate exposures and O:C ratios (0.8–6 days and O:C ~1.10–1.25), as seen in Fig. 8a. OA mass loss, i.e. $ER_{OA} < 1$, is observed together with the highest O:C ratios at the highest ages, which suggests OA fragmentation by heterogeneous oxidation results in the highest oxygen content remaining in the aerosol. With increasing age, H:C decreases continuously with OH_{exp} (Fig. 8b), with H:C ~1.00–1.15 for the periods of maximum reactor OA enhancement. A qualitatively similar trend is observed in the reactor studies of Lambe et al. (2012) for SOA from OH oxidation of alkane precursors (Fig. 8a) although starting with lower O:C and with a steeper slope at higher ages, and also by Ortega et al. (2013) for aging of biomass burning smoke.

Average carbon oxidation state (OS_C) has been proposed as a metric to characterize the formation and evolution of OA (Kroll et al., 2011). OS_C can be approximated as ~2×O:C–H:C. Figure 8c shows OS_C vs. photochemical age for ambient and reactor data. While ambient OS_C is within the range of previous observed urban/anthropogenic OA, reactor OS_C extends this significantly up to +2.0, consistent with ambient low-volatility OA observations up to +1.9 (Kroll et al., 2011). At the same OH exposure, i.e. 8 days, ~~-~~higher OS_C is observed (~1) for conditions of high reactor SOA production (ER_{OA} ~ 2) ~~at intermediate ages~~compared to no net SOA production (ER_{OA} ~ 1, OS_C ~ 0). The highest values of OS_C are observed for the highest ages, where heterogeneous oxidation leading to OA mass loss dominates. This indicates that heterogeneous oxidation adds substantial oxygen and reduces hydrogen from molecules to the particles to increase OS_C despite overall mass loss.

Formatted: Subscript

Formatted: Subscript

Formatted: Subscript

4 Discussion

4.1 Evolution of ~~Net~~ Urban OA with Photochemical Age

The identity of the SOA precursors responsible for urban SOA formation remains unclear. Combustion emissions such as those from vehicles are thought to be a major source of urban SOA (e.g. Hayes et al., 2015), and urban non-combustion sources of SOA precursors, if important, are finely spatially intermingled with combustion sources. CO is often used as a tracer of the initial concentration of urban SOA precursors in an airmass and thus allow an implicit correction for dilution occurring in parallel with aging. For this reason, the ratio of OA to CO concentration (above background level) vs. photochemical age is often used to investigate the evolution of urban SOA (de Gouw et al., 2005; DeCarlo et al., 2010).

Fig. ure 9 shows the results of this analysis for our reactor and ambient measurements. Background CO during CalNex-LA is on average ~105 ppb (ranging from 85—125 ppb, Hayes et al., 2013). A range of ± 20 ppb uncertainty in background CO, results in an average ± 6 μg m^{-3} ppm^{-1} uncertainty in OA/ΔCO. ~~Ambient photochemical age is calculated from the VOC ratio method as in Hayes et al. (2013). Reactor total photochemical age is the sum of ambient photochemical age (of the air ingested into the reactor at each time) and reactor age. The range observed in previous field campaigns in the Northeastern US and Mexico City are shown for reference (DeCarlo et al., 2010). LA Basin outflow data are also shown, from aircraft measurements aboard the NOAA WP-3D during CalNex (Bahreini et al., 2012b), averaged for 1–2 days of photochemical age, falling in the middle of the range of previous ambient observations.~~

~~Fig. 9 shows the data averages for 7% quantiles of total photochemical age, to better illustrate the average trends of the observations without the higher noise level of 2.5 min. measurements. All~~

~~data points for the sample period are shown for ambient and reactor measurements in Fig. S9a for reference.~~ An increase in OA/ΔCO with aging is observed for ambient and reactor dark data (where reactor age = ambient photochemical age in the absence of internal reactor OH_{exp}), consistent with previous studies and as discussed in Hayes et al. (2013; 2015). ~~Reactor data are shown without and with the vapor loss correction applied (see Sect. 2.3).~~ The reactor data is consistent with SOA formation being dominated by shorter-lived precursors, as little increase in OA/ΔCO is observed after about a day of total age, consistent with the SIMPLE parameterization of urban SOA (Hodzic and Jimenez, 2011; Hayes et al., 2015).

To constrain the lifetimes of the important urban SOA precursors, the OH decays of three example gas-phase species (benzene, toluene, and 1,3,5-trimenthylbenzene (TMB)) are shown are overlaid in Fig. S10, together with data from Fig. 9 that illustrates the timescale over which OA/ΔCO increases. The correlation of different VOCs with maximum SOA formation in the reactor is shown vs. their reaction rate constants with OH (k_{OH}) in Figure 10. This analysis constrains the rate constants of the most important urban SOA precursors to the approximate $k_{OH} \sim 3–5\times10^{-11}$ cm^3 $molec^{-1}$ s^{-1}. This constraint suggests that polyalkyl monoaromatics (such as TMB), substituted polyaromatics such as alkyl naphthalenes (Phousongphouang and Arey, 2002), or large alkanes with ~23 or more carbons (Calvert et al., 2008), or branched / cyclic species of similar size are (as a group) important contributors. The latter species are semivolatile and intermediate volatility species (S/IVOCs), and thus our results suggests a very important role for such species in urban SOA formation. ~~To further illustrate the lifetimes of important urban SOA precursors, OH decay curves of gas-phase benzene, toluene, and 1,3,5-trimenthylbenzene (TMB) are overlaid in Fig. S9a with data from Fig. 9.~~ The timescale of SOA formation is in between those of TMB and toluene

Formatted: Font: Italic
Formatted: Font: Italic, Subscript
Formatted: Superscript
Formatted: Superscript
Formatted: Superscript
Formatted: Superscript

decays, mostly shorter than toluene decay and definitely shorter than benzene decay, again consistent with the previous discussion.

We note that in Fig. 9 aging of CO (decay of CO from reacting with OH in the reactor or atmosphere) was not included in the evolution of OA/ΔCO analysis, as the purpose of ΔCO is to serve as an inert tracer of the urban SOA precursors emitted into each airmass. However, when comparing with aged pollution observed in the field after e.g. a week of transport, the aging to the urban CO needs to be taken into account. This is shown in Fig. ~~S9b~~S10b, and indicates that ambient observations of very aged pollution would not show a decrease in OA/ΔCO due to photochemistry since the decreases in OA and CO at long photochemical ages have similar timescales. We note that a decrease in the OA/ΔCO ratio for ambient aged pollution may still be observed for other reasons such as wet deposition (Dunlea et al., 2009). Production of CO from urban VOCs is expected to be less than 1/10 of the directly emitted CO (Hallquist et al., 2009) and is neglected here.

4.2 ~~Fit to the Observed Ambient and Reactor~~ Parameterization of the Amount and Timescale for Urban SOA Formation~~Evolution~~

The evolution of urban SOA vs. photochemical age follows a similar trend in different field studies with a rapid increase in the first day followed by a plateau at longer ages. Previously, this evolution has been fit with the SIMPLE parameterization, a 2-parameter model in which a single VOC precursor (VOC^*) is oxidized with a single rate constant with OH to produce non-volatile SOA. This parameterization has been shown to fit ambient data as well or better than more complex models (Hodzic and Jimenez, 2011; Hayes et al., 2015). However, the evolution of OA/ΔCO ~~evolution~~ past the initial ~2 days is almost completely unconstrained by ambient observations,

due to the difficulty of identifying urban pollution-dominated air masses after advection for several days, and of determining ΔCO when it is of the order of the uncertainties in the CO background. The reactor data from our study offer a unique opportunity to extend the model fit to much longer photochemical ages. The fit in Eqn. 1 was modified from Hayes et al. (2015)'s 2-parameter model for this purpose, where (POA+BGSOA)/CO is the primary OA plus background SOA, constrained at 16 μg m^{-3} ppm^{-1} (Hayes et al., 2015), VOC^*/CO is the VOC^* emission ratio, and *t* is photochemical age, using measurements at local temperature and pressure.

$$\frac{OA}{\Delta CO} = \left\{\frac{POA + BGSOA}{CO} + \frac{VOC^*}{CO}\left[1 - e^{\left(\frac{-t}{\tau_1}\right)}\right]\right\} e^{\left(\frac{-t}{\tau_2}\right)} \qquad (1)$$

Fitting the reactor data in this way requires the addition of a 2nd timescale to account for loss of OA at long ages, as done in Eqn. 1. Fitting all ambient plus vapor loss-corrected data results in VOC*/CO = 56±5 μg m^{-3} ppm^{-1}, τ_1 = 0.3±0.1 days, and τ_2 = 50±10 days (Fig. 9, all data points, i.e. before averaged into quantiles is in Fig. ~~S9a~~S10a). In this parameterization, τ_1 is the timescale for urban SOA formation and τ_2 is the timescale for net OA mass loss due to fragmentation, likely dominated by heterogeneous oxidation. Kroll et al. (2015)'s laboratory examination of heterogeneous oxidation of OA found a volatilization lifetime of 70±20 days, supporting the 50±10 days timescales found in this work.

4.3 Comparison of Reactor output to Urban SOA Model Results

It is of interest to compare the SOA formation constrained from our reactor and ambient data to SOA models used in 3D modeling studies, as those models remain poorly constrained (e.g. Hayes et al., 2015). Here we used two of the model variants recently described in Hayes et al. (2015), and compare to our data in Fig. ~~10~~11. The first model variant is a "traditional model" with SOA

Formatted: Justified

formation from VOCs using pre-2007 yields (Koo et al., 2003), which has been shown before to underpredict urban SOA formation by over an order-of-magnitude (Dzepina et al., 2009; Morino et al., 2014; Hayes et al., 2015). This comparison is still of interest as several SOA models still use this approach (e.g. Morino et al., 2014; Baker et al., 2015; Hayes et al., 2015).

The second model variant represents SOA formation ~~from VOCs and primary~~ semivolatile and intermediate volatility precursors (P-S/IVOC; Robinson et al., 2007) in addition to VOCs, and has been shown to predict SOA formation adequately at short timescales (<1 day) but to overpredict at long ages (Dzepina et al., 2011; Hayes et al., 2015). SOA formation from VOCs uses the Tsimpidi et al. (2010) formulation, including "aging" of the SOA, and using the high NO_x yields since the observed SOA formation mostly occurs in the urban environment where RO_2 react mainly with NO (Hayes et al., 2015). SOA from P-S/IVOCs is represented using the Robinson et al. (2007) parameterization. Recent results suggest that P-S/IVOC are needed to explain SOA formation observed in ambient air during CalNex (Zhao et al., 2014; Hayes et al., 2015), consistent with other locations (Dzepina et al., 2009; Hodzic et al., 2010).

Figure ~~10a~~ 11a shows the comparison of the SOA models against our ambient and reactor results. The traditional model predicts SOA a factor of 10 lower than our observations, consistent with previous studies. The updated model performance is mixed: the magnitude of SOA formation at short times (<1 day) is somewhat slower but similar to the ambient data. SOA formation at long ages (>1 day) is significantly overpredicted by a factor of ~3. This model does not include heterogeneous oxidation reactions leading to fragmentation which could decrease predicted OA at high photochemical ages, resulting in a wider discrepancy at very long ages (>10 days). Figure ~~10b~~ 11b shows the same comparison using lower IVOCs as suggested from field measurements (Zhao et al., 2014). The same model was used, but with the initial concentrations of primary IVOCs

decreased by one-half to better match the ambient observations of Zhao et al. (2014), as described by Hayes et al. (2015). This difference is due to the different methods used to estimate the background SOA. Briefly, in this work as well as in Hayes et al. (2015), the background SOA is estimated to be equal to the minimum low-volatility oxygenated organic aerosol (LV-OOA) concentration in the diurnal cycle. Whereas in Hayes et al. (2013), the background SOA was estimated to be equal to the mean LV-OOA concentration for photochemical ages less than 1.2 h. Decreasing IVOCs brings down overall SOA predictions, increasing the discrepancy at shorter ages and still overestimating SOA concentrations compared to reactor measurements at the longest ages. This result suggests that the reduced IVOC concentrations cannot account for all model discrepancies. It is of interest to compare the reactor results with those of other SOA mechanisms in the future.

4.4 Evolution at High Photochemical Ages

The photochemical evolution of OA at long ages is of high interest as it partially controls the background of OA at remote locations where it may influence climate more strongly, due to the higher sensitivity of clouds to aerosols at low aerosol concentrations (Reutter et al., 2009). Heald et al. (2011) noted that a process that consumed OA with a timescale of ~10 days was needed in order to avoid overpredictions of OA in remote air. Heterogeneous oxidation is thought to play an important role for long photochemical ages, while being too slow to compete at timescales of a day or so (DeCarlo et al., 2008; George and Abbatt, 2010). Fig. ~~11a~~ 12a compares our CalNex results to heterogeneous OH oxidation of ambient air from George and Abbatt (2010) using a similar oxidation flow reactor (Toronto Photo-Oxidation Tube, TPOT), but with gas-phase SOA precursors removed by a denuder. Note that no SOA formation is observed for the George and Abbatt case due to the use of a denuder, and thus only the data for $ER_{OA} < 1$ can be approximately

compared. The two datasets show a similar trend with the start of a net decrease around 2 weeks of oxidation and a similar evolution. A decrease in SOA yields at high ages (>7 days) was also observed by Lambe et al. (2012), in experiments where SOA was formed from gaseous precursors. Note that the George and Abbatt (2010) vs. Lambe et al. (2012) studies are qualitatively different, and thus the explanations of the decrease in OA at high ages may be different. George and Abbatt (2010) started their oxidation experiment with particles only, after removing gases with a denuder. Any decreases in OA in their study must result from heterogeneous oxidation. The Lambe et al. (2012) study started with gas-phase precursors only and no particles. Thus the reduction in SOA at high OH_{exp} may be due to either gas-phase fragmentation of condensable species, so that SOA is never formed, or to formation of SOA followed by its heterogeneous oxidation and revolatilization. Results in Fig. S7 suggest that gas-phase oxidation would prevent the formation of SOA, and thus the second explanation is more likely. ~~However it is likely that the decrease in that study is dominated by gas-phase fragmentation of condensable species leading to lack of SOA formation, rather than by SOA formation followed by its heterogeneous oxidation (e.g. Fig. S6).~~

To evaluate directly whether heterogeneous oxidation could explain the gain of oxygen observed in the aerosol, we follow the method outlined in appendix A of DeCarlo et al. (2008). Fig. ~~S10~~ S11 shows the ratio of the gain of oxygen of OA observed in the reactor (ΔOxygen in OA = $O_{atoms,\ reactor} - O_{atoms,\ ambient}$) to the total number of OH collisions with OA in the reactor, plotted vs. total photochemical age. Heterogeneous oxidation calculations use surface-weighted diameter calculated from the peak of the mass distribution and estimated particle density from AMS components (DeCarlo et al., 2004), assume every collision results in reaction (γ = 1). If it is assumed that each OH collision with OA results in one O atom addition, the number of O atoms added is underpredicted by a factor of ~~7~~5 at ages ~ 1 day, decreasing to a factor of 2 at ~ 10 days,

Formatted: Subscript

Formatted: Subscript

Formatted: Subscript

and lower values at high ages (> 10 days). This analysis supports that heterogeneous oxidation is not dominant in contributing to SOA mass at low-to-intermediate ages, but it likely plays a role in OA evolution at the highest photochemical ages in the reactor.~~shows an estimate of the total number of OH collisions with OA in the reactor vs. total photochemical age. Heterogeneous oxidation calculations use volume equivalent diameter (d_{ve}) of 285 nm(DeCarlo et al., 2004) as calculated using the peak of the mass distribution and estimated particle density from AMS components, assume every collision results in reaction (γ = 1). The measured net oxygen added (ΔOxygen in OA = $O_{atoms,reactor}$ – $O_{atoms,ambient}$) vs. OH_{exp}, is also shown. If it is assumed that each OH collision with OA results in one O atom addition, the number of O atoms added is underpredicted by a factor of 10 at ages ~ 1 day, decreasing to a factor of 2 at ~10 days, and lower values at high ages (>10 days). This analysis supports that heterogeneous oxidation is not dominant in forming SOA at low-to-intermediate ages, but it likely plays a role in OA evolution at the highest photochemical ages in the reactor.~~

An alternative explanation for the loss of OA at high photochemical ages is that the reaction of semivolatile gas species with OH (leading to fragmentation and thus non-condensing species) can lead to OA evaporation as the semivolatile species in the particles evaporate to re-establish equilibrium partitioning. However, most of OA has too low volatility to evaporate in response to the removal of semivolatile species from the gas phase. Fig. ~~S11~~ S12 shows the volatility distribution estimated for CalNex OA using concurrent thermal denuder measurements (Huffman et al., 2008; Faulhaber et al., 2009). As observed in other locations (Cappa and Jimenez, 2010), only ~20% of the OA is susceptible of evaporation upon removal of the gas phase. Losing ~60% of the OA would be the equivalent of heating to 100˚C in a thermal denuder. Thus, there is not enough semivolatile material available to account for that degree of loss observed in our reactor

measurements. We note that some models predict SOA that is too volatile (Dzepina et al., 2009), and if applied in a flow reactor context they may wrongly predict a large effect from semivolatile evaporation. Additionally, timescales for ambient OA evaporation upon removal of gas-phase organics from field measurements has been shown to be slow and size dependent, with fast evaporation up to only ~20% of OA mass happening on the order of ~100 min, followed by much slower evaporation of the order of days (Vaden et al., 2011). Given the short residence time utilized in the reactor during this study (< 5 minutes), there is not significant time to allow for substantial repartitioning of OA in equilibrium with semivolatile gas-phase organics.

4.5 Comparison to a recent Reactor Study in a Tunnel

It is of interest to compare the evolution of urban SOA vs. photochemical age determined in this work with a recently published study with a similar flow reactor in a vehicle tunnel in Pittsburgh, PA (Tkacik et al., 2014). Whether urban SOA is formed predominantly from vehicle emissions has been the subject of recent debate (Ensberg et al., 2014). The data are compared in Fig. ~~11b~~ 12b as SOA/ΔCO, where ambient POA and background OA have been subtracted from our reactor data to compare to Tkacik et al. (2014)'s SOA-only measurement. Since the tunnel data has not been corrected for vapor losses in the reactor, we only show uncorrected CalNex reactor data for this comparison.

The tunnel experiment shows qualitatively similar results, with an initial increase to a peak of the same order, followed by a decrease in SOA/ΔCO at high ages. The initial SOA rise and peak occur at higher OH_{exp} than observed in CalNex ambient data and in previous ambient urban studies, as well as our flow reactor data. The difference at low ages between the tunnel and the other studies may be due to several reasons:

(1) Possible OH_{exp} overestimation in the tunnel study. OH_{exp} in flow reactors can be reduced by 1-2 orders of magnitude by high levels of OH reactivity from high concentrations of very fresh emissions, such as those present in the tunnel environment (Li et al., 2015; Peng et al., 2015). OH_{exp} was corrected for OH suppression in the tunnel study using laboratory experiments with NO levels similar to the tunnel. However, the OH reactivity of NO_x is expected to decay much faster than that of VOCs and their reaction products. Thus the OH suppression in the tunnel study was likely underestimated (Peng et al., 2015) as OH suppression from VOCs was not considered. Since OH suppression is largest at low OH_{exp} that effect may account for the deviation observed at low ages while having a much smaller effect on the tunnel data at high ages.

(2) There may be substantial losses of semivolatiles in the inlet of the tunnel study. In contrast, our flow reactor was operated without an inlet to minimize the loss of semivolatiles, based on an observation in a previous study of a substantial reduction in SOA formation when any inlet or an inlet plate was used (Ortega et al., 2013). Since semivolatile primary species are larger molecules with faster OH rate constants (Ziemann and Atkinson, 2012), that could explain the lack of SOA formation at ages below a day, compared to the large amount of SOA formed for those ages in the ambient CalNex observations (Hayes et al., 2013; 2015). However the fact that the magnitude of eventual SOA formation is larger in the tunnel study argues against this possibility.

(3) It may appear at first that the tunnel SOA may have have been dominated by RO_2+NO, compared to RO_2+HO_2 for our ambient air results, thus making the results less comparable. However, while the initial NO levels in the tunnel may be high, the lifetime of NO under the conditions of the OFR is typically very low (Li et al., 2015). O_3 levels in OFR185 are typically 1–25 ppm, which result in NO lifetimes of 0.1–2 s. Since HO_2 levels are greatly enhanced by the reactor chemistry, the majority of the RO_2 radicals are still expected to react via RO_2 + HO_2 under

Formatted: Subscript
Formatted: Subscript
Formatted: Subscript
Formatted: Subscript
Formatted: Subscript
Formatted: Subscript
Formatted: Subscript
Formatted: Subscript

the tunnel conditions, similar to our study. The model of Peng et al. (2015) was used to estimate the fraction of RO_2 reacting with NO vs. HO_2 for the tunnel study. At the point of peak SOA production we estimate that 81% of the RO_2 radicals are reacting with HO_2 and 19% with NO. Therefore the chemistry of the OFR in the tunnel study is proceeding mostly through the HO_2 channel, similar to our ambient study.

(4) A difference between the studies that may explain somewhat higher SOA formation in the tunnel study is the larger partitioning of semivolatile species, given the higher OA concentrations (~50 μg m^{-3} in the tunnel vs ~15 μg m^{-3} for our study). However this effect is estimated to be a factor of ~1.5 for the aromatic and alkane precursors that are thought to dominate SOA formation from vehicle emissions (Barsanti et al., 2013), and ~~would~~it ~~go in the opposite direction than~~reduces the difference observed here, ~~and~~ thus ~~it does not impact~~further supporting our conclusions.

~~However the fact that the magnitude of eventual SOA formation is larger in the tunnel study argues against this possibility.~~ Thus it is most likely that the observed difference between the tunnel and our study is due to overestimation of OH_{exp} at lower ages in the tunnel study. We have used the model of Peng et al. (2015) to estimate the corrected OH_{exp} under the tunnel conditions. The corrected curve is also shown in Fig. 12b, and shows much improved agreement with our urban air observations.

A recent study examining the ambient SOA results from CalNex concluded that either vehicle emissions are not the dominant source of SOA in the LA Basin, or that the ambient SOA mass yields are much larger than what has been derived experimentally (Ensberg et al., 2014). Given the similar magnitude and timing (after correction for OH suppression) of SOA formation in the tunnel vs. ambient data and the fact that most urban CO arises from motor vehicles, ~~as well as the~~

Formatted: Subscript
Formatted: Subscript
Formatted: Subscript
Formatted: Subscript
Formatted: Subscript
Formatted: Superscript
Formatted: Superscript

likely overestimation of OH_{exp} at low ages in the tunnel study, the combination of both studies strongly suggests that motor vehicles are the dominant source of urban SOA, and that the SOA yields from vehicle emissions are much larger than estimated from measured VOCs as by Ensberg et al. (2014). The contribution of typically unmeasured S/IVOCs to SOA may explain the missing vehicle SOA, as discussed in section 4.3.

5 Summary and Conclusions

Real-time measurement of SOA formation and OA aging was carried out with a photochemical oxidation flow reactor coupled to an AMS and SMPS during the CalNex field campaign and targeted urban emissions. This work represents the first applications of an oxidation flow reactor to investigate SOA formation from ambient urban air, to our knowledge. Continuous ambient air sampling through the reactor provides complementary information to the analysis of ambient data at the site, and provides constraints on the evolution of urban SOA at long ages that are very difficult to observe with ambient measurements. Additionally, these uninterrupted reactor measurements over a two-week period allowed for observations over a prolonged period of stagnant air accumulating urban emissions.

OA enhancement peaked between 0.8–6 days of atmospheric equivalent aging (OH_{exp} = 1.0–5.2×10^{11} molec. cm^{-3} s). Reactor OA mass showed net destruction decreasing below ambient concentrations after two weeks of atmospheric equivalent aging (OH_{exp} above 2×10^{12} molec. cm^{-3} s) suggesting a shift from chemistry dominated by functionalization/condensation to one dominated by heterogeneous oxidation leading to fragmentation/evaporation, but with functionalization still occurring. Comparison to reactor experiments of heterogeneous oxidation of ambient air shows similar trends to those observed for high ages in this study. High OA

799 enhancement was observed at night (ER_{OA} ~2, delta OA ~5μg/m^3) with reactor-aged OA mass
800 peaking at concentrations similar to peak daytime ambient OA mass. Reactor-derived OA mass
801 enhancement correlates with 1,3,5-trimethylbenzene, and has an inverse relationship with O_x and
802 ambient OOA, suggesting that short-lived precursors (τ_{OH} ~ few hours) dominate SOA formation
803 in the LA-Basin.

804 The chemical evolution of OA in the reactor was examined with a Van Krevelen diagram (H:C vs.
805 O:C). Reactor-aged OA produces a similar slope (~ -0.65) to that observed in ambient OA, thus is
806 consistent with the reactor producing similar functionalization to ambient oxidation. While total
807 OA mass was observed to decrease at very high OH exposures, O:C continued to increase.
808 Oxidation state of carbon peaked at high values (OS_C ~2 at highest OH_{exp}), similar to ambient
809 observations of low volatility OA.

810 Modeling results indicate predicted maximum SOA from traditional models is a factor of 10 less
811 than the maximum OA mass enhancement observed from aging ambient air in the reactor,
812 consistent with previous comparisons using ambient data. Updated VBS-based models including
813 both VOC and S/IVOC overpredict SOA formation by a factor of 2–3 at intermediate to high ages.
814 If the IVOC emissions are reduced by a factor of 2 in the updated model to fit recent CalNex
815 observations, the discrepancy between model and observation is reduced but these models cannot
816 capture the reduction of SOA mass concentration that is observed with the OFR at longer OH
817 exposures.

818 Evolution of the ratio of OA/ΔCO vs. photochemical age shows the reactor produces results
819 consistent with the ambient data. At ages beyond those reliably observed for ambient OA, the
820 reactor observations show a leveling and then decrease in OA/ΔCO. A fit of this data results in a

timescale of SOA formation ~0.3 days and fragmentation-dominated heterogeneous oxidation and net mass loss with a timescale of ~50 days. The fit derived in this work may be useful in future studies, e.g. as a check on proposed model-parameterizations of urban SOA formation. Comparison to a similar reactor experiment aging vehicular emissions in a tunnel shows consistent results with our study, ~~especially if~~once a likely overestimation of OH_{exp} at low ages in the tunnel is taken into account. The combination of both studies strongly suggests that vehicle emissions do dominate urban SOA formation and their SOA formation potential is higher than when only VOCs are considered.

This study shows that oxidation flow reactors are useful tools as part of ambient field studies, as they allow real-time measurement of SOA formation potential and oxidation across a wide range of photochemical ages. These results help constrain SOA models not only for the growth phase of the SOA but also for the decay phase, when further aging removes SOA mass. Future studies should apply this technique in other cities and other environments such as forested regions and the outflow from polluted continents, in order to further constrain the SOA formation potential and timescales for different sources and regions.

Acknowledgements

We thank CARB 08-319 and 11-305, DOE (BER, ASP Program) DE-SC0006035 and DE-SC0011105, NOAA NA13OAR4310063, and NSF AGS-1243354 and AGS-1360834 for partial support of this work. AMO and PLH acknowledge fellowships from the DOE SCGP Fellowship Program (ORAU, ORISE) and the CIRES Visiting Fellowship program, respectively. WHB acknowledges the support by NSF (grant ATM-0919079). We thank Phil Stevens' research group

(Indiana University) for use of OH reactivity data from the CalNex Pasadena ground site. We are grateful to Jochen Stutz (UCLA), John Seinfeld (Caltech), and Jason Surratt (UNC-Chapel Hill) for co-organization of the CalNex Supersite, and to CARB for supporting the infrastructure at the site. We also thank John S. Holloway (NOAA) for providing CO data, Roya Bahreini (University of California-Riverside), and Ann M. Middlebrook (NOAA) for providing OA data from the NOAA WP-3D. We thank Carlos Martinez (Univ. Jaen) for useful discussions about CFD modeling of the OFR.

References

Aiken, A. C., DeCarlo, P. F., Kroll, J. H., Worsnop, D. R., Huffman, J. A., Docherty, K. S., Ulbrich, I. M., Mohr, C., Kimmel, J. R., Sueper, D., Sun, Y., Zhang, Q., Trimborn, A., Northway, M., Ziemann, P. J., Canagaratna, M. R., Onasch, T. B., Alfarra, M. R., Prevot, A. S. H., Dommen, J., Duplissy, J., Metzger, A., Baltensperger, U., and Jimenez, J. L.: O/C and OM/OC Ratios of Primary, Secondary, and Ambient Organic Aerosols with High-Resolution Time-of-Flight Aerosol Mass Spectrometry, Environmental Science & Technology, 42, 4478-4485, 10.1021/es703009q, 2008.

Atkinson, R., Baulch, D. L., Cox, R. A., Crowley, J. N., Hampson, R. F., Hynes, R. G., Jenkin, M. E., Rossi, M. J., Troe, J., and Subcommittee, I.: Evaluated kinetic and photochemical data for atmospheric chemistry: Volume II: gas phase reactions of organic species, Atmos. Chem. Phys., 6, 3625-4055, 10.5194/acp-6-3625-2006, 2006.

Bahreini, R., Middlebrook, A. M., Brock, C. A., de Gouw, J. A., McKeen, S. A., Williams, L. R., Daumit, K. E., Lambe, A. T., Massoli, P., Canagaratna, M. R., Ahmadov, R., Carrasquillo, A. J., Cross, E. S., Ervens, B., Holloway, J. S., Hunter, J. F., Onasch, T. B., Pollack, I. B., Roberts, J. M., Ryerson, T. B., Warneke, C., Davidovits, P., Worsnop, D. R., and Kroll, J. H.: Mass Spectral Analysis of Organic Aerosol Formed Downwind of the Deepwater Horizon Oil Spill: Field Studies and Laboratory Confirmations, Environmental Science & Technology, 46, 8025-8034, 10.1021/es301691k, 2012a.

Bahreini, R., Middlebrook, A. M., de Gouw, J. A., Warneke, C., Trainer, M., Brock, C. A., Stark, H., Brown, S. S., Dube, W. P., Gilman, J. B., Hall, K., Holloway, J. S., Kuster, W. C., Perring, A. E., Prevot, A. S. H., Schwarz, J. P., Spackman, J. R., Szidat, S., Wagner, N. L., Weber, R. J., Zotter, P., and Parrish, D. D.: Gasoline emissions dominate over diesel in formation of secondary organic aerosol mass, Geophysical Research Letters, 39, 10.1029/2011gl050718, 2012b.

Baker, K. R., Carlton, A. G., Kleindienst, T. E., Offenberg, J. H., Beaver, M. R., Gentner, D. R., Goldstein, A. H., Hayes, P. L., Jimenez, J. L., Gilman, J. B., de Gouw, J. A., Woody, M. C., Pye, H. O. T., Kelly, J. T., Lewandowski, M., Jaoui, M., Stevens, P. S., Brune, W. H., Lin, Y. H., Rubitschun, C. L., and Surratt, J. D.: Gas and aerosol carbon in California: comparison of measurements and model predictions in Pasadena and Bakersfield, Atmos. Chem. Phys., 15, 5243-5258, 10.5194/acp-15-5243-2015, 2015.

Barsanti, K. C., Carlton, A. G., and Chung, S. H.: Analyzing experimental data and model parameters: implications for predictions of SOA using chemical transport models, Atmos. Chem. Phys., 13, 12073-12088, 10.5194/acp-13-12073-2013, 2013.

Borbon, A., Gilman, J. B., Kuster, W. C., Grand, N., Chevaillier, S., Colomb, A., Dolgorouky, C., Gros, V., Lopez, M., Sarda-Esteve, R., Holloway, J., Stutz, J., Petetin, H., McKeen, S., Beekmann, M., Warneke, C., Parrish, D. D., and de Gouw, J. A.: Emission ratios of anthropogenic volatile organic compounds in northern mid-latitude megacities: Observations versus emission inventories in Los Angeles and Paris, Journal of Geophysical Research: Atmospheres, 118, 2041-2057, 10.1002/jgrd.50059, 2013.

Bruns, E. A., El Haddad, I., Keller, A., Klein, F., Kumar, N. K., Pieber, S. M., Corbin, J. C., Slowik, J. G., Brune, W. H., Baltensperger, U., and Prévôt, A. S. H.: Inter-comparison of laboratory smog chamber and flow reactor systems on organic aerosol yield and composition, Atmos. Meas. Tech. Discuss., 8, 309-352, 10.5194/amtd-8-309-2015, 2015.

Calvert, J. G., Derwent, R. G., Orlando, J. J., Tyndall, G. S., and Wallington, T. J.: Mechanisms of Atmospheric Oxidation of the Alkanes, Oxford University Press, 2008.

Canagaratna, M. R., Jayne, J. T., Jimenez, J. L., Allan, J. D., Alfarra, M. R., Zhang, Q., Onasch, T. B., Drewnick, F., Coe, H., Middlebrook, A., Delia, A., Williams, L. R., Trimborn, A. M., Northway, M. J., DeCarlo, P. F., Kolb, C. E., Davidovits, P., and Worsnop, D. R.: Chemical and microphysical characterization of ambient aerosols with the aerodyne aerosol mass spectrometer, Mass Spectrom Rev, 26, 185-222, Doi 10.1002/Mas.20115, 2007.

Canagaratna, M. R., Jimenez, J. L., Kroll, J. H., Chen, Q., Kessler, S. H., Massoli, P., Hildebrandt Ruiz, L., Fortner, E., Williams, L. R., Wilson, K. R., Surratt, J. D., Donahue, N. M., Jayne, J. T., and Worsnop, D. R.: Elemental ratio measurements of organic compounds using aerosol mass spectrometry: characterization, improved calibration, and implications, Atmos. Chem. Phys., 15, 253-272, 10.5194/acp-15-253-2015, 2015.

Cao, G., and Jang, M.: Effects of particle acidity and UV light on secondary organic aerosol formation from oxidation of aromatics in the absence of NOx, Atmospheric Environment, 41, 7603-7613, http://dx.doi.org/10.1016/j.atmosenv.2007.05.034, 2007.

Cappa, C. D., and Jimenez, J. L.: Quantitative estimates of the volatility of ambient organic aerosol, Atmos. Chem. Phys., 10, 5409-5424, 10.5194/acp-10-5409-2010, 2010.

Cubison, M. J., Ortega, A. M., Hayes, P. L., Farmer, D. K., Day, D., Lechner, M. J., Brune, W. H., Apel, E., Diskin, G. S., Fisher, J. A., Fuelberg, H. E., Hecobian, A., Knapp, D. J., Mikoviny, T., Riemer, D., Sachse, G. W., Sessions, W., Weber, R. J., Weinheimer, A. J., Wisthaler, A., and Jimenez, J. L.: Effects of aging on organic aerosol from open biomass burning smoke in aircraft and laboratory studies, Atmos Chem Phys, 11, 12049-12064, 2011.

de Gouw, J., and Jimenez, J. L.: Organic Aerosols in the Earth's Atmosphere, Environmental Science & Technology, 43, 7614-7618, 10.1021/es9006004, 2009.

de Gouw, J. A., Middlebrook, A. M., Warneke, C., Goldan, P. D., Kuster, W. C., Roberts, J. M., Fehsenfeld, F. C., Worsnop, D. R., Canagaratna, M. R., Pszenny, A. A. P., Keene, W. C., Marchewka, M., Bertman, S. B., and Bates, T. S.: Budget of organic carbon in a polluted atmosphere: Results from the New England Air Quality Study in 2002, J. Geophys. Res., 110, D16305, 10.1029/2004jd005623, 2005.

DeCarlo, P. F., Slowik, J. G., Worsnop, D. R., Davidovits, P., and Jimenez, J. L.: Particle morphology and density characterization by combined mobility and aerodynamic diameter measurements. Part 1: Theory, Aerosol Sci Tech, 38, 1185-1205, 2004.

DeCarlo, P. F., Kimmel, J. R., Trimborn, A., Northway, M. J., Jayne, J. T., Aiken, A. C., Gonin, M., Fuhrer, K., Horvath, T., Docherty, K., Worsnop, D. R., and Jimenez, J. L.: Field-Deployable, High-Resolution, Time-of-Flight Aerosol Mass Spectrometer, Analytical Chemistry, 78, 8281-8289, 2006.

DeCarlo, P. F., Dunlea, E. J., Kimmel, J. R., Aiken, A. C., Sueper, D., Crounse, J., Wennberg, P. O., Emmons, L., Shinozuka, Y., Clarke, A., Zhou, J., Tomlinson, J., Collins, D. R., Knapp, D., Weinheimer, A. J., Montzka, D. D., Campos, T., and Jimenez, J. L.: Fast airborne aerosol size and chemistry measurements above Mexico City and Central Mexico during the MILAGRO campaign, Atmos. Chem. Phys., 8, 4027-4048, 10.5194/acp-8-4027-2008, 2008.

DeCarlo, P. F., Ulbrich, I. M., Crounse, J., de Foy, B., Dunlea, E. J., Aiken, A. C., Knapp, D., Weinheimer, A. J., Campos, T., Wennberg, P. O., and Jimenez, J. L.: Investigation of the sources and processing of organic aerosol over the Central Mexican Plateau from aircraft measurements during MILAGRO, Atmos. Chem. Phys., 10, 5257-5280, 10.5194/acp-10-5257-2010, 2010.

929 Docherty, K. S., Stone, E. A., Ulbrich, I. M., DeCarlo, P. F., Snyder, D. C., Schauer, J. J., Peltier, R. E., Weber, R.
930 J., Murphy, S. M., Seinfeld, J. H., Grover, B. D., Eatough, D. J., and Jimenez, J. L.: Apportionment of Primary and
931 Secondary Organic Aerosols in Southern California during the 2005 Study of Organic Aerosols in Riverside
932 (SOAR-1), Environmental Science & Technology, 42, 7655-7662, 10.1021/es8008166, 2008.

933 Docherty, K. S., Aiken, A. C., Huffman, J. A., Ulbrich, I. M., DeCarlo, P. F., Sueper, D., Worsnop, D. R., Snyder,
934 D. C., Peltier, R. E., Weber, R. J., Grover, B. D., Eatough, D. J., Williams, B. J., Goldstein, A. H., Ziemann, P. J.,
935 and Jimenez, J. L.: The 2005 Study of Organic Aerosols at Riverside (SOAR-1): instrumental intercomparisons and
936 fine particle composition, Atmos. Chem. Phys., 11, 12387-12420, 10.5194/acp-11-12387-2011, 2011.

937 Donahue, N. M., Robinson, A. L., Stanier, C. O., and Pandis, S. N.: Coupled Partitioning, Dilution, and Chemical
938 Aging of Semivolatile Organics, Environmental Science & Technology, 40, 2635-2643, 10.1021/es052297c, 2006.

939 Donahue, N. M., Chuang, W., Epstein, S. A., Kroll, J. H., Worsnop, D. R., Robinson, A. L., Adams, P. J., and
940 Pandis, S. N.: Why do organic aerosols exist? Understanding aerosol lifetimes using the two-dimensional volatility
941 basis set, Environ Chem, 10, 151-157, Doi 10.1071/En13022, 2013.

942 Drewnick, F., Hings, S. S., DeCarlo, P., Jayne, J. T., Gonin, M., Fuhrer, K., Weimer, S., Jimenez, J. L., Demerjian,
943 K. L., Borrmann, S., and Worsnop, D. R.: A New Time-of-Flight Aerosol Mass Spectrometer (TOF-AMS)—
944 Instrument Description and First Field Deployment, Aerosol Science and Technology, 39, 637-658,
945 10.1080/02786820500182040, 2005.

946 Dunlea, E. J., DeCarlo, P. F., Aiken, A. C., Kimmel, J. R., Peltier, R. E., Weber, R. J., Tomlinson, J., Collins, D. R.,
947 Shinozuka, Y., McNaughton, C. S., Howell, S. G., Clarke, A. D., Emmons, L. K., Apel, E. C., Pfister, G. G., van
948 Donkelaar, A., Martin, R. V., Millet, D. B., Heald, C. L., and Jimenez, J. L.: Evolution of Asian aerosols during
949 transpacific transport in INTEX-B, Atmos. Chem. Phys., 9, 7257-7287, 10.5194/acp-9-7257-2009, 2009.

950 Dzepina, K., Volkamer, R. M., Madronich, S., Tulet, P., Ulbrich, I. M., Zhang, Q., Cappa, C. D., Ziemann, P. J., and
951 Jimenez, J. L.: Evaluation of recently-proposed secondary organic aerosol models for a case study in Mexico City,
952 Atmos. Chem. Phys., 9, 5681-5709, 10.5194/acp-9-5681-2009, 2009.

953 Dzepina, K., Cappa, C. D., Volkamer, R. M., Madronich, S., DeCarlo, P. F., Zaveri, R. A., and Jimenez, J. L.:
954 Modeling the Multiday Evolution and Aging of Secondary Organic Aerosol During MILAGRO 2006,
955 Environmental Science & Technology, 45, 3496-3503, 10.1021/es103186f, 2011.

956 Ensberg, J. J., Hayes, P. L., Jimenez, J. L., Gilman, J. B., Kuster, W. C., de Gouw, J. A., Holloway, J. S., Gordon, T.
957 D., Jathar, S., Robinson, A. L., and Seinfeld, J. H.: Emission factor ratios, SOA mass yields, and the impact of
958 vehicular emissions on SOA formation, Atmos. Chem. Phys., 14, 2383-2397, 10.5194/acp-14-2383-2014, 2014.

959 Ervens, B., Turpin, B. J., and Weber, R. J.: Secondary organic aerosol formation in cloud droplets and aqueous
960 particles (aqSOA): a review of laboratory, field and model studies, Atmos. Chem. Phys., 11, 11069-11102,
961 10.5194/acp-11-11069-2011, 2011.

962 Faulhaber, A. E., Thomas, B. M., Jimenez, J. L., Jayne, J. T., Worsnop, D. R., and Ziemann, P. J.: Characterization
963 of a thermodenuder-particle beam mass spectrometer system for the study of organic aerosol volatility and
964 composition, Atmos. Meas. Tech., 2, 15-31, 10.5194/amt-2-15-2009, 2009.

965 George, I. J., and Abbatt, J. P. D.: Heterogeneous oxidation of atmospheric aerosol particles by gas-phase radicals,
966 Nat Chem, 2, 713-722, 2010.

967 Hallquist, M., Wenger, J. C., Baltensperger, U., Rudich, Y., Simpson, D., Claeys, M., Dommen, J., Donahue, N. M.,
968 George, C., Goldstein, A. H., Hamilton, J. F., Herrmann, H., Hoffmann, T., Iinuma, Y., Jang, M., Jenkin, M. E.,
969 Jimenez, J. L., Kiendler-Scharr, A., Maenhaut, W., McFiggans, G., Mentel, T. F., Monod, A., Prévôt, A. S. H.,
970 Seinfeld, J. H., Surratt, J. D., Szmigielski, R., and Wildt, J.: The formation, properties and impact of secondary
971 organic aerosol: current and emerging issues, Atmos. Chem. Phys., 9, 5155-5236, 10.5194/acp-9-5155-2009, 2009.

972 Hayes, P. L., Ortega, A. M., Cubison, M. J., Froyd, K. D., Zhao, Y., Cliff, S. S., Hu, W. W., Toohey, D. W., Flynn,
973 J. H., Lefer, B. L., Grossberg, N., Alvarez, S., Rappenglück, B., Taylor, J. W., Allan, J. D., Holloway, J. S., Gilman,
974 J. B., Kuster, W. C., de Gouw, J. A., Massoli, P., Zhang, X., Liu, J., Weber, R. J., Corrigan, A. L., Russell, L. M.,
975 Isaacman, G., Worton, D. R., Kreisberg, N. M., Goldstein, A. H., Thalman, R., Waxman, E. M., Volkamer, R., Lin,
976 Y. H., Surratt, J. D., Kleindienst, T. E., Offenberg, J. H., Dusanter, S., Griffith, S., Stevens, P. S., Brioude, J.,
977 Angevine, W. M., and Jimenez, J. L.: Organic aerosol composition and sources in Pasadena, California, during the
978 2010 CalNex campaign, Journal of Geophysical Research: Atmospheres, 118, 9233-9257, 10.1002/jgrd.50530,
979 2013.

980 Hayes, P. L., Carlton, A. G., Baker, K. R., Ahmadov, R., Washenfelder, R. A., Alvarez, S., Rappenglück, B.,
981 Gilman, J. B., Kuster, W. C., de Gouw, J. A., Zotter, P., Prévôt, A. S. H., Szidat, S., Kleindienst, T. E., Offenberg, J.
982 H., Ma, P. K., and Jimenez, J. L.: Modeling the formation and aging of secondary organic aerosols in Los Angeles
983 during CalNex 2010, Atmos. Chem. Phys., 15, 5773-5801, 10.5194/acp-15-5773-2015, 2015.

984 Heald, C. L., Kroll, J. H., Jimenez, J. L., Docherty, K. S., DeCarlo, P. F., Aiken, A. C., Chen, Q., Martin, S. T.,
985 Farmer, D. K., and Artaxo, P.: A simplified description of the evolution of organic aerosol composition in the
986 atmosphere, Geophys. Res. Lett., 37, L08803, 10.1029/2010gl042737, 2010.

987 Heald, C. L., Coe, H., Jimenez, J. L., Weber, R. J., Bahreini, R., Middlebrook, A. M., Russell, L. M., Jolleys, M.,
988 Fu, T. M., Allan, J. D., Bower, K. N., Capes, G., Crosier, J., Morgan, W. T., Robinson, N. H., Williams, P. I.,
989 Cubison, M. J., DeCarlo, P. F., and Dunlea, E. J.: Exploring the vertical profile of atmospheric organic aerosol:
990 comparing 17 aircraft field campaigns with a global model, Atmos. Chem. Phys., 11, 12673-12696, 10.5194/acp-11-
991 12673-2011, 2011.

992 Herndon, S. C., Onasch, T. B., Wood, E. C., Kroll, J. H., Canagaratna, M. R., Jayne, J. T., Zavala, M. A., Knighton,
993 W. B., Mazzoleni, C., Dubey, M. K., Ulbrich, I. M., Jimenez, J. L., Seila, R., de Gouw, J. A., de Foy, B., Fast, J.,
994 Molina, L. T., Kolb, C. E., and Worsnop, D. R.: Correlation of secondary organic aerosol with odd oxygen in
995 Mexico City, Geophysical Research Letters, 35, L15804, 10.1029/2008gl034058, 2008.

996 Hersey, S. P., Craven, J. S., Schilling, K. A., Metcalf, A. R., Sorooshian, A., Chan, M. N., Flagan, R. C., and
997 Seinfeld, J. H.: The Pasadena Aerosol Characterization Observatory (PACO): chemical and physical analysis of the
998 Western Los Angeles basin aerosol, Atmos. Chem. Phys., 11, 7417-7443, 10.5194/acp-11-7417-2011, 2011.

999 Hodzic, A., Jimenez, J. L., Madronich, S., Canagaratna, M. R., DeCarlo, P. F., Kleinman, L., and Fast, J.: Modeling
1000 organic aerosols in a megacity: potential contribution of semi-volatile and intermediate volatility primary organic
1001 compounds to secondary organic aerosol formation, Atmos. Chem. Phys., 10, 5491-5514, 10.5194/acp-10-5491-
1002 2010, 2010.

1003 Hodzic, A., and Jimenez, J. L.: Modeling anthropogenically controlled secondary organic aerosols in a megacity: a
1004 simplified framework for global and climate models, Geosci. Model Dev., 4, 901-917, 10.5194/gmd-4-901-2011,
1005 2011.

1006 Huffman, J. A., Ziemann, P. J., Jayne, J. T., Worsnop, D. R., and Jimenez, J. L.: Development and Characterization
1007 of a Fast-Stepping/Scanning Thermodenuder for Chemically-Resolved Aerosol Volatility Measurements, Aerosol
1008 Science and Technology, 42, 395-407, 10.1080/02786820802104981, 2008.

1009 Huffman, J. A., Docherty, K. S., Aiken, A. C., Cubison, M. J., Ulbrich, I. M., DeCarlo, P. F., Sueper, D., Jayne, J.
1010 T., Worsnop, D. R., Ziemann, P. J., and Jimenez, J. L.: Chemically-resolved aerosol volatility measurements from
1011 two megacity field studies, Atmos Chem Phys, 9, 7161-7182, 2009.

1012 Jimenez, J. L., Canagaratna, M. R., Donahue, N. M., Prevot, A. S. H., Zhang, Q., Kroll, J. H., DeCarlo, P. F., Allan,
1013 J. D., Coe, H., Ng, N. L., Aiken, A. C., Docherty, K. S., Ulbrich, I. M., Grieshop, A. P., Robinson, A. L., Duplissy,
1014 J., Smith, J. D., Wilson, K. R., Lanz, V. A., Hueglin, C., Sun, Y. L., Tian, J., Laaksonen, A., Raatikainen, T.,
1015 Rautiainen, J., Vaattovaara, P., Ehn, M., Kulmala, M., Tomlinson, J. M., Collins, D. R., Cubison, M. J., Dunlea, E.
1016 J., Huffman, J. A., Onasch, T. B., Alfarra, M. R., Williams, P. I., Bower, K., Kondo, Y., Schneider, J., Drewnick, F.,
1017 Borrmann, S., Weimer, S., Demerjian, K., Salcedo, D., Cottrell, L., Griffin, R., Takami, A., Miyoshi, T.,
1018 Hatakeyama, S., Shimono, A., Sun, J. Y., Zhang, Y. M., Dzepina, K., Kimmel, J. R., Sueper, D., Jayne, J. T.,
1019 Herndon, S. C., Trimborn, A. M., Williams, L. R., Wood, E. C., Middlebrook, A. M., Kolb, C. E., Baltensperger, U.,
1020 and Worsnop, D. R.: Evolution of Organic Aerosols in the Atmosphere, Science, 326, 1525-1529, 2009.

1021 Kang, E., Root, M. J., Toohey, D. W., and Brune, W. H.: Introducing the concept of Potential Aerosol Mass (PAM),
1022 Atmos. Chem. Phys., 7, 5727-5744, 10.5194/acp-7-5727-2007, 2007.

1023 Kang, E., Toohey, D. W., and Brune, W. H.: Dependence of SOA oxidation on organic aerosol mass concentration
1024 and OH exposure: experimental PAM chamber studies, Atmos. Chem. Phys., 11, 1837-1852, 10.5194/acp-11-1837-
1025 2011, 2011.

1026 Knote, C., Hodzic, A., and Jimenez, J. L.: The effect of dry and wet deposition of condensable vapors on secondary
1027 organic aerosols concentrations over the continental US, Atmos. Chem. Phys., 15, 1-18, 10.5194/acp-15-1-2015,
1028 2015.

1029 Koo, B., Ansari, A. S., and Pandis, S. N.: Integrated approaches to modeling the organic and inorganic atmospheric
1030 aerosol components, Atmospheric Environment, 37, 4757-4768, http://dx.doi.org/10.1016/j.atmosenv.2003.08.016,
1031 2003.

1032 Kroll, J. H., Donahue, N. M., Jimenez, J. L., Kessler, S. H., Canagaratna, M. R., Wilson, K. R., Altieri, K. E.,
1033 Mazzoleni, L. R., Wozniak, A. S., Bluhm, H., Mysak, E. R., Smith, J. D., Kolb, C. E., and Worsnop, D. R.: Carbon
1034 oxidation state as a metric for describing the chemistry of atmospheric organic aerosol, Nat Chem, 3, 133-139, 2011.

1035 Kroll, J. H., Lim, C. Y., Kessler, S. H., and Wilson, K. R.: Heterogeneous Oxidation of Atmospheric Organic
1036 Aerosol: Kinetics of Changes to the Amount and Oxidation State of Particle-Phase Organic Carbon, The Journal of
1037 Physical Chemistry A, 119, 10767-10783, 10.1021/acs.jpca.5b06946, 2015.

1038 Lambe, A. T., Ahern, A. T., Williams, L. R., Slowik, J. G., Wong, J. P. S., Abbatt, J. P. D., Brune, W. H., Ng, N. L.,
1039 Wright, J. P., Croasdale, D. R., Worsnop, D. R., Davidovits, P., and Onasch, T. B.: Characterization of aerosol
1040 photooxidation flow reactors: heterogeneous oxidation, secondary organic aerosol formation and cloud condensation
1041 nuclei activity measurements, Atmos. Meas. Tech., 4, 445-461, 10.5194/amt-4-445-2011, 2011a.

1042 Lambe, A. T., Onasch, T. B., Massoli, P., Croasdale, D. R., Wright, J. P., Ahern, A. T., Williams, L. R., Worsnop,
1043 D. R., Brune, W. H., and Davidovits, P.: Laboratory studies of the chemical composition and cloud condensation
1044 nuclei (CCN) activity of secondary organic aerosol (SOA) and oxidized primary organic aerosol (OPOA), Atmos.
1045 Chem. Phys., 11, 8913-8928, 10.5194/acp-11-8913-2011, 2011b.

1046 Lambe, A. T., Onasch, T. B., Croasdale, D. R., Wright, J. P., Martin, A. T., Franklin, J. P., Massoli, P., Kroll, J. H.,
1047 Canagaratna, M. R., Brune, W. H., Worsnop, D. R., and Davidovits, P.: Transitions from Functionalization to

Fragmentation Reactions of Laboratory Secondary Organic Aerosol (SOA) Generated from the OH Oxidation of Alkane Precursors, Environmental Science & Technology, 46, 5430–5437, 10.1021/es300274t, 2012.

Lambe, A. T., Chhabra, P. S., Onasch, T. B., Brune, W. H., Hunter, J. F., Kroll, J. H., Cummings, M. J., Brogan, J. F., Parmar, Y., Worsnop, D. R., Kolb, C. E., and Davidovits, P.: Effect of oxidant concentration, exposure time, and seed particles on secondary organic aerosol chemical composition and yield, Atmos. Chem. Phys., 15, 3063-3075, 10.5194/acp-15-3063-2015, 2015.

Li, R., Palm, B. B., Borbon, A., Graus, M., Warneke, C., Ortega, A. M., Day, D. A., Brune, W. H., Jimenez, J. L., and de Gouw, J. A.: Laboratory Studies on Secondary Organic Aerosol Formation from Crude Oil Vapors, Environmental Science & Technology, 47, 12566-12574, 10.1021/es402265y, 2013.

Li, R., Palm, B. B., Ortega, A. M., Hlywiak, J. A., Hu, W., Peng, Z., Day, D. A., Knote, C., Brune, W. H., de Gouw, J. A., and Jimenez, J. L.: Modeling the Radical Chemistry in an Oxidation Flow Reactor: Radical Formation and Recycling, Sensitivities, and OH Exposure Estimation Equation, The Journal of Physical Chemistry A, 10.1021/jp509534k, 2015.

Mao, J., Ren, X., Brune, W. H., Olson, J. R., Crawford, J. H., Fried, A., Huey, L. G., Cohen, R. C., Heikes, B., Singh, H. B., Blake, D. R., Sachse, G. W., Diskin, G. S., Hall, S. R., and Shetter, R. E.: Airborne measurement of OH reactivity during INTEX-B, Atmos. Chem. Phys., 9, 163-173, 10.5194/acp-9-163-2009, 2009.

Massoli, P., Lambe, A. T., Ahern, A. T., Williams, L. R., Ehn, M., Mikkilä, J., Canagaratna, M. R., Brune, W. H., Onasch, T. B., Jayne, J. T., Petäjä, T., Kulmala, M., Laaksonen, A., Kolb, C. E., Davidovits, P., and Worsnop, D. R.: Relationship between aerosol oxidation level and hygroscopic properties of laboratory generated secondary organic aerosol (SOA) particles, Geophys. Res. Lett., 37, L24801, 10.1029/2010gl045258, 2010.

McMurry, P. H., and Grosjean, D.: Gas and aerosol wall losses in Teflon film smog chambers, Environmental Science & Technology, 19, 1176-1182, 10.1021/es00142a006, 1985.

Morino, Y., Tanabe, K., Sato, K., and Ohara, T.: Secondary organic aerosol model intercomparison based on secondary organic aerosol to odd oxygen ratio in Tokyo, Journal of Geophysical Research: Atmospheres, 119, 2014JD021937, 10.1002/2014jd021937, 2014.

Murphy, D. M., Cziczo, D. J., Froyd, K. D., Hudson, P. K., Matthew, B. M., Middlebrook, A. M., Peltier, R. E., Sullivan, A., Thomson, D. S., and Weber, R. J.: Single-particle mass spectrometry of tropospheric aerosol particles, Journal of Geophysical Research: Atmospheres, 111, D23S32, 10.1029/2006jd007340, 2006.

Myhre, G., Shindell, D., Bréon, F.-M., Collins, W., Fuglestvedt, J., Huang, J., Koch, D., Lamarque, J.-F., Lee, D., Mendoza, B., Nakajima, T., Robock, A., Stephens, G., Takemura, T., and Zhang, H.: Anthropogenic and Natural Radiative Forcing, in Climate Change 2013: The Physical Science Basis. Contribution of Working Group I to the Fifth Assessment Report of the Intergovernmental Panel on Climate Change, edited by V. B. and P. M. M. Stocker, T.F., D. Qin, G.-K. Plattner, M. Tignor, S.K. Allen, J. Boschung, A. Nauels, Y. Xia, Cambridge University Press, Cambridge, United Kingdom and New York, NY, USA., 2013.

Ng, N. L., Canagaratna, M. R., Zhang, Q., Jimenez, J. L., Tian, J., Ulbrich, I. M., Kroll, J. H., Docherty, K. S., Chhabra, P. S., Bahreini, R., Murphy, S. M., Seinfeld, J. H., Hildebrandt, L., Donahue, N. M., DeCarlo, P. F., Lanz, V. A., Prévôt, A. S. H., Dinar, E., Rudich, Y., and Worsnop, D. R.: Organic aerosol components observed in Northern Hemispheric datasets from Aerosol Mass Spectrometry, Atmos. Chem. Phys., 10, 4625-4641, 10.5194/acp-10-4625-2010, 2010.

1087 Ng, N. L., Canagaratna, M. R., Jimenez, J. L., Chhabra, P. S., Seinfeld, J. H., and Worsnop, D. R.: Changes in
1088 organic aerosol composition with aging inferred from aerosol mass spectra, Atmos Chem Phys, 11, 6465-6474,
1089 2011a.

1090 Ng, N. L., Canagaratna, M. R., Jimenez, J. L., Zhang, Q., Ulbrich, I. M., and Worsnop, D. R.: Real-Time Methods
1091 for Estimating Organic Component Mass Concentrations from Aerosol Mass Spectrometer Data, Environ Sci
1092 Technol, 45, 910-916, 2011b.

1093 Ortega, A. M., Day, D. A., Cubison, M. J., Brune, W. H., Bon, D., de Gouw, J. A., and Jimenez, J. L.: Secondary
1094 organic aerosol formation and primary organic aerosol oxidation from biomass-burning smoke in a flow reactor
1095 during FLAME-3, Atmos. Chem. Phys., 13, 11551-11571, 10.5194/acp-13-11551-2013, 2013.

1096 Palm, B. B., Campuzano-Jost, P., Ortega, A. M., Day, D. A., Kaser, L., Jud, W., Karl, T., Hansel, A., Hunter, J. F.,
1097 Cross, E. S., Kroll, J. H., Peng, Z., Brune, W. H., and Jimenez, J. L.: In situ secondary organic aerosol formation
1098 from ambient pine forest air using an oxidation flow reactor, Atmos. Chem. Phys., 16, 2943-2970, 10.5194/acp-16-
1099 2943-2016, 2016.

1100 Pankow, J. F.: An absorption model of gas/particle partitioning of organic compounds in the atmosphere,
1101 Atmospheric Environment, 28, 185-188, http://dx.doi.org/10.1016/1352-2310(94)90093-0, 1994.

1102 Peng, Z., Day, D. A., Stark, H., Li, R., Lee-Taylor, J., Palm, B. B., Brune, W. H., and Jimenez, J. L.: HOx radical
1103 chemistry in oxidation flow reactors with low-pressure mercury lamps systematically examined by modeling,
1104 Atmos. Meas. Tech., 8, 4863-4890, 10.5194/amt-8-4863-2015, 2015.

1105 Peng, Z., Day, D. A., Ortega, A. M., Palm, B. B., Hu, W. W., Stark, H., Li, R., Tsigaridis, K., Brune, W. H., and
1106 Jimenez, J. L.: Non-OH chemistry in oxidation flow reactors for the study of atmospheric chemistry systematically
1107 examined by modeling, Atmos. Chem. Phys., 2016, 4283-4305, 10.5194/acp-16-4283-2016, 2016.

1108 Phousongphouang, P. T., and Arey, J.: Rate Constants for the Gas-Phase Reactions of a Series of Alkylnaphthalenes
1109 with the OH Radical, Environ Sci Technol, 36, 1947-1952, 10.1021/es011434c, 2002.

1110 Pirjola, L., Kulmala, M., Wilck, M., Bischoff, A., Stratmann, F., and Otto, E.: Formation of Sulphuric Acid Aerosols
1111 and Cloud COndensation Nuclei: An Expresion for Significant Nucleation and Model Comprarison, Journal of
1112 Aerosol Science, 30, 1079-1094, http://dx.doi.org/10.1016/S0021-8502(98)00776-9, 1999.

1113 Pope, C. A., Burnett, R. T., Thun, M. J., Calle, E. E., Krewski, D., Ito, K., and Thurston, G. D.: Lung cancer,
1114 cardiopulmonary mortality, and long-term exposure to fine particulate air pollution, Jama-Journal of the American
1115 Medical Association, 287, 1132-1141, 10.1001/jama.287.9.1132, 2002.

1116 Reutter, P., Su, H., Trentmann, J., Simmel, M., Rose, D., Gunthe, S. S., Wernli, H., Andreae, M. O., and Pöschl, U.:
1117 Aerosol- and updraft-limited regimes of cloud droplet formation: influence of particle number, size and
1118 hygroscopicity on the activation of cloud condensation nuclei (CCN), Atmos. Chem. Phys., 9, 7067-7080,
1119 10.5194/acp-9-7067-2009, 2009.

1120 Robinson, A. L., Donahue, N. M., Shrivastava, M. K., Weitkamp, E. A., Sage, A. M., Grieshop, A. P., Lane, T. E.,
1121 Pierce, J. R., and Pandis, S. N.: Rethinking Organic Aerosols: Semivolatile Emissions and Photochemical Aging,
1122 Science, 315, 1259-1262, 10.1126/science.1133061, 2007.

1123 Ryerson, T. B., Andrews, A. E., Angevine, W. M., Bates, T. S., Brock, C. A., Cairns, B., Cohen, R. C., Cooper, O.
1124 R., de Gouw, J. A., Fehsenfeld, F. C., Ferrare, R. A., Fischer, M. L., Flagan, R. C., Goldstein, A. H., Hair, J. W.,
1125 Hardesty, R. M., Hostetler, C. A., Jimenez, J. L., Langford, A. O., McCauley, E., McKeen, S. A., Molina, L. T.,
1126 Nenes, A., Oltmans, S. J., Parrish, D. D., Pederson, J. R., Pierce, R. B., Prather, K., Quinn, P. K., Seinfeld, J. H.,
1127 Senff, C. J., Sorooshian, A., Stutz, J., Surratt, J. D., Trainer, M., Volkamer, R., Williams, E. J., and Wofsy, S. C.:
1128 The 2010 California Research at the Nexus of Air Quality and Climate Change (CalNex) field study, Journal of
1129 Geophysical Research: Atmospheres, 118, 5830-5866, 10.1002/jgrd.50331, 2013.

1130 Tkacik, D. S., Lambe, A. T., Jathar, S., Li, X., Presto, A. A., Zhao, Y., Blake, D., Meinardi, S., Jayne, J. T., Croteau,
1131 P. L., and Robinson, A. L.: Secondary Organic Aerosol Formation from in-Use Motor Vehicle Emissions Using a
1132 Potential Aerosol Mass Reactor, Environmental Science & Technology, 48, 11235-11242, 10.1021/es502239v,
1133 2014.

1134 Tsimpidi, A. P., Karydis, V. A., Zavala, M., Lei, W., Molina, L., Ulbrich, I. M., Jimenez, J. L., and Pandis, S. N.:
1135 Evaluation of the volatility basis-set approach for the simulation of organic aerosol formation in the Mexico City
1136 metropolitan area, Atmos. Chem. Phys., 10, 525-546, 10.5194/acp-10-525-2010, 2010.

1137 Vaden, T. D., Imre, D., Beránek, J., Shrivastava, M., and Zelenyuk, A.: Evaporation kinetics and phase of laboratory
1138 and ambient secondary organic aerosol, Proceedings of the National Academy of Sciences, 108, 2190-2195,
1139 10.1073/pnas.1013391108, 2011.

1140 Volkamer, R., Jimenez, J. L., San Martini, F., Dzepina, K., Zhang, Q., Salcedo, D., Molina, L. T., Worsnop, D. R.,
1141 and Molina, M. J.: Secondary organic aerosol formation from anthropogenic air pollution: Rapid and higher than
1142 expected, Geophys. Res. Lett., 33, L17811, 10.1029/2006gl026899, 2006.

1143 Warneke, C., de Gouw, J. A., Edwards, P. M., Holloway, J. S., Gilman, J. B., Kuster, W. C., Graus, M., Atlas, E.,
1144 Blake, D., Gentner, D. R., Goldstein, A. H., Harley, R. A., Alvarez, S., Rappenglueck, B., Trainer, M., and Parrish,
1145 D. D.: Photochemical aging of volatile organic compounds in the Los Angeles basin: Weekday-weekend effect,
1146 Journal of Geophysical Research: Atmospheres, 118, 5018-5028, 10.1002/jgrd.50423, 2013.

1147 Washenfelder, R. A., Young, C. J., Brown, S. S., Angevine, W. M., Atlas, E. L., Blake, D. R., Bon, D. M., Cubison,
1148 M. J., de Gouw, J. A., Dusanter, S., Flynn, J., Gilman, J. B., Graus, M., Griffith, S., Grossberg, N., Hayes, P. L.,
1149 Jimenez, J. L., Kuster, W. C., Lefer, B. L., Pollack, I. B., Ryerson, T. B., Stark, H., Stevens, P. S., and Trainer, M.
1150 K.: The glyoxal budget and its contribution to organic aerosol for Los Angeles, California, during CalNex 2010,
1151 Journal of Geophysical Research: Atmospheres, 116, D00V02, 10.1029/2011jd016314, 2011.

1152 Watson, J. G.: Visibility: Science and regulation, Journal of the Air & Waste Management Association, 52, 628-713,
1153 2002.

1154 Wood, E. C., Canagaratna, M. R., Herndon, S. C., Onasch, T. B., Kolb, C. E., Worsnop, D. R., Kroll, J. H.,
1155 Knighton, W. B., Seila, R., Zavala, M., Molina, L. T., DeCarlo, P. F., Jimenez, J. L., Weinheimer, A. J., Knapp, D.
1156 J., Jobson, B. T., Stutz, J., Kuster, W. C., and Williams, E. J.: Investigation of the correlation between odd oxygen
1157 and secondary organic aerosol in Mexico City and Houston, Atmos. Chem. Phys., 10, 8947-8968, 10.5194/acp-10-
1158 8947-2010, 2010.

1159 Zhang, Q., Jimenez, J. L., Canagaratna, M. R., Allan, J. D., Coe, H., Ulbrich, I., Alfarra, M. R., Takami, A.,
1160 Middlebrook, A. M., Sun, Y. L., Dzepina, K., Dunlea, E., Docherty, K., DeCarlo, P. F., Salcedo, D., Onasch, T.,
1161 Jayne, J. T., Miyoshi, T., Shimono, A., Hatakeyama, S., Takegawa, N., Kondo, Y., Schneider, J., Drewnick, F.,
1162 Borrmann, S., Weimer, S., Demerjian, K., Williams, P., Bower, K., Bahreini, R., Cottrell, L., Griffin, R. J.,
1163 Rautiainen, J., Sun, J. Y., Zhang, Y. M., and Worsnop, D. R.: Ubiquity and dominance of oxygenated species in

organic aerosols in anthropogenically-influenced Northern Hemisphere midlatitudes, Geophys. Res. Lett., 34, L13801, 10.1029/2007gl029979, 2007.

Zhang, Q. J., Beekmann, M., Freney, E., Sellegri, K., Pichon, J. M., Schwarzenboeck, A., Colomb, A., Bourrianne, T., Michoud, V., and Borbon, A.: Formation of secondary organic aerosol in the Paris pollution plume and its impact on surrounding regions, Atmos. Chem. Phys. Discuss., 15, 8073-8111, 10.5194/acpd-15-8073-2015, 2015.

Zhang, X., Cappa, C. D., Jathar, S. H., McVay, R. C., Ensberg, J. J., Kleeman, M. J., and Seinfeld, J. H.: Influence of vapor wall loss in laboratory chambers on yields of secondary organic aerosol, Proceedings of the National Academy of Sciences, 111, 5802-5807, 10.1073/pnas.1404727111, 2014.

Zhao, Y., Hennigan, C. J., May, A. A., Tkacik, D. S., de Gouw, J. A., Gilman, J. B., Kuster, W. C., Borbon, A., and Robinson, A. L.: Intermediate-Volatility Organic Compounds: A Large Source of Secondary Organic Aerosol, Environmental Science & Technology, 48, 13743-13750, 10.1021/es5035188, 2014.

Ziemann, P. J., and Atkinson, R.: Kinetics, products, and mechanisms of secondary organic aerosol formation, Chemical Society Reviews, 41, 6582-6605, 10.1039/c2cs35122f, 2012.

Figure Captions

Figure 1: (a) Schematic of the oxidation flow reactor (OFR) coupled to an Aerodyne high-resolution time-of-flight aerosol mass spectrometer (AMS), scanning-mobility particle sizer (SMPS), and ozone (O_3) monitor. An ambient sampling line allowed for direct sampling of ambient air. Computer-controlled switching valves allowed for sampling in alternation from the reactor and ambient lines. Voltage supplied to UV lamps were varied via programmable computer control to step through oxidant concentrations in the reactor. Ring flow was via a PTFE Teflon line and was used for gas-phase measurements. Center flow was a copper line that continuously pulled the sample for aerosol analysis. **(b)** Photograph of the reactor with a sun / rain cover and of the ambient aerosol inlet (right, covered by foil insulation) on the trailer roof during CalNex. **(c)** Photograph of the sampling site showing the different trailers and inlets. The OFR can be seen on top of the leftmost trailer, next to the AMS and SMPS ambient inlets.

Figure 2: A typical ~~oxidant cycle showing~~OFR sampling cycle, including four steps in lamp intensity in the reactor. Top: reactor oxidant concentrations. Bottom: OA concentration for ambient and reactor output sampling. The UV light intensity color scale corresponds to the sum of the AC voltages applied to the two lamps in the reactor. Only at the highest lamp setting are both lamps on, while at lower settings only one of the lamps is used.

Figure 3: (a) Time series of reactor and ambient species mass concentrations during the sampling period. **(b)** Zoom on the time series of the species mass concentrations for one representative day. Daytime and nighttime are marked. **(c)** Average fraction contribution from organic, nitrate, sulfate, ammonium, and chloride to total AMS aerosol measurements for ambient and reactor (excluding dark reactor, "lights off" periods, i.e. periods are included only if OH_{exp} > ambient). The pie chart areas are proportional to the total mass concentrations.

Formatted: Font: Bold

Formatted: Subscript

Figure 4: (a) Relative OA enhancement (ER_{OA} = reactor OA / ambient OA) vs.estimated reactor photochemical age for the sampling period. **(b)** Absolute OA mass concentration enhancement (ΔOA Mass = reactor OA - ambient OA) versus photochemical age. The data has been averaged into 6% quantiles for day and night measurements, with vertical error bars indicating standard errors.

Figure 5: Reactor OA mass enhancement vs. ambient O_x, (odd oxygen; O_3+NO_2) for all data in ~3.7 and ~23.5 day reactor age ranges during the sample period, colored by nighttime and daytime. Average for 10% quantiles are shown for ~3.7 days and ~23.5 days of photochemical age, with error bars indicating standard errors. Note that ambient O_x is not itself playing a role in reactor aging, but rather is a proxy for ambient photochemistry.

Formatted: Subscript

Figure 6: Times series of benzene, 1,3,5-trimethylbenzene, ambient total oxygenated organic aerosol (OOA), reactor organic mass enhancement, and maximum reactor organic mass enhancement. Inset is a scatter plot of maximum reactor OA mass enhancement (for each OH_{exp} cycle) vs. ambient 1,3,5-trimethylbenzene, with a linear ODR regression fit.

Figure 7: (a) Fractional contribution of *m/z* 44 (f_{44}) vs. *m/z* 43 (f_{43}) to OA for the ambient and reactor data in this work. The region of ambient observations from Ng et al. (2011b), and for reactor laboratory observations and oxalic acid from Lambe et al. (2011a) are shown. **(b)** Van Krevelen diagram for ambient and reactor measurements for the sampling period. Functionalization slopes from Heald et al. (2010), and oxidation state from Kroll et al. (2011) are shown for reference. Elemental analysis has been calculated with the Improved-Ambient method from Canagaratna et al. (2015). Reactor measurements are colored by total photochemical age in days (at OH = 1.5×10^6 molec. cm^{-3}) and ambient PMF-derived HOA, SV- and LV-OOA factors are shown from Hayes et al. (2013).

Figure 8: (a) Oxygen-to-carbon (O:C) and **(b)** hydrogen-to-carbon (H:C) elemental ratios for OA mass measured from the reactor vs. total photochemical age in days (at OH = 1.5×10^6 molec. cm^{-3}). Results using similar reactors for alkane oxidation from Lambe et al. (2012), and for aging of biomass burning smoke (Ortega et al., 2013) are also shown. **(c)** Average oxidation state (OS_C= 2O:C – H:C) vs. OH_{exp}. Data are colored by the relative organic enhancement (ER_{OA} = reactor OA / ambient OA).

Figure 9: Ratio of OA to excess carbon monoxide (above background levels) vs. total photochemical age in days (at OH = 1.5×10^6 molec. cm^{-3}) for ambient and reactor data, with vertical error bars indicating standard errors. Also shown in the value for LA Basin outflow from aircraft measurements from the NOAA WP-3D during CalNex (Bahreini et al., 2012b). See Hayes et al. (2013) for a discussion of the determination of CO background levels. Averages for quantiles of ambient (7%), reactor (7%), reactor dark (25%, internal OH_{exp}= 0) and reactor vapor loss-corrected (12%) data are shown. A fit to reactor data is also shown, including background (BG) SOA, and primary organic aerosol (POA; (see text for details). Results from field studies in

the northeastern US and Mexico City are shown in the background (DeCarlo et al., 2010). Note that the LVOC loss correction can only be applied when reactor output OA is larger than ambient OA, which reduces the number of datapoints.

Figure 10: R^2 between the concentrations of different VOCs and the maximum amount of SOA formation in the OFR, plotted vs. the reaction rate constant of each VOC with OH (k_{OH}).

Figure ~~10~~11: Comparison of reactor data with model results for evolution of OA/ΔCO vs. total photochemical age in days (at OH = 1.5×10^6 molec. cm^{-3}) with **(a)** traditional SOA formation model, high NO_x Robinson + Tsimpidi model from Hayes et al. (2015). Also shown is the summary of urban aged ratios from de Gouw and Jimenez (2009). **(b)** High NO_x Robinson + Tsimpidi model from Hayes et al. (2015) run with one-half IVOCs per the results of Zhao et al. (2014). (POA+BGSOA)/ΔCO is 21 μg m^{-3} ppm^{-1}, which somewhat is higher than the value of 16 μg m^{-3} ppm^{-1} previously reported by Hayes et al. (2013). ~~This difference is due to the different methods used to estimate the background SOA. Briefly, in this work as well as in Hayes et al. (2015), the background SOA is estimated to be equal to the minimum low-volatility oxygenated organic aerosol (LV-OOA) concentration in the diurnal cycle. Whereas in Hayes et al. (2013), the background SOA was estimated to be equal to the mean LV-OOA concentration for photochemical ages less than 1.2 h.~~

Figure ~~11~~12: (a) Relative organic aerosol enhancement (ER_{OA}) from all reactor data in this study (including 6% quantiles), with vertical error bars indicating standard errors, and from a heterogeneous oxidation study (George and Abbatt, 2010) plotted vs. total photochemical age in days (at OH = 1.5×10^6 molec. cm^{-3}). **(b)** SOA/ΔCO vs. photochemical age for our study and for aging of vehicle exhaust with a similar reactor at a tunnel near Pittsburgh, PA (Tkacik et al., 2014). Results from field studies in the northeastern US and Mexico City are shown in the background (DeCarlo et al., 2010).

Formatted: Font: Bold
Formatted: Superscript
Formatted: Font: Italic
Formatted: Font: Italic, Subscript

Figure 1.

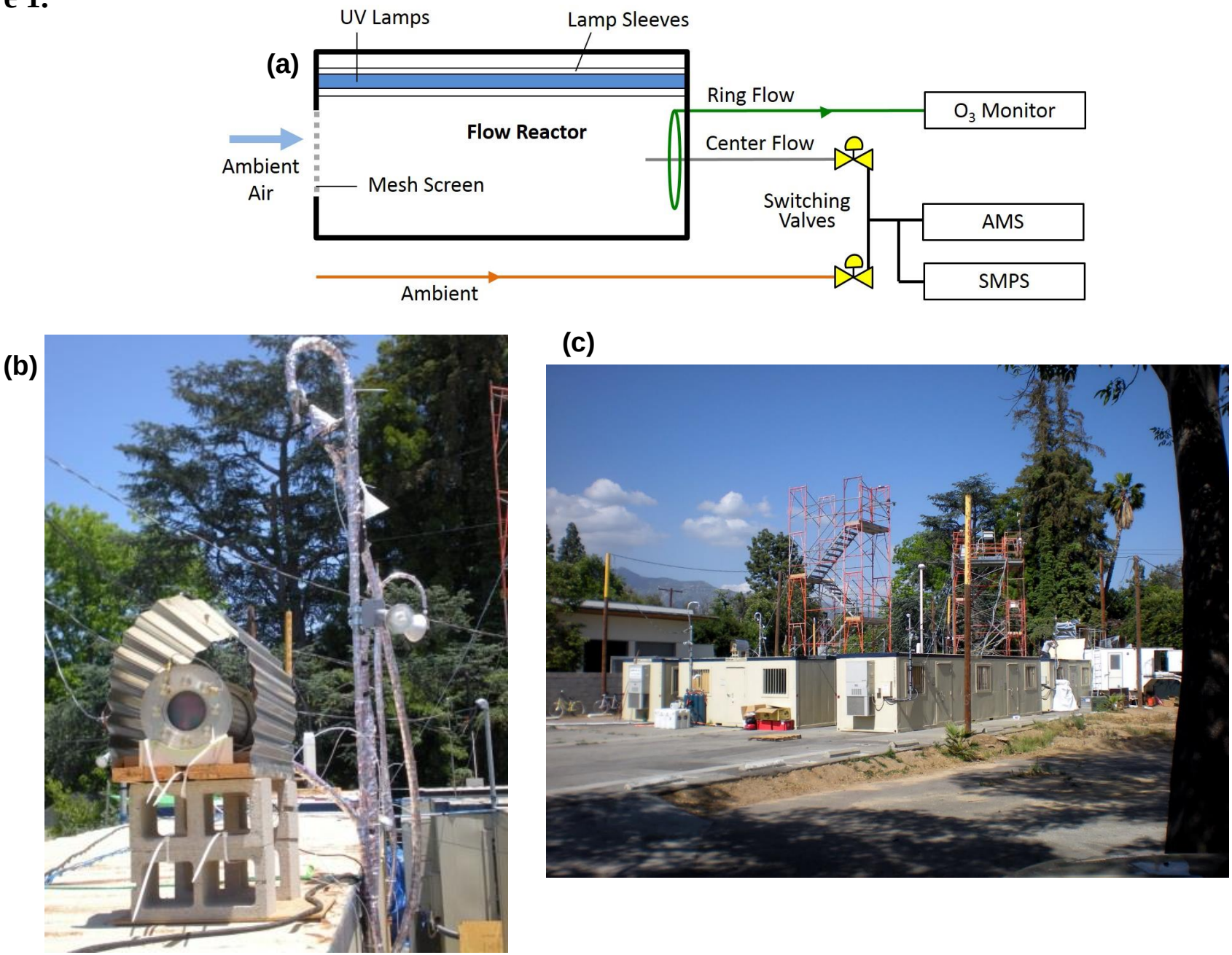
(a)
UV Lamps
Lamp Sleeves
Flow Reactor
Ambient Air
Mesh Screen
Ring Flow
O_3 Monitor
Center Flow
Switching Valves
AMS
SMPS
Ambient
(b)
(c)

Figure 2.

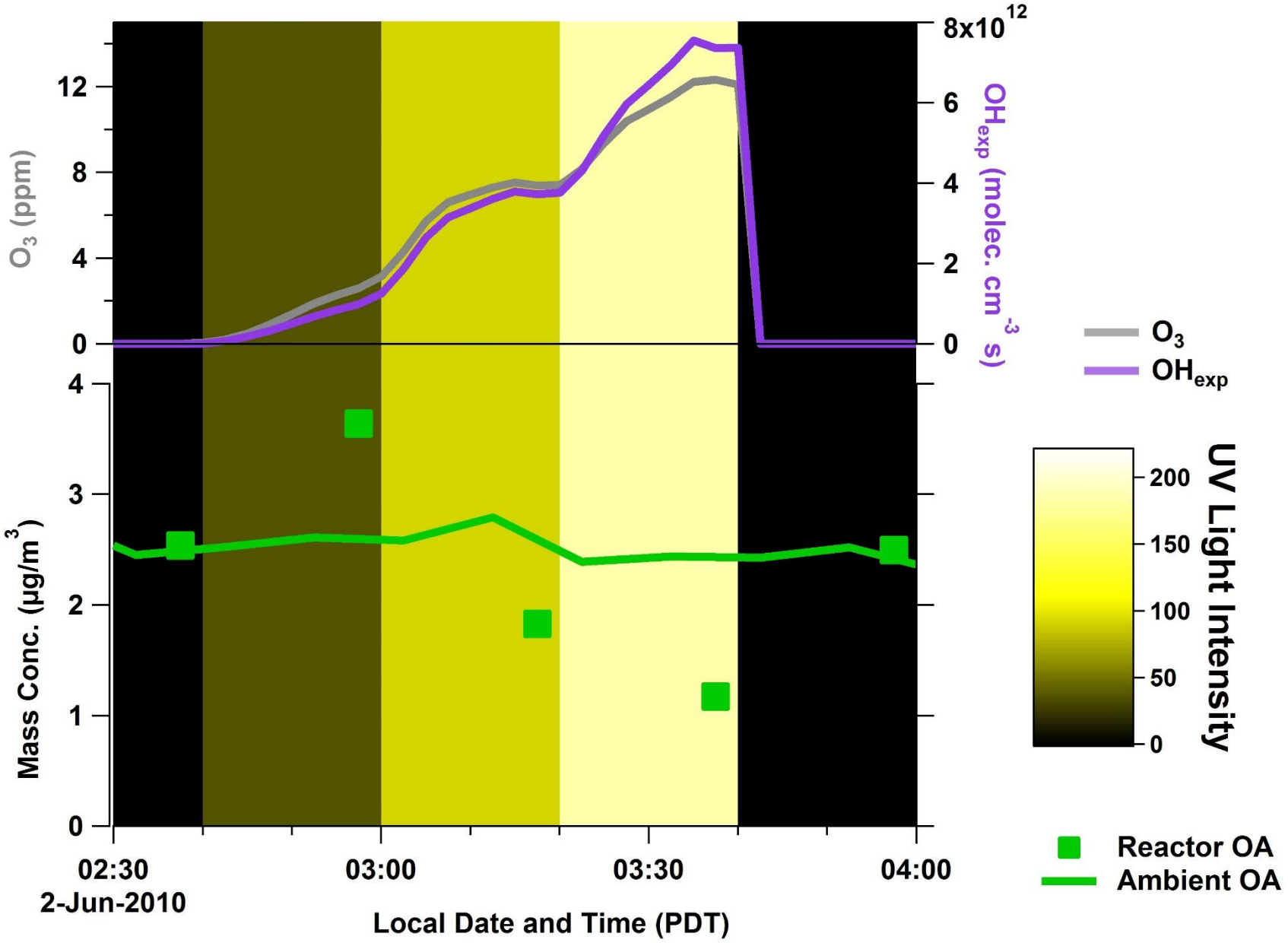
8x10^12
12
6
8
4
4
2
0
0
O3 (ppm)
OHexp (molec. cm-3 s)
O3
OHexp
4
3
2
1
0
Mass Conc. (µg/m3)
200
150
100
50
0
UV Light Intensity
Reactor OA
Ambient OA
02:30
2-Jun-2010
03:00
03:30
04:00
Local Date and Time (PDT)

Figure 3.

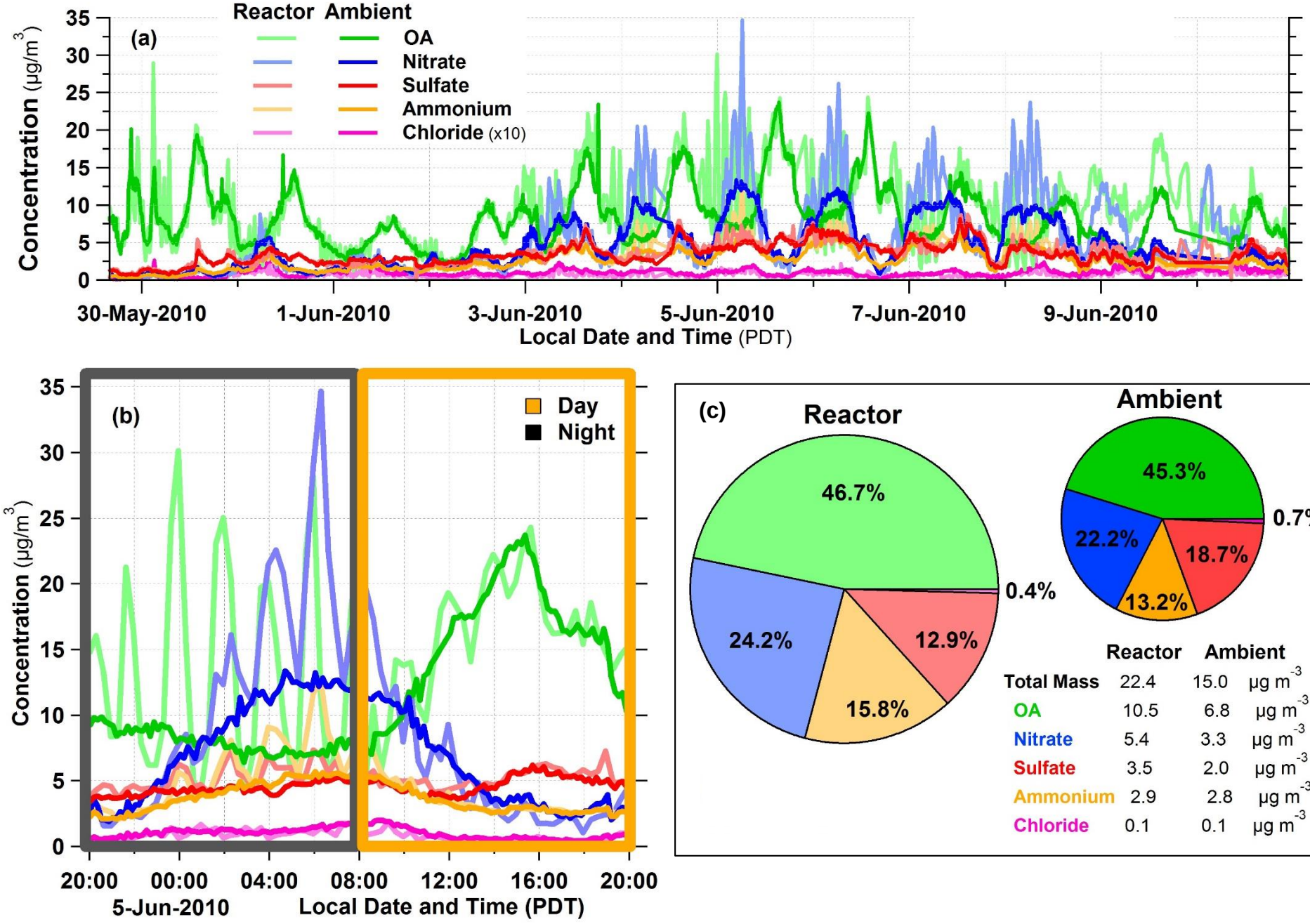

	Reactor	Ambient	
Total Mass	22.4	15.0	μg m^{-3}
OA	10.5	6.8	μg m^{-3}
Nitrate	5.4	3.3	μg m^{-3}
Sulfate	3.5	2.0	μg m^{-3}
Ammonium	2.9	2.8	μg m^{-3}
Chloride	0.1	0.1	μg m^{-3}

Figure 4.

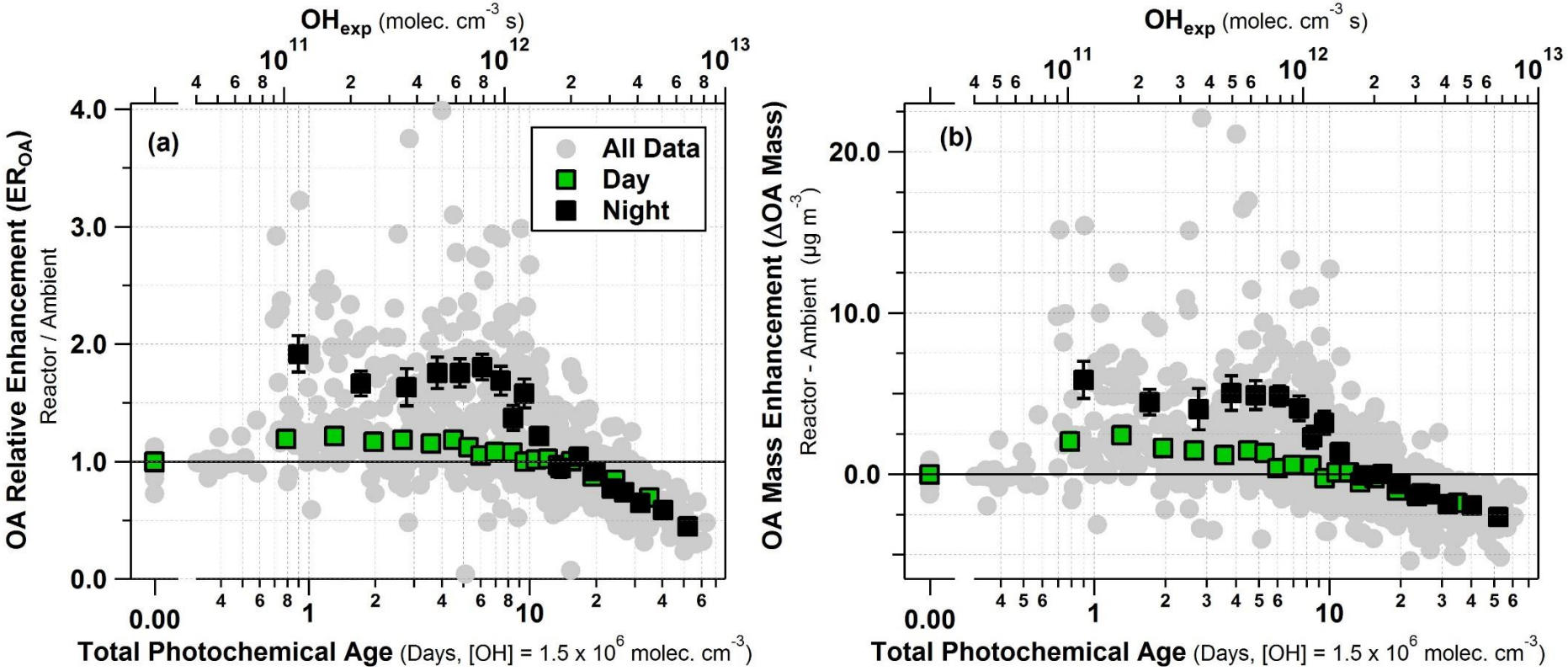
OH$_{exp}$ (molec. cm^{-3} s)
(a)
All Data
Day
Night
OA Relative Enhancement (ER$_{OA}$)
Reactor / Ambient
Total Photochemical Age (Days, [OH] = 1.5 x 10^{6} molec. cm^{-3})
(b)
OA Mass Enhancement (ΔOA Mass)
Reactor - Ambient (μg m^{-3})

Figure 5.

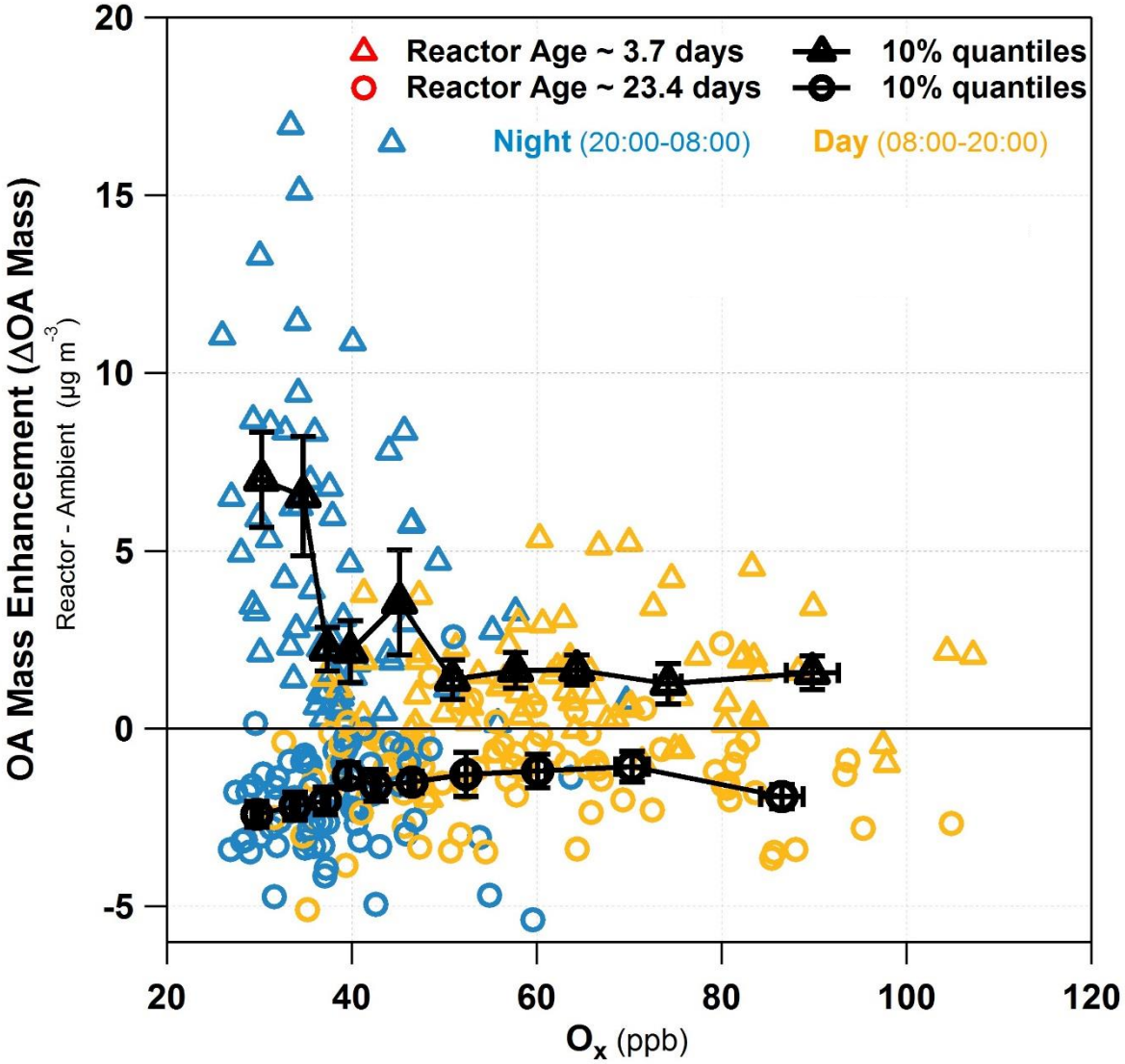
Reactor Age ~ 3.7 days
Reactor Age ~ 23.4 days
10% quantiles
10% quantiles
Night (20:00-08:00)
Day (08:00-20:00)
OA Mass Enhancement (ΔOA Mass)
Reactor - Ambient (μg m-3)
20
15
10
5
0
-5
20
40
60
80
100
120
Ox (ppb)

Figure 6.

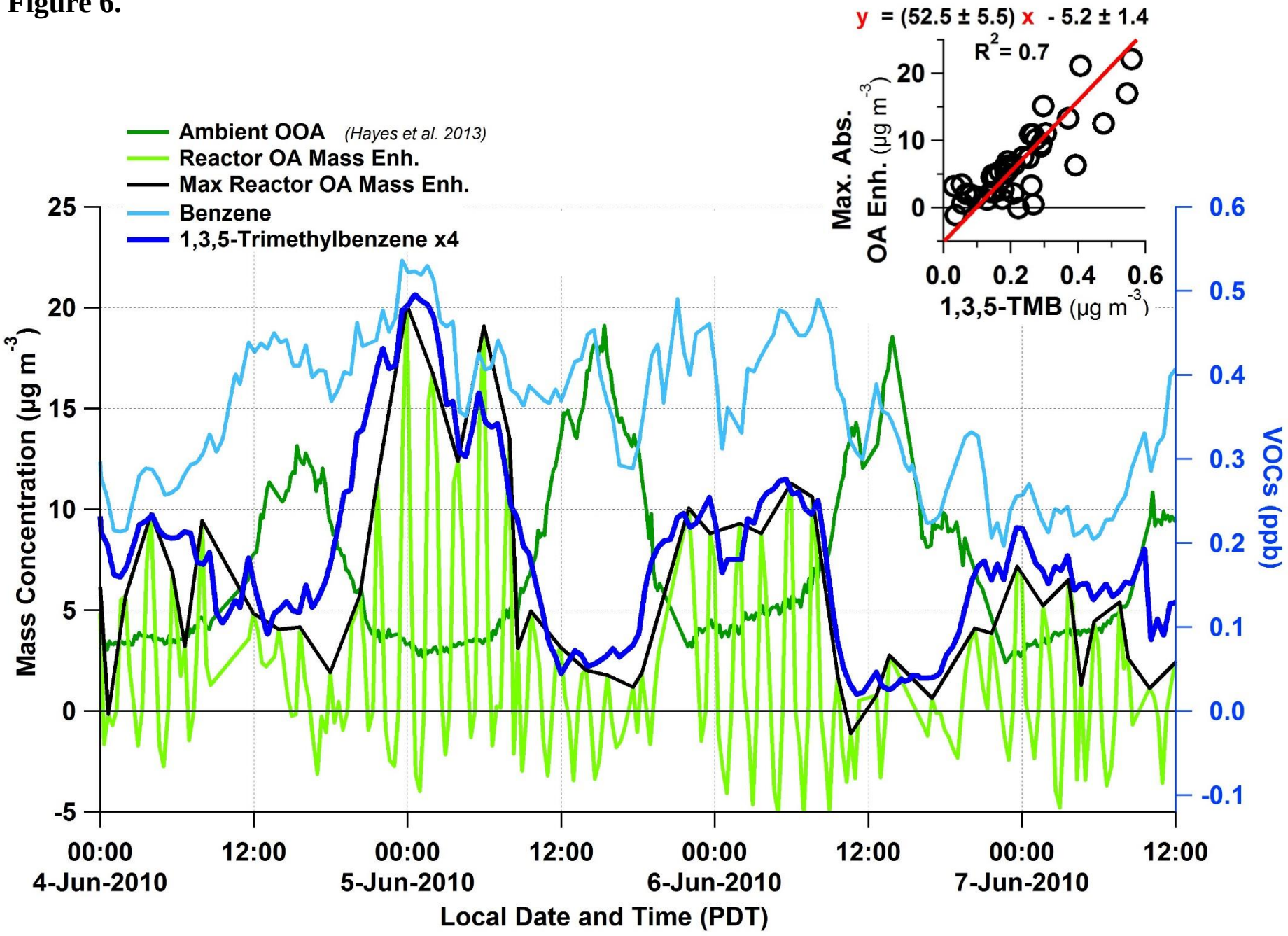
y = (52.5 ± 5.5) x - 5.2 ± 1.4
R2 = 0.7
Max. Abs. OA Enh. (µg m-3)
1,3,5-TMB (µg m-3)
Ambient OOA (Hayes et al. 2013)
Reactor OA Mass Enh.
Max Reactor OA Mass Enh.
Benzene
1,3,5-Trimethylbenzene x4
Mass Concentration (µg m-3)
VOCs (ppb)
00:00 4-Jun-2010
12:00
00:00 5-Jun-2010
12:00
00:00 6-Jun-2010
12:00
00:00 7-Jun-2010
12:00
Local Date and Time (PDT)

Figure 7.

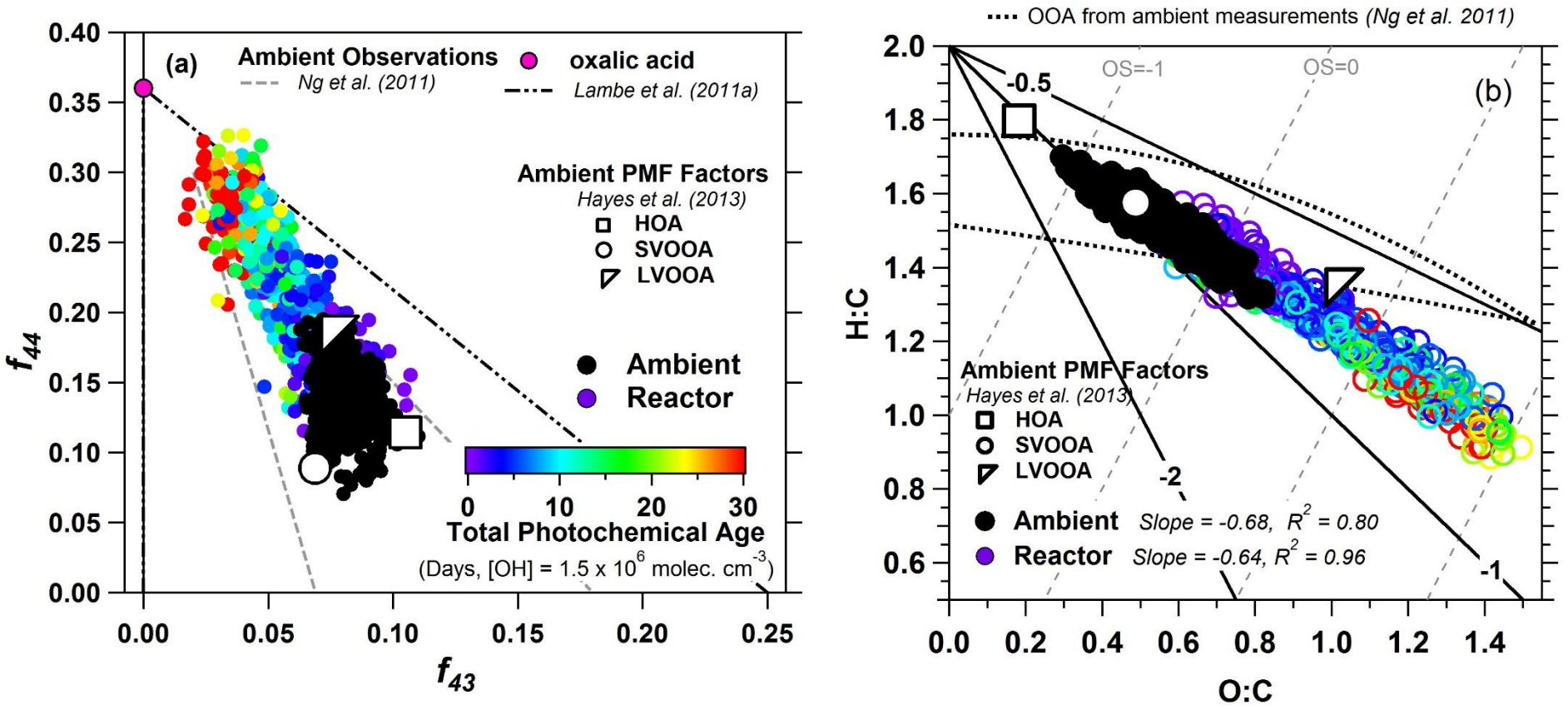
(a)
Ambient Observations
Ng et al. (2011)
oxalic acid
Lambe et al. (2011a)
Ambient PMF Factors
Hayes et al. (2013)
HOA
SVOOA
LVOOA
Ambient
Reactor
0
10
20
30
Total Photochemical Age
(Days, [OH] = 1.5 x 10^6 molec. cm^-3)
f44
f43
0.00
0.05
0.10
0.15
0.20
0.25
0.30
0.35
0.40
OOA from ambient measurements (Ng et al. 2011)
(b)
OS=-1
OS=0
-0.5
-1
-2
Ambient PMF Factors
Hayes et al. (2013)
HOA
SVOOA
LVOOA
Ambient Slope = -0.68, R2 = 0.80
Reactor Slope = -0.64, R2 = 0.96
H:C
O:C
0.6
0.8
1.0
1.2
1.4
1.6
1.8
2.0
0.0
0.2
0.4
0.6
0.8
1.0
1.2
1.4

Figure 8.

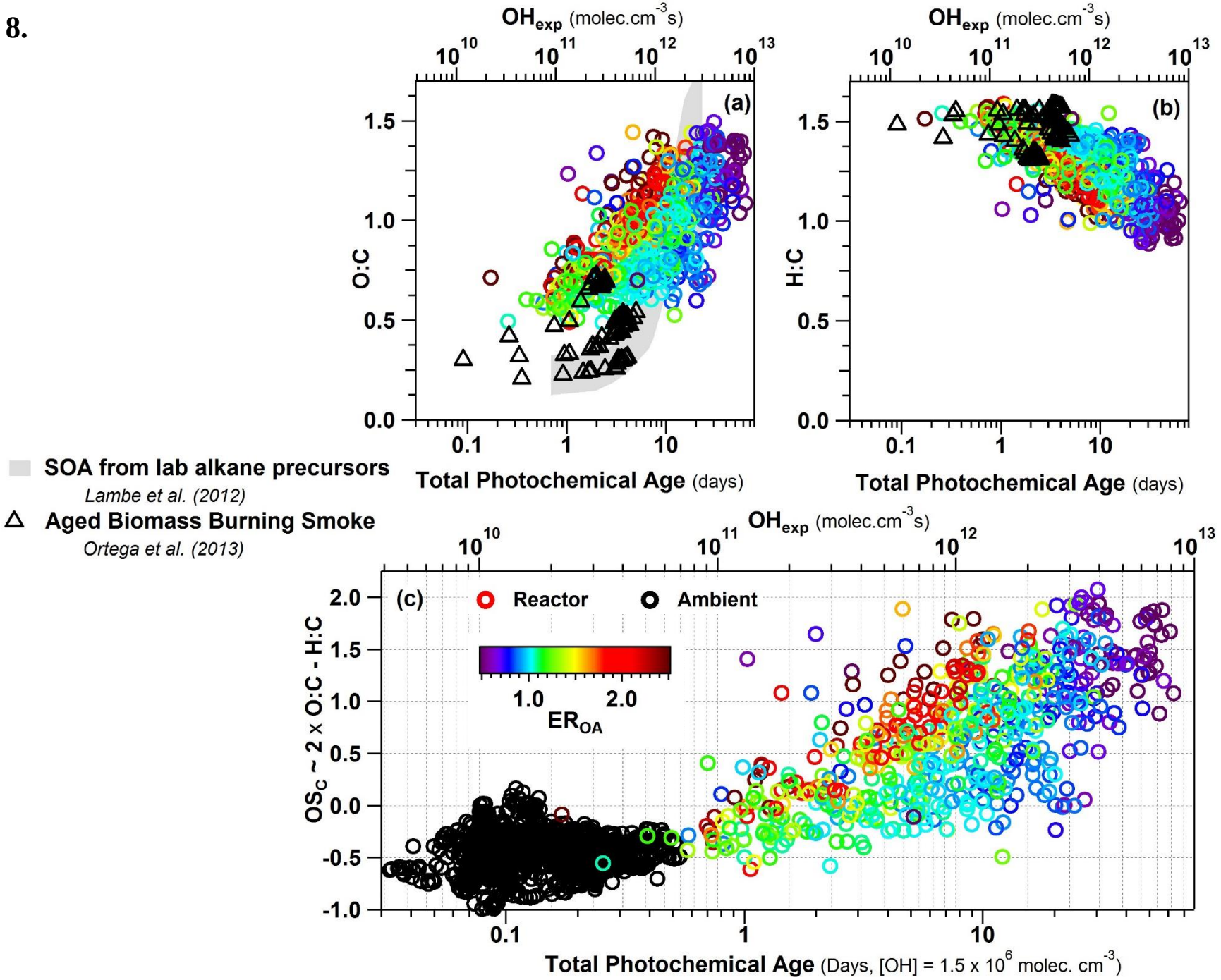
OH_exp (molec.cm^-3 s)
10^10
10^11
10^12
10^13
(a)
(b)
(c)
O:C
H:C
1.5
1.0
0.5
0.0
0.1
1
10
Total Photochemical Age (days)
SOA from lab alkane precursors
Lambe et al. (2012)
Aged Biomass Burning Smoke
Ortega et al. (2013)
Reactor
Ambient
ER_OA
1.0
2.0
OS_C ~ 2 x O:C - H:C
2.0
-0.5
-1.0
Total Photochemical Age (Days, [OH] = 1.5 x 10^6 molec. cm^-3)

Figure 9.

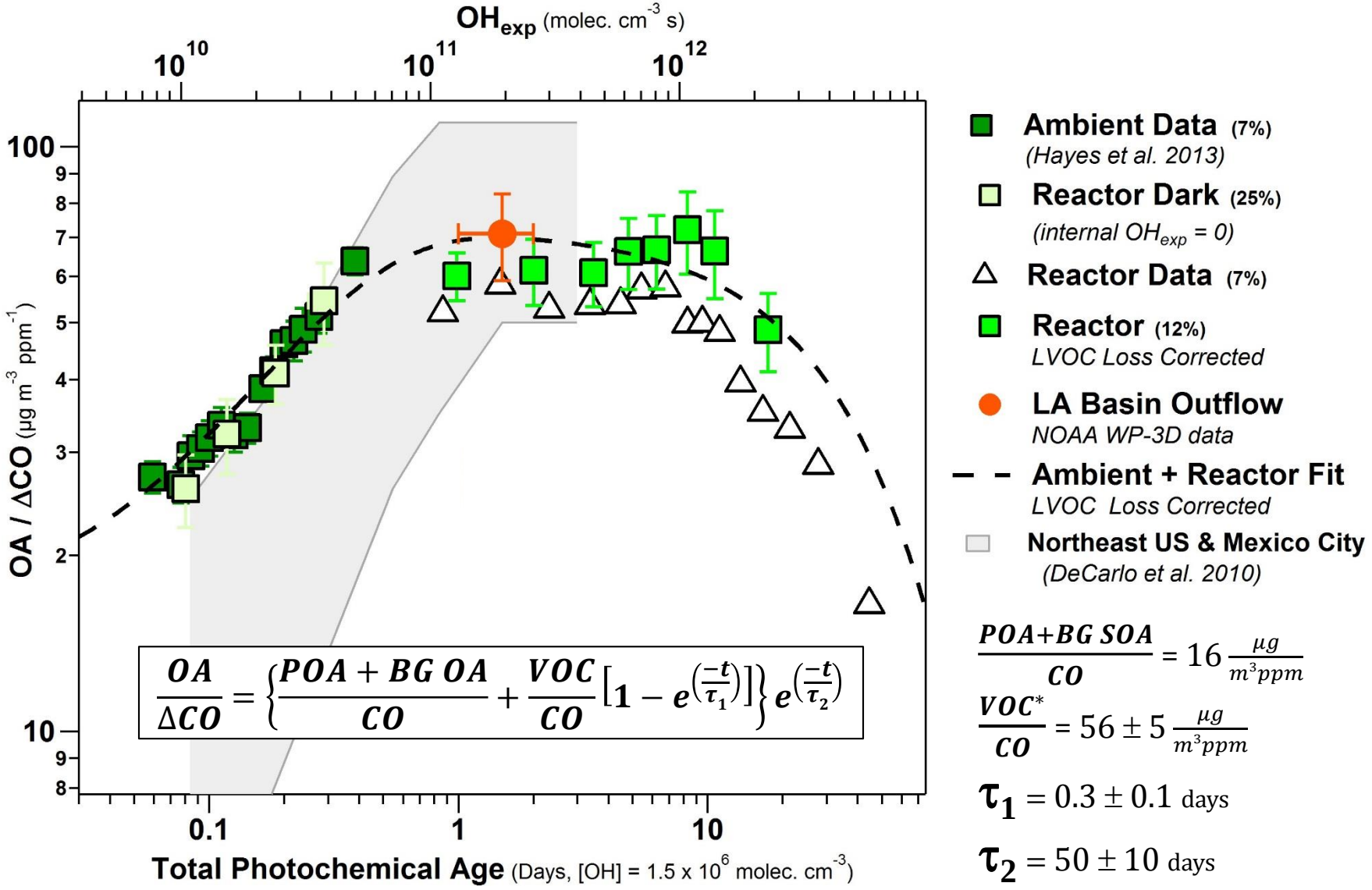

$$\frac{POA+BG\ SOA}{CO} = 16\ \frac{\mu g}{m^3 ppm}$$

$$\frac{VOC^*}{CO} = 56 \pm 5\ \frac{\mu g}{m^3 ppm}$$

$$\tau_1 = 0.3 \pm 0.1 \text{ days}$$

$$\tau_2 = 50 \pm 10 \text{ days}$$

Figure 10.

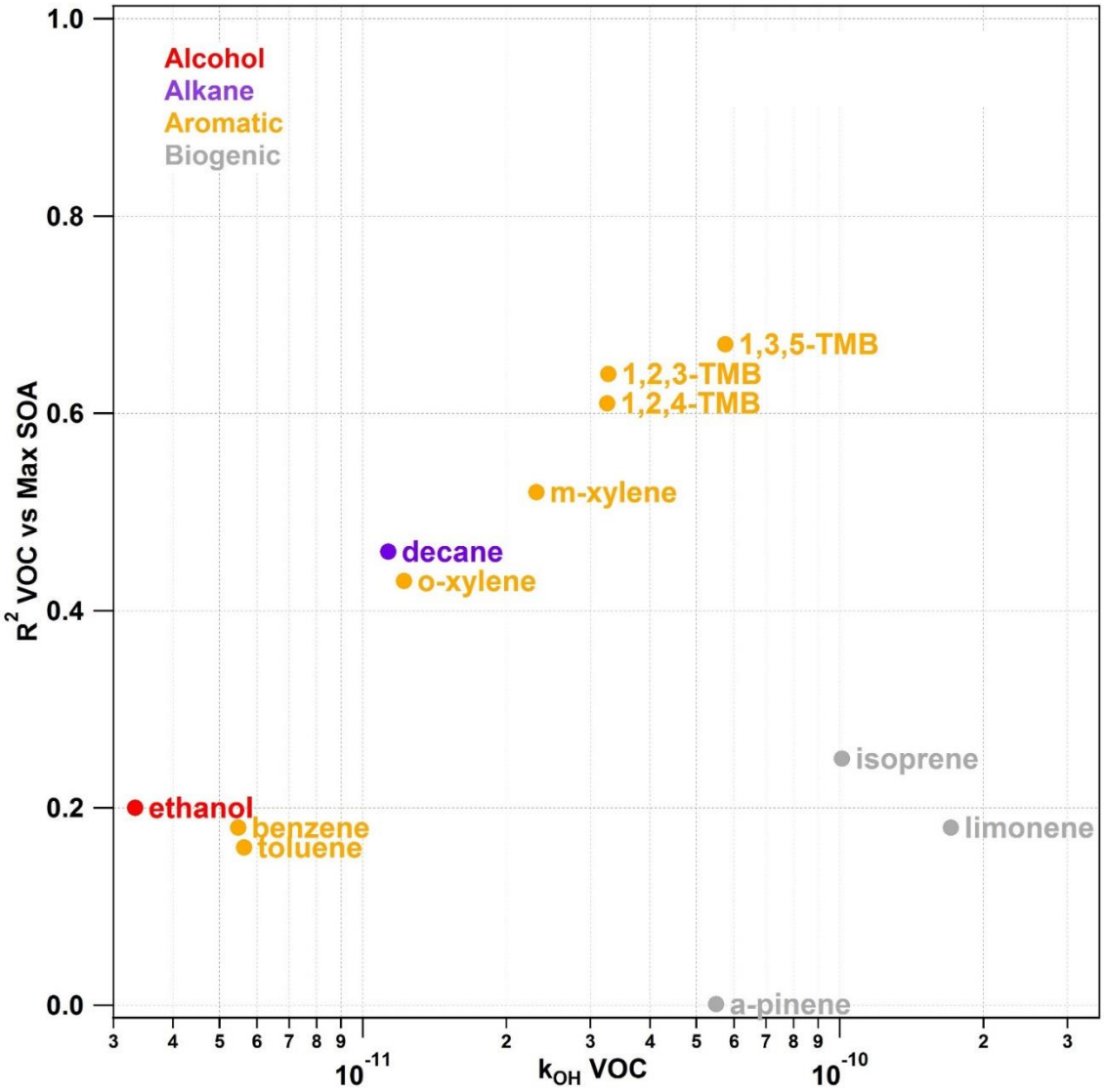
Alcohol
Alkane
Aromatic
Biogenic
1.0
0.8
0.6
0.4
0.2
0.0
R2 VOC vs Max SOA
1,3,5-TMB
1,2,3-TMB
1,2,4-TMB
m-xylene
decane
o-xylene
isoprene
limonene
ethanol
benzene
toluene
a-pinene
3 4 5 6 7 8 9
10-11
2 3 4 5 6 7 8 9
kOH VOC
10-10
2 3

Figure 11.

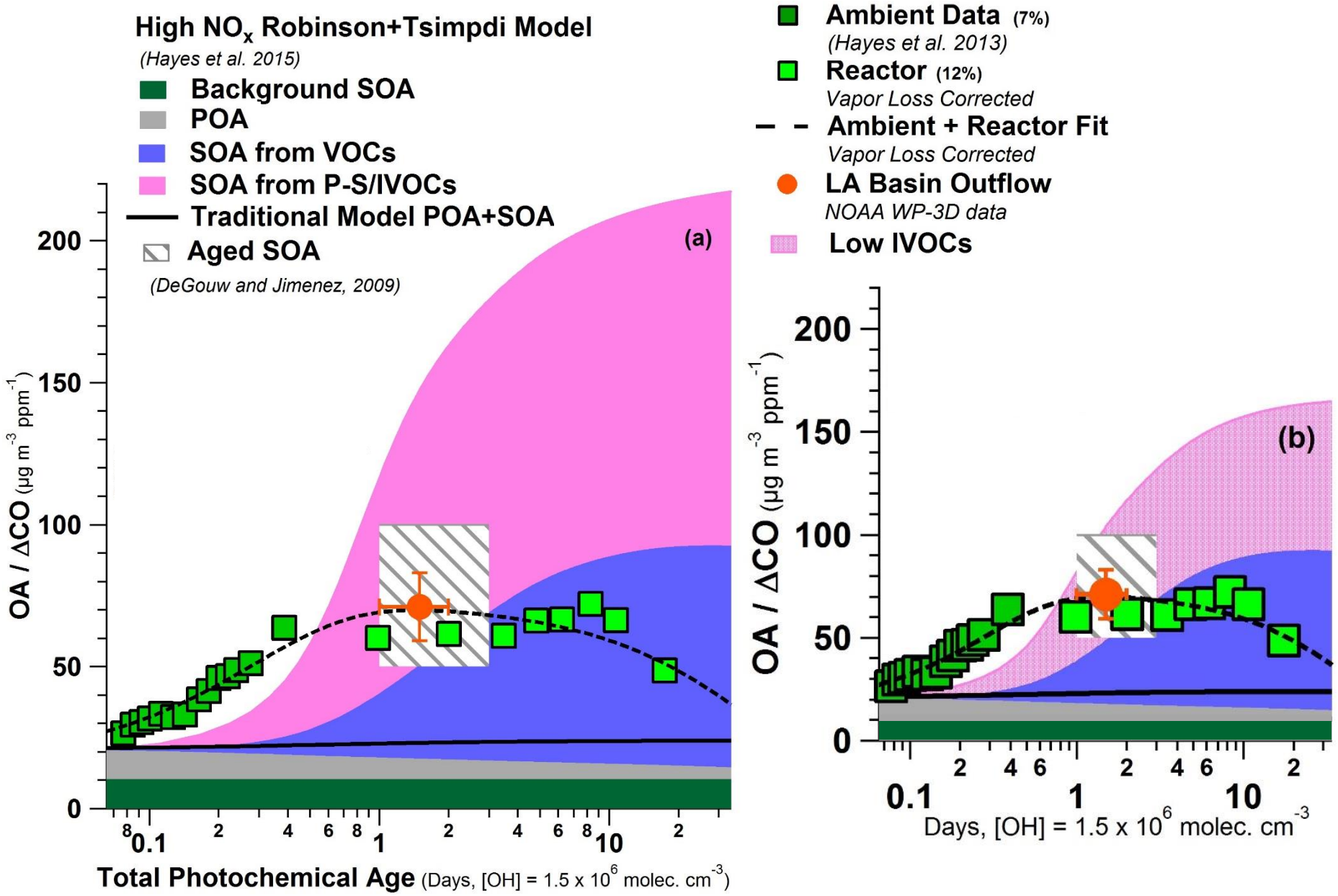
High NOx Robinson+Tsimpdi Model
(Hayes et al. 2015)
Background SOA
POA
SOA from VOCs
SOA from P-S/IVOCs
Traditional Model POA+SOA
Aged SOA
(DeGouw and Jimenez, 2009)
(a)
OA / ΔCO (μg m-3 ppm-1)
Total Photochemical Age (Days, [OH] = 1.5 x 10^6 molec. cm-3)
Ambient Data (7%)
(Hayes et al. 2013)
Reactor (12%)
Vapor Loss Corrected
Ambient + Reactor Fit
Vapor Loss Corrected
LA Basin Outflow
NOAA WP-3D data
Low IVOCs
(b)
Days, [OH] = 1.5 x 10^6 molec. cm-3

Figure 12.

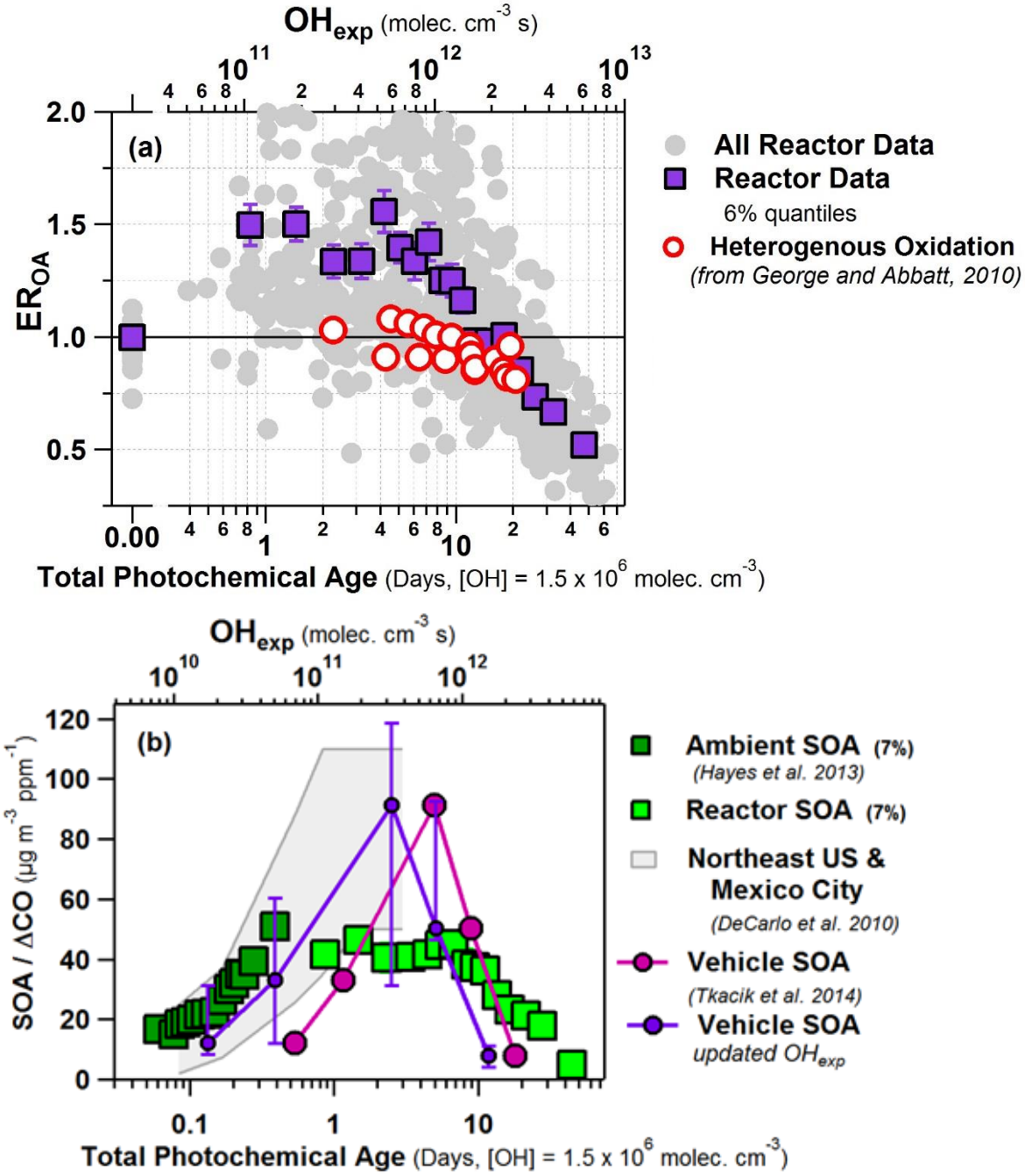
OHexp (molec. cm-3 s)
(a)
ERoA
All Reactor Data
Reactor Data
6% quantiles
Heterogenous Oxidation
(from George and Abbatt, 2010)
Total Photochemical Age (Days, [OH] = 1.5 x 10^6 molec. cm^-3)
(b)
SOA / ΔCO (μg m^-3 ppm^-1)
Ambient SOA (7%)
(Hayes et al. 2013)
Reactor SOA (7%)
Northeast US & Mexico City
(DeCarlo et al. 2010)
Vehicle SOA
(Tkacik et al. 2014)
Vehicle SOA
updated OHexp
Total Photochemical Age (Days, [OH] = 1.5 x 10^6 molec. cm^-3)

1 Quantification of AMS Reactor Data

All aspects of quantification of AMS data are the same as described by Hayes et al. (2013). Here we describe only those aspects where additional analysis or corrections are needed specifically for the reactor output data.

1.1 AMS Collection Efficiency

Quantification of AMS concentration data requires a correction for particle bounce at the vaporizer, referred to as the collection efficiency (CE; Canagaratna et al., 2007). The composition-dependent CE formulation of Middlebrook et al. (2012) was used by Hayes et al. (2013) to estimate CE for the ambient data, leading to good intercomparisons with multiple collocated instruments as documented by that study. The same methodology has also been applied to reactor output measurements.

Although the focus of this paper is OA formation and aging, a brief summary of the observed evolution of the inorganic species: (a) Sulfate formation proceeds as expected from the OH + SO_2 reaction. A quantitative analysis of sulfate formation is shown in Palm et al. (2016), which reports results from a similar experiment from our group, but in a forest environment. That analysis provides evidence that the corrections for losses of low volatility species developed in that work are appropriate. (b) Nitrate formation is more complex since OH + NO_2 is a fast reaction, but HNO_3 is semivolatile and the formation of NH_4NO_3 also depends on the availability of NH_3(g). (c) The aerosols in the output of the flow reactor during CalNex are neutralized, similarly to the ambient aerosols (Hayes et al., 2013).

Fig. ~~S1a~~ S2a shows the time series of reactor and ambient aerosol concentrations and estimated CE. Ambient CE periodically rises above 0.5 due to larger fractions of ammonium nitrate aerosol, which leads to reduced particle bounce (Middlebrook et al., 2012). The reactor typically formed additional ammonium sulfate and ammonium nitrate beyond ambient concentrations at the same time as ambient levels peak for those compounds, thus the reactor CE profile has a very similar temporal structure to ambient. However, Fig. ~~S1b~~ S2b shows that the estimated CE increases at the highest reactor OH_{exp}, due to additional ammonium nitrate formation in the reactor with increased photochemical age.

Highly acidic particles, as indicated by the ammonium balance, can also lead to increased CE in the AMS (Middlebrook et al., 2012). The ammonium balance method compares the measured ammonium to that required to fully neutralize observed sulfate, nitrate, and chloride (Zhang et al., 2007), as shown in Fig. ~~S2~~S3. Ambient and reactor results have near identical slopes that are indistinguishable from the one-to-one line within the uncertainties of the measurements, signifying full neutralization for both. Furthermore, this comparison indicates that the reactor is producing similar inorganic composition to that observed in the atmosphere as nitric acid and sulfuric acid gases are formed in the reactor and fully neutralized by ammonium forming ammonium nitrate and ammonium sulfate. Thus no correction of CE due to the presence of highly acidic particles are needed in this study.

Comparison of AMS and SMPS measurements for ambient and reactor data, shows that ambient data falls along a one-to-one line, indicating both instruments are measuring the same amount of mass within the uncertainties (Fig. ~~S3a~~S4a). Reactor output data has a slightly higher slope of 1.14, i.e. the AMS measures ~14% higher mass than the SMPS from the reactor and also shows a cluster of points where SMPS>AMS due to periods where substantial mass is formed at small

particle sizes (see below). Both slopes are within the combined uncertainties of the two measurements. Fig. ~~S3b~~ S4b shows the relative increase in aerosol concentration in the reactor (i.e. ratio of reactor to ambient concentrations) for the SMPS vs. AMS which also compare well, on average (slope = 1.05), but with considerable scatter, most of which is likely due to additional measurement noise introduced from ratioing multiple short measurements. Evaporation of freshly formed NH_4NO_3 in the longer residence times in the SMPS (compared to the faster AMS analysis) where the sheath flow may have reduced NH_3 and HNO_3 gas concentrations, has been observed with this experimental setup, and may be a cause of the slightly larger slope for reactor output conditions. A~~n~~ small underestimation of AMS CE for the reactor conditions could also result in this observation.

It is also possible that the AMS relative ionization efficiency (RIE) of organic species is lower for more oxidized species (Jimenez et al., 2003; D. Murphy, pers. Comm. 2015), although no clear evidence has been reported for ambient data (e.g. Docherty et al., 2011). If that effect played a dominant role here, we would expect the reactor slopes to be lower, rather than slightly higher than 1. Thus we conclude that any RIE changes are small and cannot be separated from other effects such as small changes in CE, nitrate evaporation in the SMPS, or differences in particle transmission (next section).

1.2 Accounting for Particle Mass below the AMS Lens Transmission

As the reactor exposed ambient air to high levels of OH and O_3, new particle formation and growth was sometimes observed. To fully account for the mass of all particles formed in the reactor, it is necessary to quantify the mass of small particles below the AMS lens transmission size (Zhang et al., 2004). SMPS data was used to estimate the total mass concentration below the AMS size cut.

First, particle transmission from plumbing line losses was corrected using the Particle Loss Calculator (von der Weiden et al., 2009) for this experimental plumbing and flowrate configuration for both reactor and ambient SMPS data, with transmission curves as shown in Fig. ~~S4~~S5. Second, the measured SMPS mass that is below the AMS transmission curve was estimated using a published AMS lens transmission parameterization (Knote et al., 2011) multiplying the SMPS size-dependent mass by the size-dependent AMS lens fractional loss (1-transmission). Figure ~~S5a~~ S6a shows a time series of estimated reactor and ambient mass missed by the AMS due to transmission losses. Since corrections needed to account for the contribution of these small sizes to total mass is small for ambient data (on average 1.7%), Hayes et al. (2013) did not apply a correction to AMS ambient data. Fig. ~~S5b~~ S6b shows the estimated fraction of the reactor output mass that is below the AMS lens transmission size vs. total photochemical age in days (at OH = 1.5×10^6 molec. cm^{-3}). An average of 6.2% of the total reactor output mass is estimated to be below the AMS lens transmission, with no dependence on photochemical age except possibly at the highest values (>20 days of age).

We note that the AMS measurements from the reactor may be biased ~6% low, on average, and sometimes as much as 20%. This non-measured mass likely has a large OA fraction (see Fig. ~~S7~~S8). Thus, reactor-reported mass enhancement above ambient may be underestimated by these amounts. Given the 6.2% AMS underestimation from particle transmission of small sizes in the reactor, and the apparent 14% overestimation in the AMS vs SMPS comparison, but overall good agreement in the relative enhancement of total aerosol between both instruments, we have not corrected for these differences as the net correction would be small and within the uncertainties of the measurement, while the correction process would introduce additional noise.

Supplementary Captions

Figure S1: Results of computerized fluid dynamics (CFD) simulations comparing two OFR configurations. **(a)** Tube inlet, similar to Lambe et al. (2011); **(b)** Large open face inlet (11.9 cm diameter) as used in this field study. Colors are contours of positive horizontal velocity. White regions involve horizontal velocities, i.e. recirculation regions. The extensive recirculation regions of case (a) are almost completely removed in case (b), resulting in a narrower residence time distribution. Simulations were conducted using the FLUENT software, using cylindrical symmetry, with air at 1 atm and 293 K.

Figure ~~S1~~S2: (a) Estimated AMS collection efficiency (CE) and corresponding AMS mass concentration time series for ambient and reactor data (after applying CE correction). **(b)** Estimated CE vs. OH exposure (OH_{exp}) in the reactor for all reactor measurements and averages for 7% quantiles.

Figure ~~S2~~S3: Measured vs. predicted ammonium assuming full neutralization ("Ammonium balance") for ambient and reactor data. Linear orthogonal distance regression fit lines, slope and R^2 for each are also shown.

Figure ~~S3~~S4: (a) Scatter plot of AMS mass vs. mass estimated from SMPS measurements for ambient and reactor data, with linear orthogonal distance regression fit slope and R^2 for each. A one-to-one line and +/-15% region is shown for reference. **(b)** Relative enhancement ratio from AMS and SMPS data with raw data, 20-minute averaged smooth data, linear orthogonal distance regression, line, fit slope and R^2 for each.

Figure ~~S4~~S5: Estimated particle transmission of inlet plumbing vs. particle diameter for reactor and ambient sampling lines for both AMS and SMPS measurements, calculated using the particle loss calculator of von der Weiden et al. (2009).

Figure ~~S5~~S6: (a) Time series of SMPS mass measured below the AMS lens transmission size for ambient and reactor measurements. **(b)** Percent of estimated mass not measured by AMS, due to on particle losses in sampling lines and the AMS lens transmission at small sizes, for the reactor vs. total photochemical age in days (at OH = 1.5×10^6 molec. cm^{-3}), where all data is colored by ΔOA mass with average 5% quantiles and standard error bars.

Figure ~~S6~~S7: Modeled fate of low volatility organic gases (LVOCs) formed in the reactor vs. OH_{exp} including wall loss, reaction with OH, condensation on aerosol, and exiting the reactor, with a fit for the fraction condensing on aerosols in the reactor.

Formatted: Font: Not Bold
Formatted: Font: Not Bold
Formatted: Font: Not Bold
Formatted: Font: Not Bold
Formatted: Font: Not Bold

Figure ~~S7~~S8: AMS mass size distribution (vs. vacuum aerodynamic diameter, d_{va}) for reactor and ambient OA, averaged from 20:00 on 2 June 2010 – 00:20 on 9 June 2010 for average nighttime ambient and reactor with no internal OH_{exp} (dark reactor), and for ~3.7 days and ~23.5 days aging.

Figure ~~S8~~S9: Times series of benzene, 1,3,5-trimethylbenzene, and toluene on top panel. Time series of ambient OOA, reactor OA mass enhancement, maximum reactor mass enhancement, and O_x on bottom panel.

Figure ~~S9~~S10: Ratio of organic aerosol to excess carbon monoxide (above background) vs. total photochemical age in days (at OH = 1.5×10^6 molec. cm^{-3}) for **(a)** the same data as Fig. 9, showing all data used to produce averages for quantiles of ambient and reactor vapor-loss corrected data. Also shown are the expected decays of benzene, toluene, and 1,3,5-trimethylbenzene in the reactor vs. total photochemical age in days (at OH = 1.5×10^6 molec. cm^{-3}), using reaction rates from Atkinson et al. (2006). **(b)** The same data as Fig. 9, showing reactor vapor loss-corrected data, but where excess CO is decreased by reaction with OH in the reactor, including means for 12% quantiles. Results from field studies in the northeastern US and Mexico City are shown for comparison to previous observations (DeCarlo et al., 2010). A fit to the data when CO is assumed to react with OH is shown.

Figure ~~S10~~S11: The ratio of the gain of oxygen of OA observed in the reactor (ΔOxygen in OA = $O_{atoms,\ reactor} - O_{atoms,\ ambient}$) to the total number of OH collisions with OA in the reactor vs. total photochemical age. ~~Measured oxygen added to OA in the reactor vs. total photochemical age in days (at OH = 1.5×10^6 molec. cm^{-3}), along with a log-normal fit to the ΔOxygen data. Reactor data is colored by OA mass enhancement.~~ The estimated number of OH collisions ~~with OA is shown,~~is calculated based on the methodology outlined in appendix A of DeCarlo et al. (2008).

Figure ~~S11~~S12: Top panel: Mass fraction remaining (MFR) for OA vs. thermal denuder temperature for this CalNex-LA dataset, using the methods described in Huffman et al. (2008; 2009). Bottom panel: estimated volatility distribution of particle- and gas-phase species, calculated from the thermal denuder profile using the method of Faulhaber et al. (2009), on bottom panel.

References

Atkinson, R., Baulch, D. L., Cox, R. A., Crowley, J. N., Hampson, R. F., Hynes, R. G., Jenkin, M. E., Rossi, M. J., Troe, J., and Subcommittee, I.: Evaluated kinetic and photochemical data for atmospheric chemistry: Volume II: gas phase reactions of organic species, Atmos. Chem. Phys., 6, 3625-4055, 10.5194/acp-6-3625-2006, 2006.

Canagaratna, M. R., Jayne, J. T., Jimenez, J. L., Allan, J. D., Alfarra, M. R., Zhang, Q., Onasch, T. B., Drewnick, F., Coe, H., Middlebrook, A., Delia, A., Williams, L. R., Trimborn, A. M., Northway, M. J., DeCarlo, P. F., Kolb, C. E., Davidovits, P., and Worsnop, D. R.: Chemical and microphysical characterization of ambient aerosols with the aerodyne aerosol mass spectrometer, Mass Spectrom Rev, 26, 185-222, Doi 10.1002/Mas.20115, 2007.

Field Code Changed

DeCarlo, P. F., Dunlea, E. J., Kimmel, J. R., Aiken, A. C., Sueper, D., Crounse, J., Wennberg, P. O., Emmons, L., Shinozuka, Y., Clarke, A., Zhou, J., Tomlinson, J., Collins, D. R., Knapp, D., Weinheimer, A. J., Montzka, D. D., Campos, T., and Jimenez, J. L.: Fast airborne aerosol size and chemistry measurements above Mexico City and Central Mexico during the MILAGRO campaign, Atmos. Chem. Phys., 8, 4027-4048, 10.5194/acp-8-4027-2008, 2008.

DeCarlo, P. F., Ulbrich, I. M., Crounse, J., de Foy, B., Dunlea, E. J., Aiken, A. C., Knapp, D., Weinheimer, A. J., Campos, T., Wennberg, P. O., and Jimenez, J. L.: Investigation of the sources and processing of organic aerosol over the Central Mexican Plateau from aircraft measurements during MILAGRO, Atmos. Chem. Phys., 10, 5257-5280, 10.5194/acp-10-5257-2010, 2010.

Docherty, K. S., Aiken, A. C., Huffman, J. A., Ulbrich, I. M., DeCarlo, P. F., Sueper, D., Worsnop, D. R., Snyder, D. C., Peltier, R. E., Weber, R. J., Grover, B. D., Eatough, D. J., Williams, B. J., Goldstein, A. H., Ziemann, P. J., and Jimenez, J. L.: The 2005 Study of Organic Aerosols at Riverside (SOAR-1): instrumental intercomparisons and fine particle composition, Atmos. Chem. Phys., 11, 12387-12420, 10.5194/acp-11-12387-2011, 2011.

Faulhaber, A. E., Thomas, B. M., Jimenez, J. L., Jayne, J. T., Worsnop, D. R., and Ziemann, P. J.: Characterization of a thermodenuder-particle beam mass spectrometer system for the study of organic aerosol volatility and composition, Atmos. Meas. Tech., 2, 15-31, 10.5194/amt-2-15-2009, 2009.

Hayes, P. L., Ortega, A. M., Cubison, M. J., Froyd, K. D., Zhao, Y., Cliff, S. S., Hu, W. W., Toohey, D. W., Flynn, J. H., Lefer, B. L., Grossberg, N., Alvarez, S., Rappenglück, B., Taylor, J. W., Allan, J. D., Holloway, J. S., Gilman, J. B., Kuster, W. C., de Gouw, J. A., Massoli, P., Zhang, X., Liu, J., Weber, R. J., Corrigan, A. L., Russell, L. M., Isaacman, G., Worton, D. R., Kreisberg, N. M., Goldstein, A. H., Thalman, R., Waxman, E. M., Volkamer, R., Lin, Y. H., Surratt, J. D., Kleindienst, T. E., Offenberg, J. H., Dusanter, S., Griffith, S., Stevens, P. S., Brioude, J., Angevine, W. M., and Jimenez, J. L.: Organic aerosol composition and sources in Pasadena, California, during the 2010 CalNex campaign, Journal of Geophysical Research: Atmospheres, 118, 9233-9257, 10.1002/jgrd.50530, 2013.

Huffman, J. A., Ziemann, P. J., Jayne, J. T., Worsnop, D. R., and Jimenez, J. L.: Development and Characterization of a Fast-Stepping/Scanning Thermodenuder for Chemically-Resolved Aerosol Volatility Measurements, Aerosol Science and Technology, 42, 395-407, 10.1080/02786820802104981, 2008.

Huffman, J. A., Docherty, K. S., Aiken, A. C., Cubison, M. J., Ulbrich, I. M., DeCarlo, P. F., Sueper, D., Jayne, J. T., Worsnop, D. R., Ziemann, P. J., and Jimenez, J. L.: Chemically-resolved aerosol volatility measurements from two megacity field studies, Atmos. Chem. Phys., 9, 7161-7182, 10.5194/acp-9-7161-2009, 2009.

Jimenez, J. L., Jayne, J. T., Shi, Q., Kolb, C. E., Worsnop, D. R., Yourshaw, I., Seinfeld, J. H., Flagan, R. C., Zhang, X. F., Smith, K. A., Morris, J. W., and Davidovits, P.: Ambient aerosol sampling using the Aerodyne Aerosol Mass Spectrometer, J Geophys Res-Atmos, 108, 2003.

Knote, C., Brunner, D., Vogel, H., Allan, J., Asmi, A., Äijälä, M., Carbone, S., van der Gon, H. D., Jimenez, J. L., Kiendler-Scharr, A., Mohr, C., Poulain, L., Prévôt, A. S. H., Swietlicki, E., and Vogel, B.: Towards an online-coupled chemistry-climate model: evaluation of trace gases and aerosols in COSMO-ART, Geosci. Model Dev., 4, 1077-1102, 10.5194/gmd-4-1077-2011, 2011.

Lambe, A. T., Onasch, T. B., Massoli, P., Croasdale, D. R., Wright, J. P., Ahern, A. T., Williams, L. R., Worsnop, D. R., Brune, W. H., and Davidovits, P.: Laboratory studies of the chemical composition and cloud condensation nuclei (CCN) activity of secondary organic aerosol (SOA) and oxidized primary organic aerosol (OPOA), Atmos Chem Phys, 11, 8913-8928, DOI 10.5194/acp-11-8913-2011, 2011.

198 Middlebrook, A. M., Bahreini, R., Jimenez, J. L., and Canagaratna, M. R.: Evaluation of Composition-Dependent
199 Collection Efficiencies for the Aerodyne Aerosol Mass Spectrometer using Field Data, Aerosol Sci Tech, 46, 258-
200 271, 2012.

201 Palm, B. B., Campuzano-Jost, P., Ortega, A. M., Day, D. A., Kaser, L., Jud, W., Karl, T., Hansel, A., Hunter, J. F.,
202 Cross, E. S., Kroll, J. H., Peng, Z., Brune, W. H., and Jimenez, J. L.: In situ secondary organic aerosol formation from
203 ambient pine forest air using an oxidation flow reactor, Atmos. Chem. Phys., 16, 2943-2970, 10.5194/acp-16-2943-
204 2016, 2016.

205 von der Weiden, S. L., Drewnick, F., and Borrmann, S.: Particle Loss Calculator – a new software tool for the
206 assessment of the performance of aerosol inlet systems, Atmos. Meas. Tech. Discuss., 2, 1099-1141, 10.5194/amtd-
207 2-1099-2009, 2009.

208 Zhang, Q., Jimenez, J. L., Canagaratna, M. R., Allan, J. D., Coe, H., Ulbrich, I., Alfarra, M. R., Takami, A.,
209 Middlebrook, A. M., Sun, Y. L., Dzepina, K., Dunlea, E., Docherty, K., DeCarlo, P. F., Salcedo, D., Onasch, T., Jayne,
210 J. T., Miyoshi, T., Shimono, A., Hatakeyama, S., Takegawa, N., Kondo, Y., Schneider, J., Drewnick, F., Borrmann,
211 S., Weimer, S., Demerjian, K., Williams, P., Bower, K., Bahreini, R., Cottrell, L., Griffin, R. J., Rautiainen, J., Sun,
212 J. Y., Zhang, Y. M., and Worsnop, D. R.: Ubiquity and dominance of oxygenated species in organic aerosols in
213 anthropogenically-influenced Northern Hemisphere midlatitudes, Geophys. Res. Lett., 34, L13801,
214 10.1029/2007gl029979, 2007.

215 Zhang, X. F., Smith, K. A., Worsnop, D. R., Jimenez, J. L., Jayne, J. T., Kolb, C. E., Morris, J., and Davidovits, P.:
216 Numerical characterization of particle beam collimation: Part II - Integrated aerodynamic-lens-nozzle system, Aerosol
217 Science and Technology, 38, 619-638, 10.1080/02786820490479833, 2004.

218

219

Formatted: Justified, Line spacing: single

Figure S1.

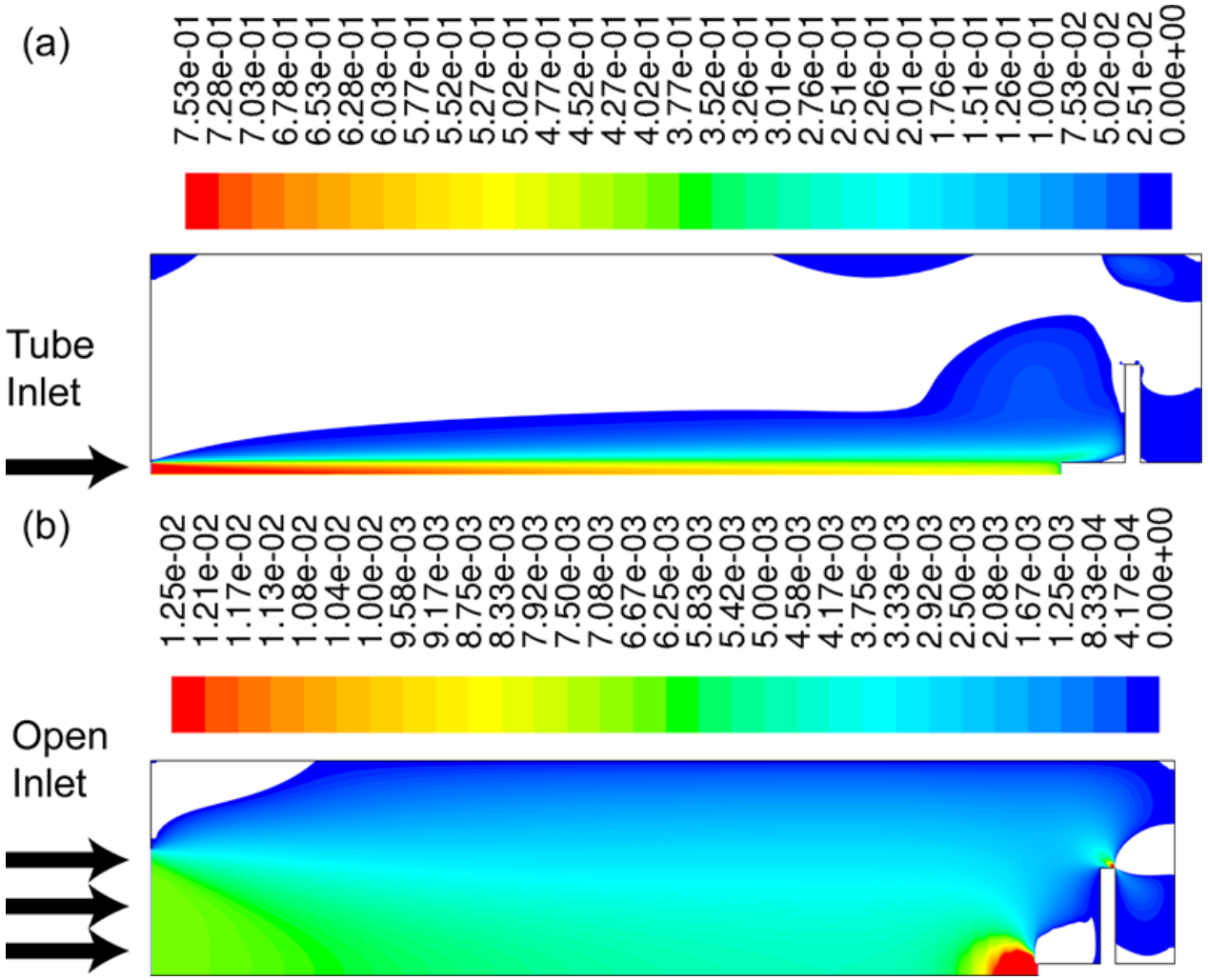
(a)
7.53e-01
7.28e-01
7.03e-01
6.78e-01
6.53e-01
6.28e-01
6.03e-01
5.77e-01
5.52e-01
5.27e-01
5.02e-01
4.77e-01
4.52e-01
4.27e-01
4.02e-01
3.77e-01
3.52e-01
3.26e-01
3.01e-01
2.76e-01
2.51e-01
2.26e-01
2.01e-01
1.76e-01
1.51e-01
1.26e-01
1.00e-01
7.53e-02
5.02e-02
2.51e-02
0.00e+00
Tube
Inlet
(b)
1.25e-02
1.21e-02
1.17e-02
1.13e-02
1.08e-02
1.04e-02
1.00e-02
9.58e-03
9.17e-03
8.75e-03
8.33e-03
7.92e-03
7.50e-03
7.08e-03
6.67e-03
6.25e-03
5.83e-03
5.42e-03
5.00e-03
4.58e-03
4.17e-03
3.75e-03
3.33e-03
2.92e-03
2.50e-03
2.08e-03
1.67e-03
1.25e-03
8.33e-04
4.17e-04
0.00e+00
Open
Inlet

Figure S2.

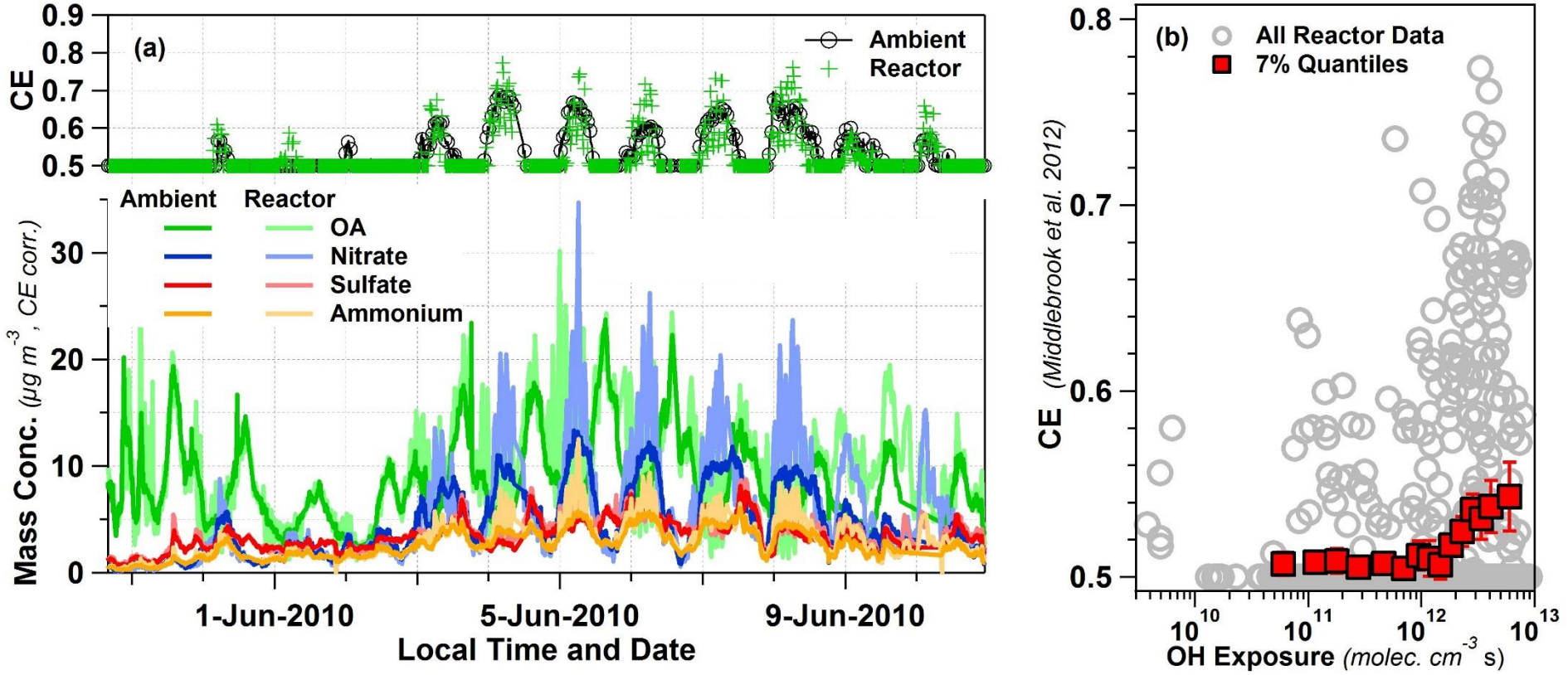
(a)
Ambient
Reactor
CE
0.9
0.8
0.7
0.6
0.5
Ambient
Reactor
OA
Nitrate
Sulfate
Ammonium
Mass Conc. (μg m-3, CE corr.)
30
20
10
0
1-Jun-2010
5-Jun-2010
9-Jun-2010
Local Time and Date
(b)
All Reactor Data
7% Quantiles
CE (Middlebrook et al. 2012)
0.8
0.7
0.6
0.5
10^10
10^11
10^12
10^13
OH Exposure (molec. cm-3 s)

Figure S3.

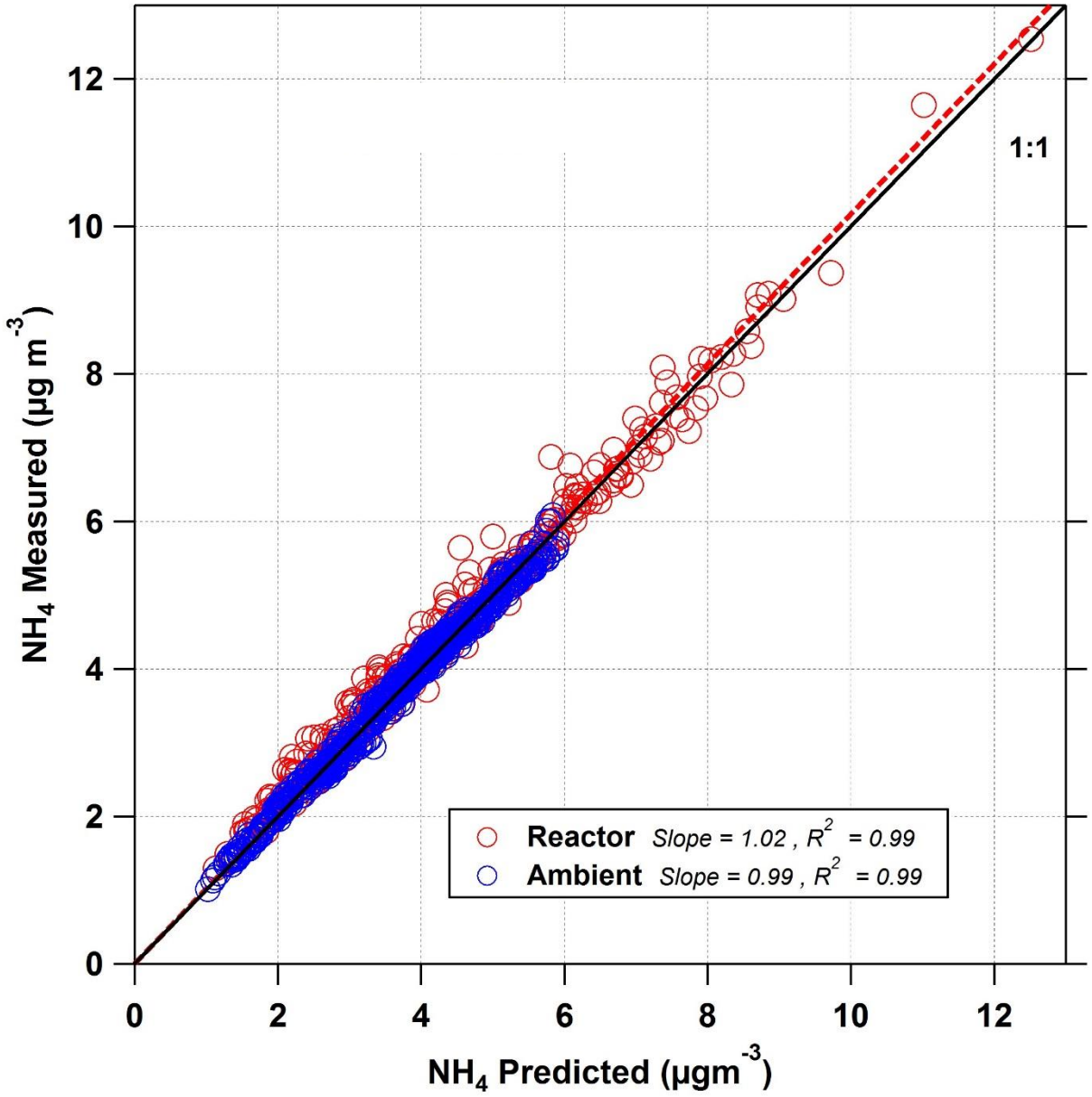
12
10
8
6
4
2
0
0
2
4
6
8
10
12
1:1
NH4 Measured (µg m-3)
NH4 Predicted (µgm-3)
Reactor Slope = 1.02 , R2 = 0.99
Ambient Slope = 0.99 , R2 = 0.99

Figure S4.

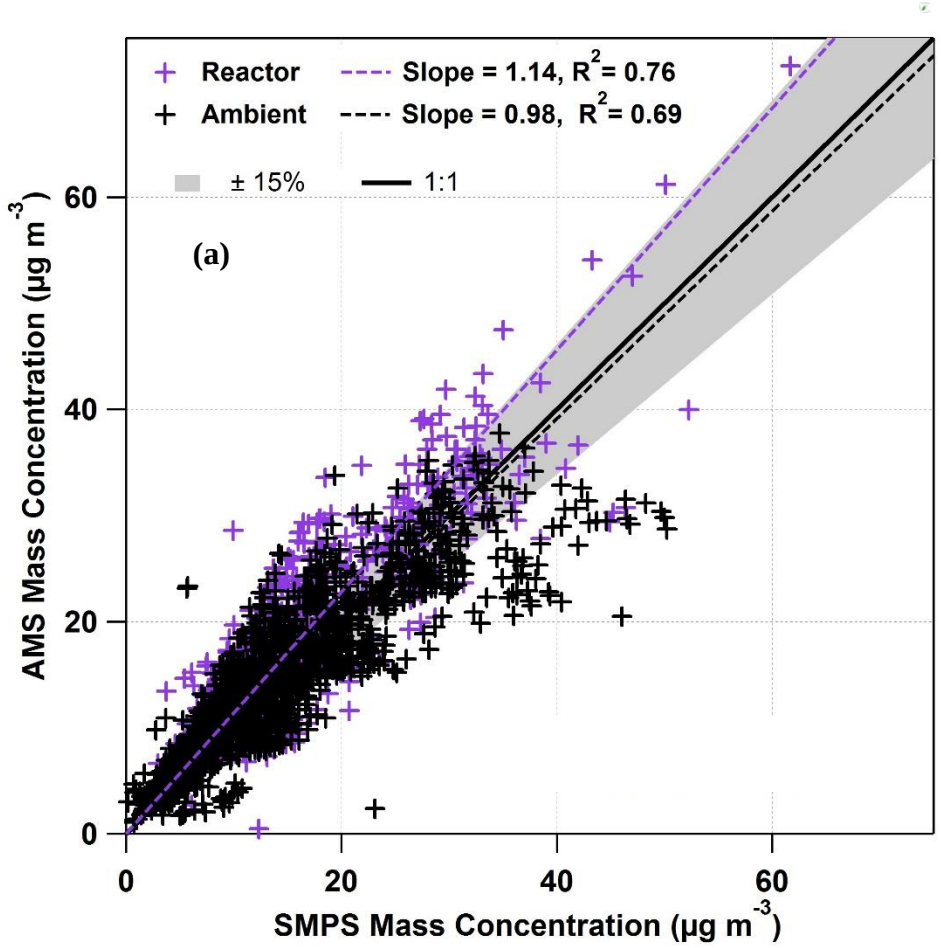
Reactor
Slope = 1.14, R2 = 0.76
Ambient
Slope = 0.98, R2 = 0.69
± 15%
1:1
(a)
AMS Mass Concentration (µg m-3)
SMPS Mass Concentration (µg m-3)
0
20
40
60

(b)

Figure S5.

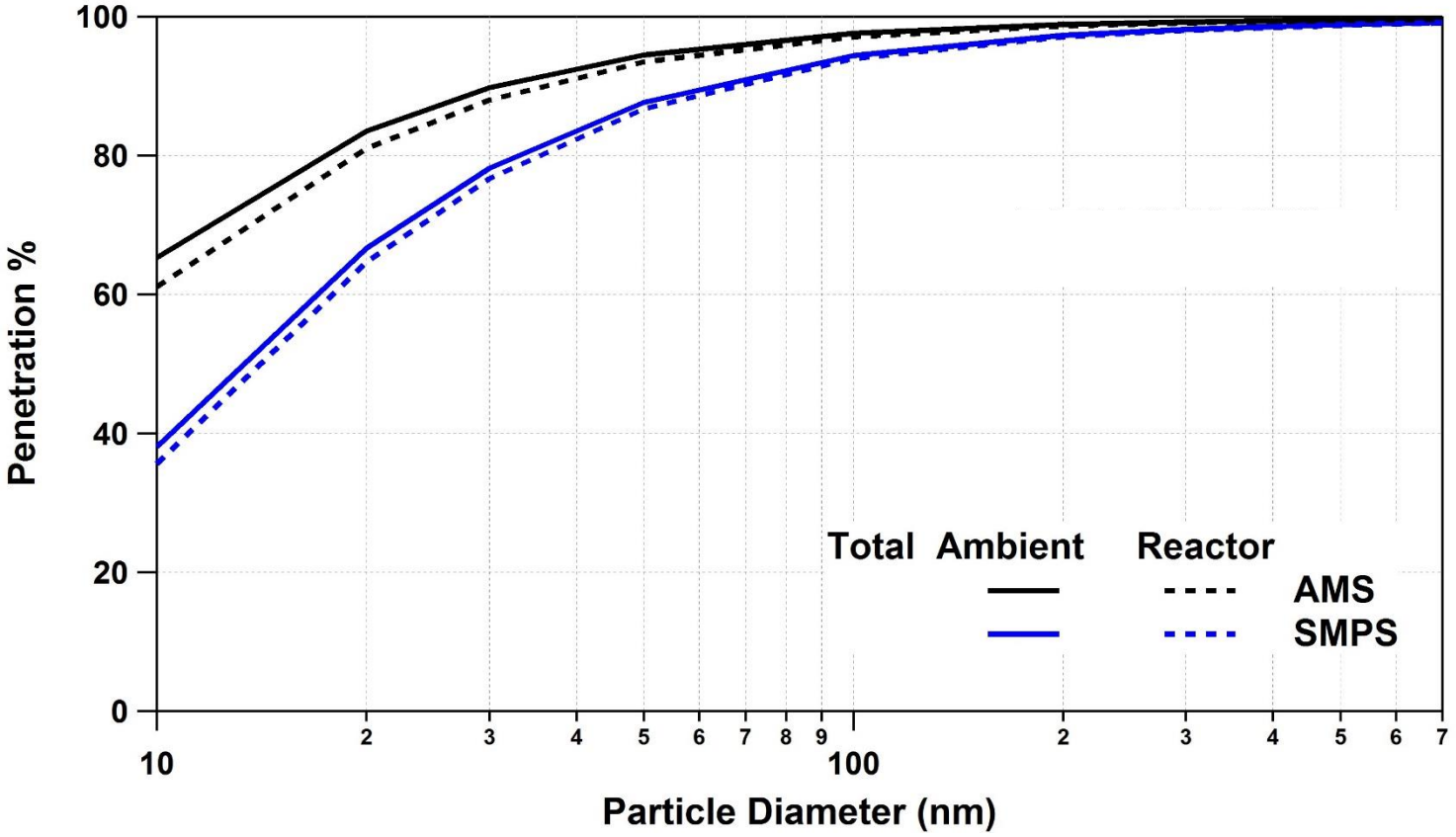
Penetration %
100
80
60
40
20
0
10
2
3
4
5
6
7
8
9
100
2
3
4
5
6
7
Particle Diameter (nm)
Total Ambient
Reactor
AMS
SMPS

Figure S6.

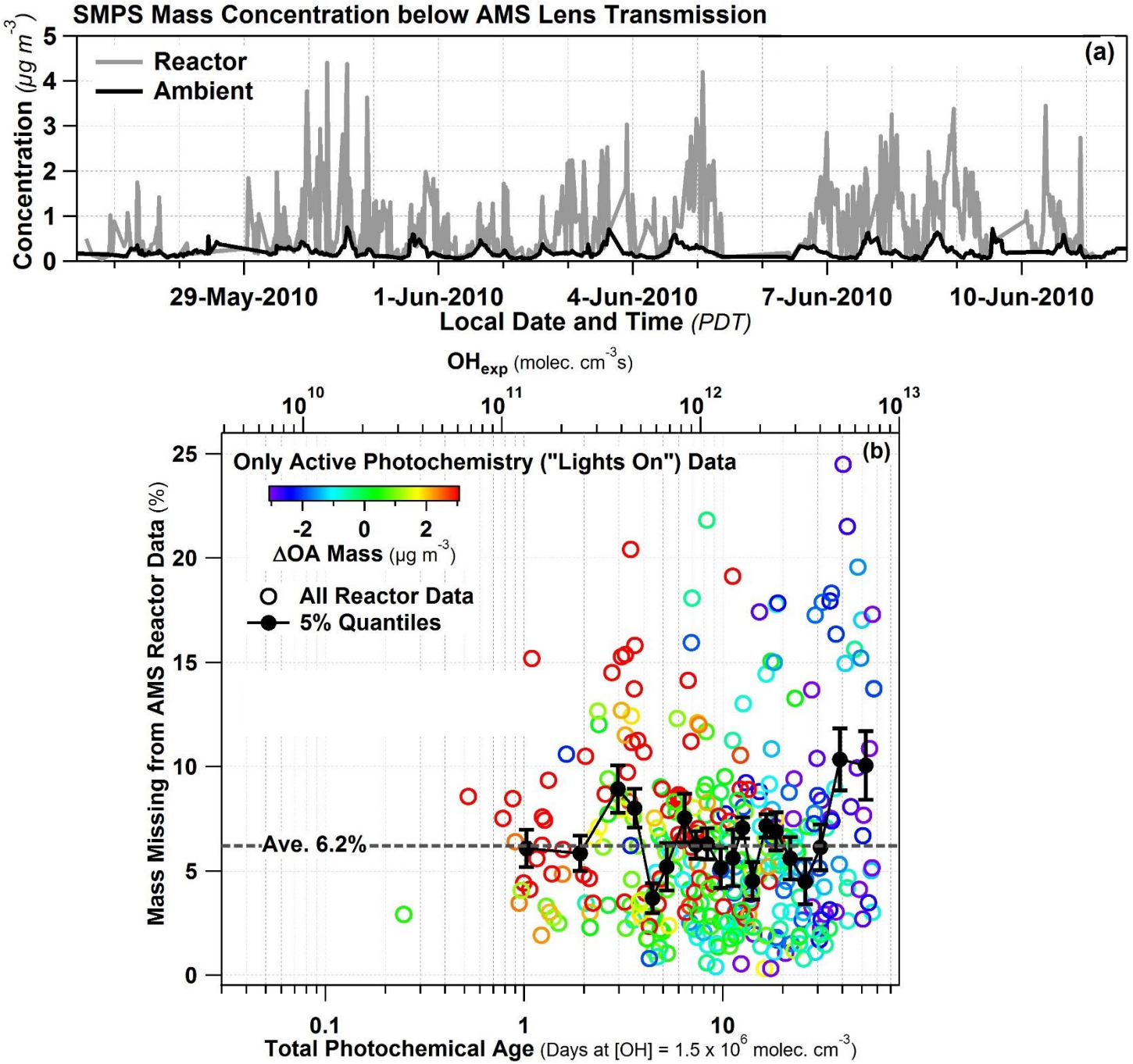
SMPS Mass Concentration below AMS Lens Transmission
Reactor
Ambient
(a)
Concentration (μg m-3)
0
1
2
3
4
5
29-May-2010
1-Jun-2010
4-Jun-2010
7-Jun-2010
10-Jun-2010
Local Date and Time (PDT)
OHexp (molec. cm-3s)
10^10
10^11
10^12
10^13
(b)
Only Active Photochemistry ("Lights On") Data
-2
0
2
ΔOA Mass (μg m-3)
All Reactor Data
5% Quantiles
Ave. 6.2%
Mass Missing from AMS Reactor Data (%)
0
5
10
15
20
25
0.1
1
10
Total Photochemical Age (Days at [OH] = 1.5 x 10^6 molec. cm-3)

Figure S7.

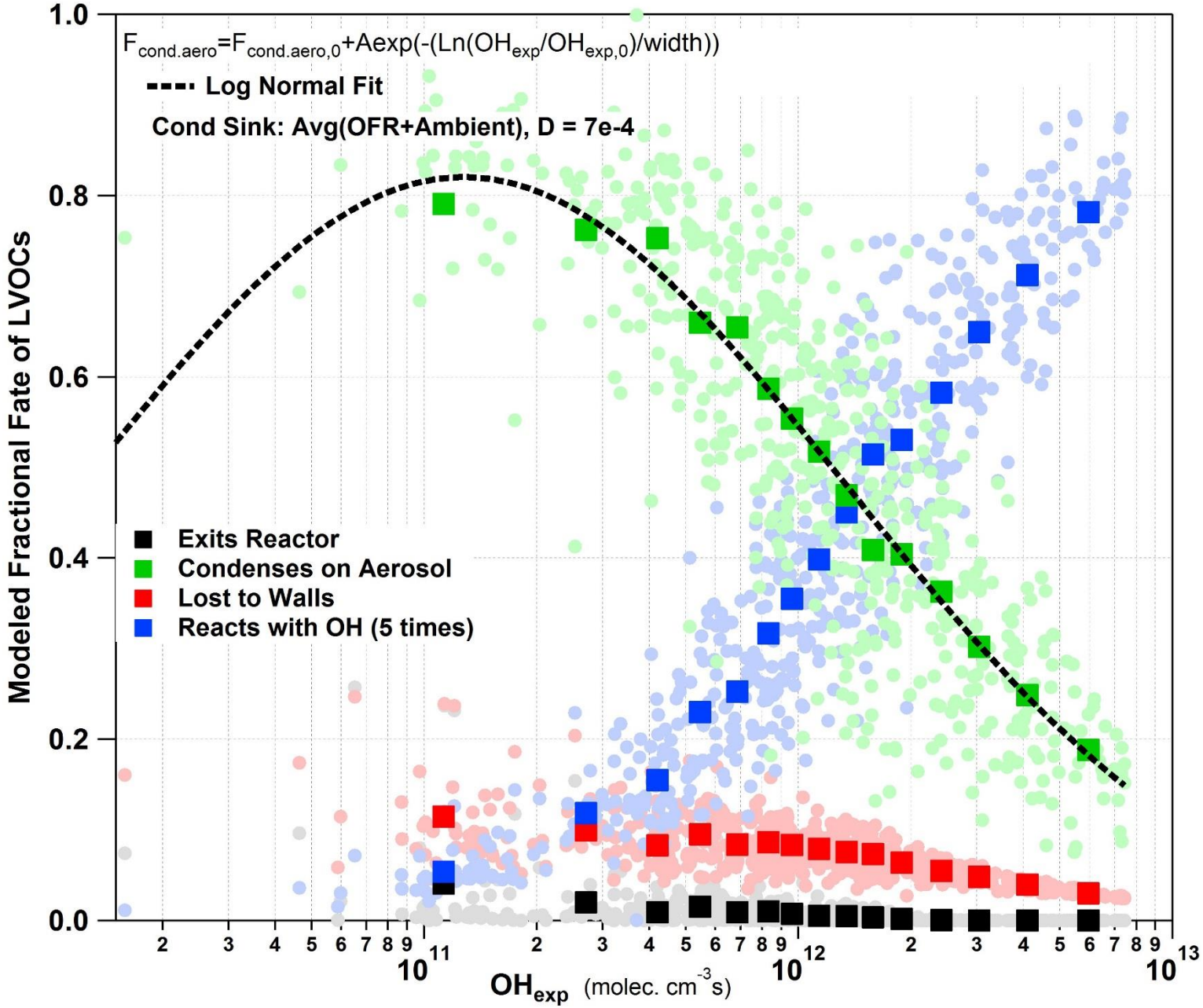
$F_{cond.aero}=F_{cond.aero,0}+Aexp(-(Ln(OH_{exp}/OH_{exp,0})/width))$
Log Normal Fit
Cond Sink: Avg(OFR+Ambient), D = 7e-4
Exits Reactor
Condenses on Aerosol
Lost to Walls
Reacts with OH (5 times)
Modeled Fractional Fate of LVOCs
1.0
0.8
0.6
0.4
0.2
0.0
2 3 4 5 6 7 8 9 10^{11} 2 3 4 5 6 7 8 9 10^{12} 2 3 4 5 6 7 8 9 10^{13}
OH_{exp} (molec. cm^{-3} s)

Figure S8.

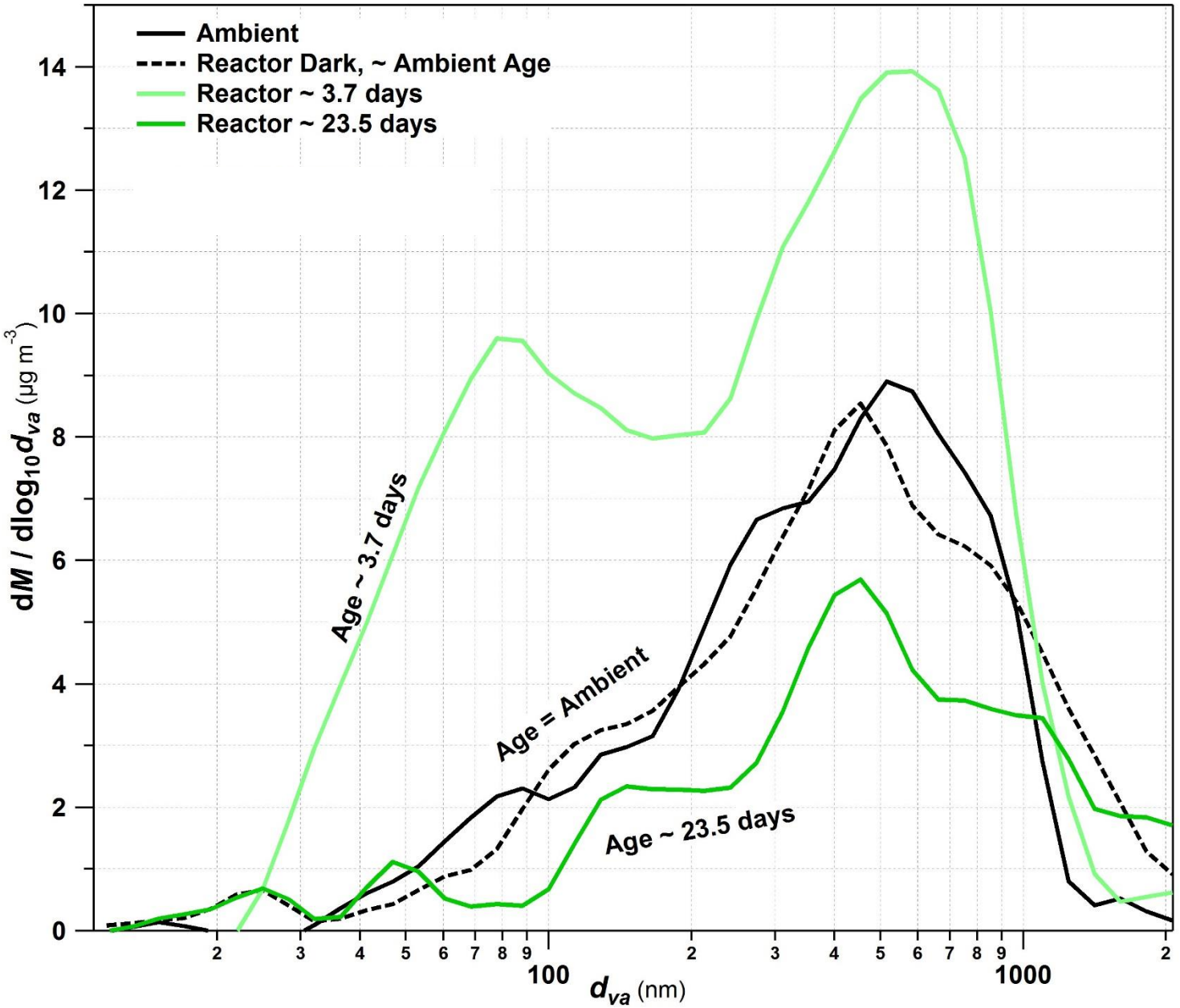
Ambient
Reactor Dark, ~ Ambient Age
Reactor ~ 3.7 days
Reactor ~ 23.5 days
Age ~ 3.7 days
Age = Ambient
Age ~ 23.5 days
dM / dlog10dva (µg m-3)
dva (nm)
0
2
4
6
8
10
12
14
100
1000

Figure S9.

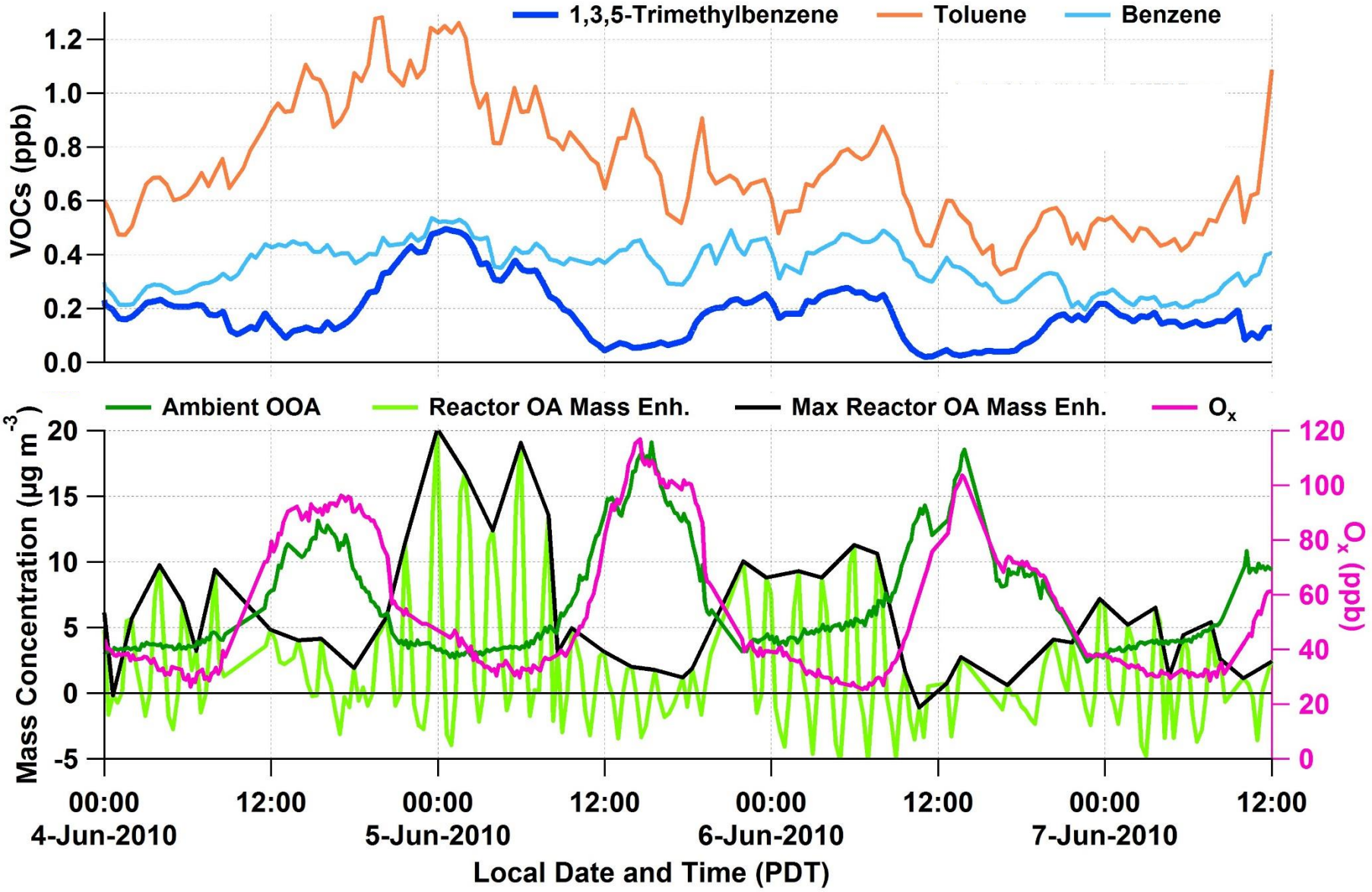
1,3,5-Trimethylbenzene
Toluene
Benzene
VOCs (ppb)
1.2
1.0
0.8
0.6
0.4
0.2
0.0
Ambient OOA
Reactor OA Mass Enh.
Max Reactor OA Mass Enh.
O_x
Mass Concentration (μg m^{-3})
20
15
10
5
0
-5
120
100
80
60
40
20
0
O_x (ppb)
00:00
12:00
00:00
12:00
00:00
12:00
00:00
12:00
4-Jun-2010
5-Jun-2010
6-Jun-2010
7-Jun-2010
Local Date and Time (PDT)

Figure S10.

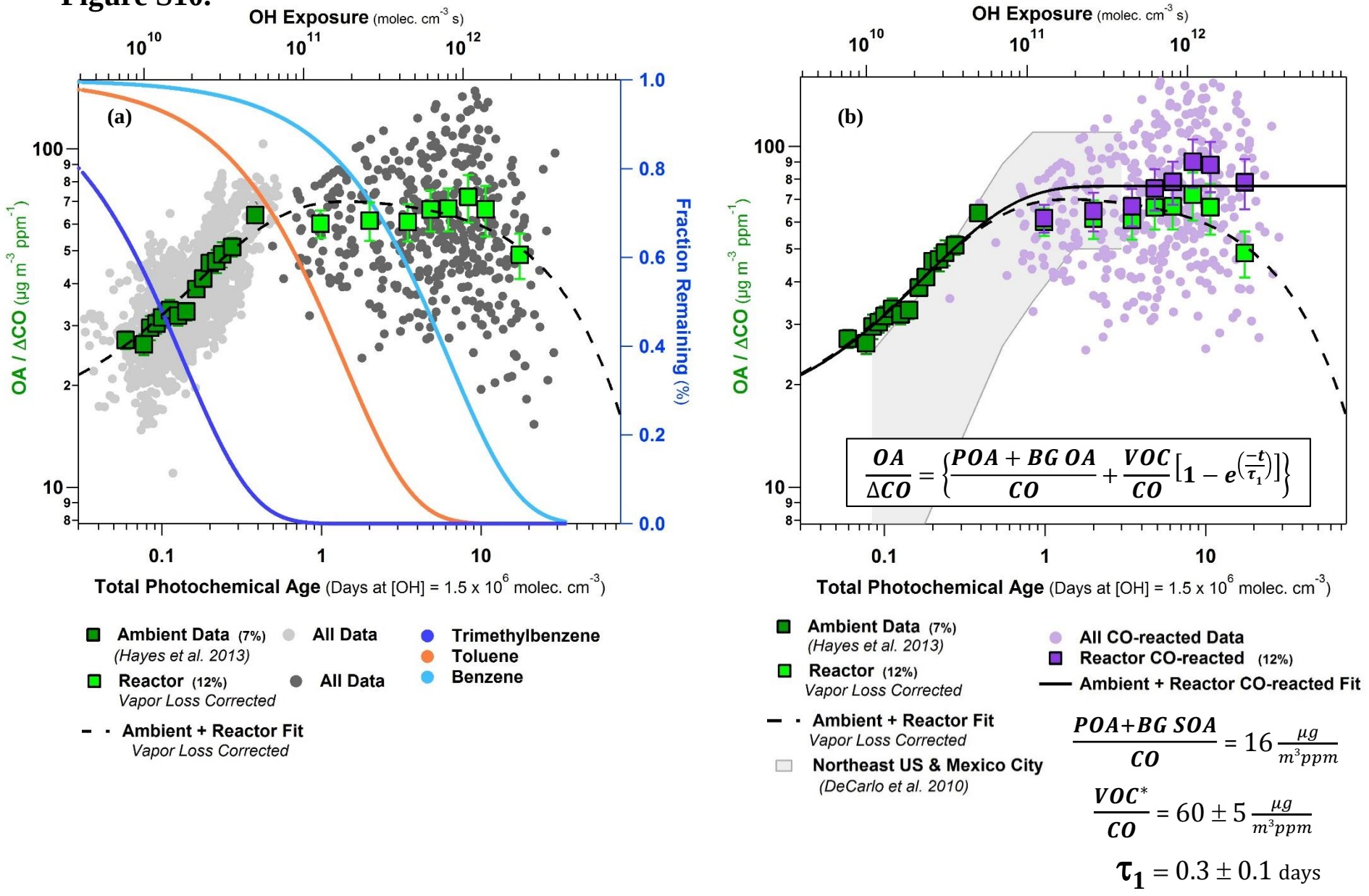
OH Exposure (molec. cm-3 s)
(a)
(b)
OA / ΔCO (μg m-3 ppm-1)
Fraction Remaining (%)
Total Photochemical Age (Days at [OH] = 1.5 x 10^6 molec. cm-3)
Ambient Data (7%)
(Hayes et al. 2013)
Reactor (12%)
Vapor Loss Corrected
Ambient + Reactor Fit
Vapor Loss Corrected
All Data
All Data
Trimethylbenzene
Toluene
Benzene
Ambient Data (7%)
(Hayes et al. 2013)
Reactor (12%)
Vapor Loss Corrected
Ambient + Reactor Fit
Vapor Loss Corrected
Northeast US & Mexico City
(DeCarlo et al. 2010)
All CO-reacted Data
Reactor CO-reacted (12%)
Ambient + Reactor CO-reacted Fit
$\frac{OA}{\Delta CO} = \left\{\frac{POA + BG\ OA}{CO} + \frac{VOC}{CO}\left[1 - e^{\left(\frac{-t}{\tau_1}\right)}\right]\right\}$
$\frac{POA+BG\ SOA}{CO} = 16\ \frac{\mu g}{m^3 ppm}$
$\frac{VOC^*}{CO} = 60 \pm 5\ \frac{\mu g}{m^3 ppm}$
$\tau_1 = 0.3 \pm 0.1$ days

Figure S11.

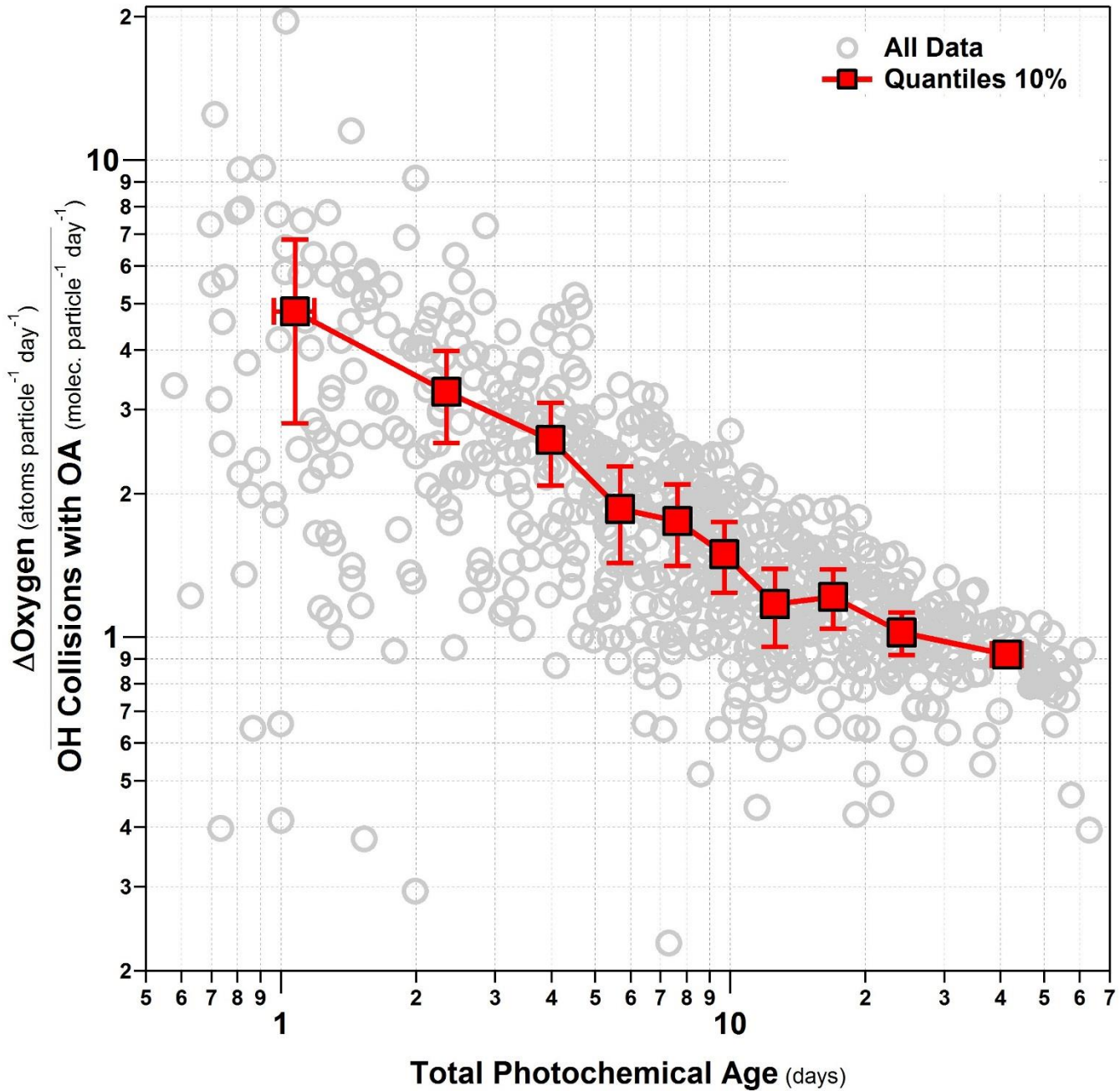
All Data
Quantiles 10%
ΔOxygen (atoms particle-1 day-1)
OH Collisions with OA (molec. particle-1 day-1)
Total Photochemical Age (days)
1
10

Figure S12.

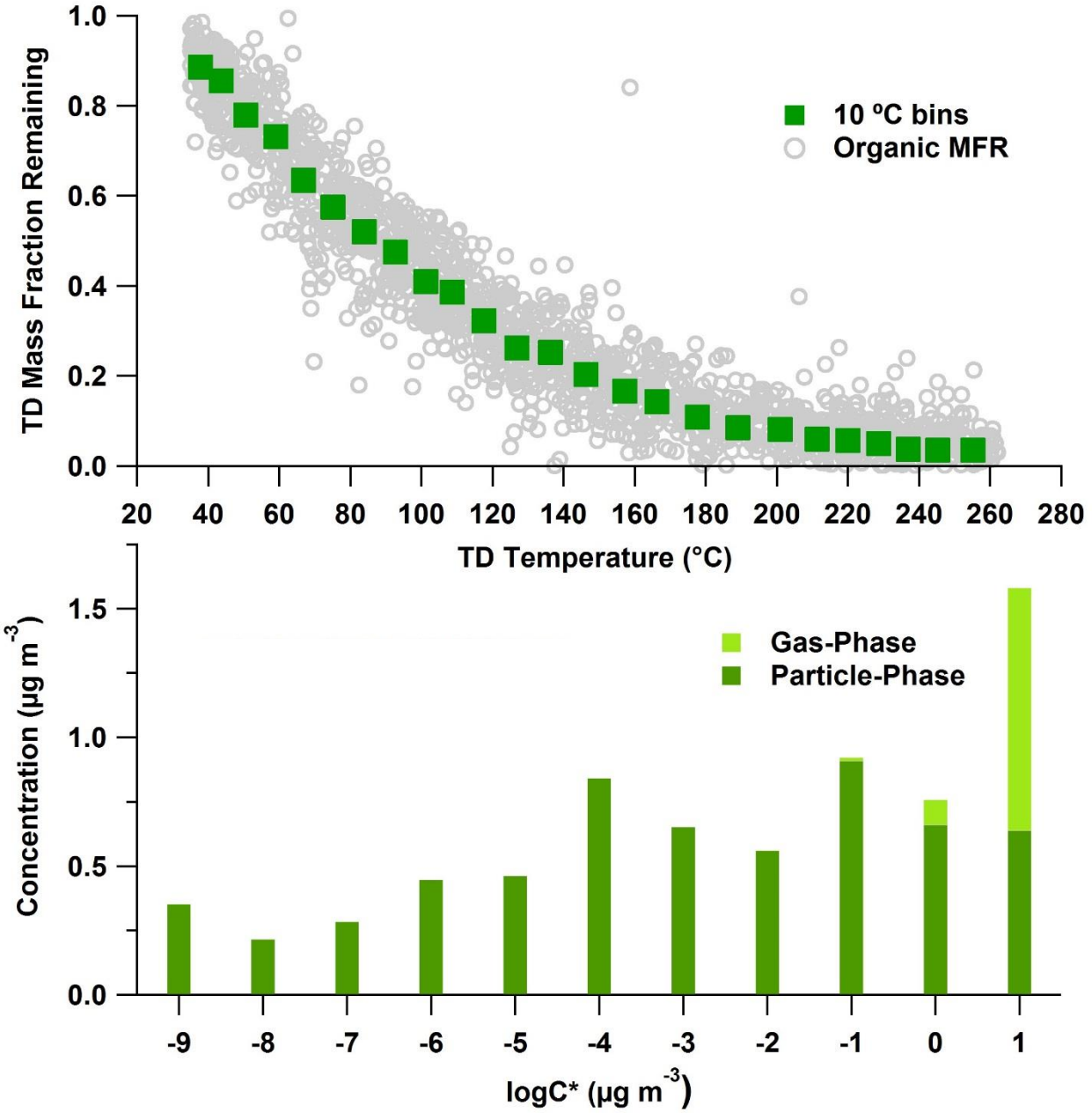
TD Mass Fraction Remaining
1.0
0.8
0.6
0.4
0.2
0.0
10 ºC bins
Organic MFR
20
40
60
80
100
120
140
160
180
200
220
240
260
280
TD Temperature (°C)
Concentration (µg m-3)
1.5
1.0
0.5
0.0
Gas-Phase
Particle-Phase
-9
-8
-7
-6
-5
-4
-3
-2
-1
0
1
logC* (µg m-3)